GHASP: an Hα kinematical survey of spiral galaxies - XIII. Distribution of luminous and dark matter in spiral and irregular nearby galaxies using Hα and HI rotation curves and WISE photometry

M. Korsaga, B. Epinat, P. Amram, C. Carignan, P. Adamczyk, A. Sorgho

Monthly Notices
of the
ROYAL ASTRONOMICAL SOCIETY

MNRAS **490,** 2977–3024 (2019)
Advance Access publication 2019 September 27

doi:10.1093/mnras/stz2678

GHASP: an H α kinematical survey of spiral galaxies – XIII. Distribution of luminous and dark matter in spiral and irregular nearby galaxies using H α and H I rotation curves and *WISE* photometry

M. Korsaga,[1,2]★ B. Epinat,[1] P. Amram,[1] C. Carignan,[2,3] P. Adamczyk[1] and A. Sorgho[2]

[1]*CNRS, CNES, LAM, Aix Marseille University, 13013 Marseille, France*
[2]*Department of Astronomy, University of Cape Town, Private Bag X3, Rondebosch 7701, South Africa*
[3]*Observatoire d'Astrophysique de l'Université de Ouagadougou, BP 7021, Ouagadougou 03, Burkina Faso*

Accepted 2019 September 17. Received 2019 September 6; in original form 2018 December 14

ABSTRACT

We present the mass models of 31 spiral and irregular nearby galaxies obtained using hybrid rotation curves (RCs) combining high-resolution GHASP Fabry–Perot H α RCs and extended WHISP H I ones together with 3.4 μm *WISE* photometry. The aim is to compare the dark matter (DM) halo properties within the optical radius using only H α RCs with the effect of including and excluding the mass contribution of the neutral gas component, and when using H I or hybrid RCs. Pseudo-isothermal (*ISO*) core and Navarro–Frenk–White (NFW) cuspy DM halo profiles are used with various fiducial fitting procedures. Mass models using H α RCs including or excluding the H I gas component provide compatible disc M/L. The correlations between DM halo and baryon parameters do not strongly depend on the RC. Clearly, the differences between the fitting procedures are larger than between the different data sets. Hybrid and H I RCs lead to higher M/L values for both *ISO* and NFW best-fitting models but lower central densities for *ISO* haloes and higher concentration for NFW haloes than when using H α RCs only. The agreement with the mass model parameters deduced using hybrid RCs, considered as a reference, is better for H I than for H α RCs. *ISO* density profiles better fit the RCs than the NFW ones, especially when using H α or hybrid RCs. Halo masses at the optical radius determined using the various data sets are compatible even if they tend to be overestimated with H α RCs. Hybrid RCs are thus ideal to study the mass distribution within the optical radius.

Key words: galaxies: haloes – galaxies: irregular – galaxies: ISM – galaxies: kinematics and dynamics – galaxies: spiral – dark matter.

1 INTRODUCTION

Since ∼50 yr, it is well observed that there is a large discrepancy between the luminous mass and the dynamical mass of galaxies (see e.g. Freeman 1970; Bosma 1978). This is usually explained by adding a more or less spherical halo of dark matter (DM) to the visible baryonic mass composed of stars and gas (see e.g. Carignan & Freeman 1985). The DM can be distributed using a theoretical or an empirical density profile. Therefore, in the literature, several density profile models are used to determine the DM distribution. The two most commonly used models are the pseudo-isothermal sphere (*ISO*; Begeman 1987) with a core density profile and the Λ cold dark matter (ΛCDM) cuspy density profile from Navarro–Frenk–White (NFW; Navarro, Frenk & White 1996, 1997).

In the last ∼10 yr, 2D-kinematics of large samples of nearby galaxies have been obtained either in the optical using Fabry–Perot interferometry of the H α line (see e.g. the GHASP sample of ∼200 galaxies, Epinat, Amram & Marcelin 2008b), at radio wavelength using aperture synthesis of the H I line [see e.g. the WHISP sample, a homogenous survey of ∼300 spiral and irregular galaxies with the Westerbork Synthesis Radio Telescope (WSRT) in Swaters et al. 2002; Noordermeer et al. 2005; van Eymeren et al. 2011 or the THINGS sample of ∼35 galaxies observed with the Very Large Array in de Blok et al. 2008] or a combination of those two types of data (see e.g. the SPARC sample of ∼175 galaxies in Lelli, McGaugh & Schombert 2016). At present, H α kinematics has ∼1–2 arcsec spatial resolution, limited by the seeing, as compared to the radio (e.g. WSRT or VLA) 15–30 arcsec resolution. Naturally, the new radio interferometers, with longer baselines, will improve

★ E-mail: marie.korsaga@lam.fr

on this and eventually get comparable resolutions. In the near future, large sample of more distant galaxies will be obtained using UV–optical–near-infrared (NIR) emission lines with IFUs on large optical/IR telescopes or H I on the new generation of large radio interferometers such as MeerKAT for nearby galaxies and in a more distant future with the SKA for thousands of distant galaxies. It is thus important to compare the results we get for nearby galaxies using either optical Hα, radio H I, or hybrid (combining Hα + H I) data sets and understand properly the effects of different spatial resolutions. When analysing the mass distribution of galaxies, it is also important to know if the derived parameters of both the luminous and dark components are affected by using those different data sets.

The main difference is expected to come from the spatial resolution of today's data because of the great sensitivity of the mass distribution parameters to the central part of the galaxies rotation curves (RCs; Blais-Ouellette, Amram & Carignan 2001), where the velocity gradient is maximal. It is that part of the RC that will constrain the free parameter of the luminous disc, namely the M/L ratio, which necessarily also has an impact of the parameters of the DM component. Many other studies have shown that the parameters of the DM distribution are very sensitive to the inner part kinematics as observed using emission line Hα observations (see e.g. Amram et al. 1992; Spano et al. 2008).

Korsaga et al. (2018) in their work, used 121 Hα RCs combined to *Wide-field Infrared Survey Explorer* (*WISE*) W_1-band photometric data to determine the DM halo distribution. Another study was also done using a sample of 100 Hα RCs combined with optical R_c-band photometric data (Korsaga et al. 2019). The main aim was to see if the luminous and DM parameters were dependant of the photometric band used (optical versus IR), since they are dominated by different stellar populations. In this paper, we aim to first construct the mass distribution of 31 galaxies using the same RCs and mid-IR photometry data mentioned earlier and considering the effect of including the contribution from the H I gas component. Secondly, the mass distribution is determined with the same photometry and gas component but using extended hybrid RCs (Hα in the inner parts extended with H I data in the outer parts). This will also be compared to purely H I kinematical data. The main goal here is to study how luminous and DM parameters depend on the data set used to derive the RCs.

The galaxy sample is presented in Section 2. In Section 3, we present the mass models and the results of the fits are described in Sections 4 and 5. A discussion of the results obtained with the different types of RCs is done in Sections 6 and 7 presents a summary and the general conclusions. In Appendix A, we present the mass models of all the galaxies. We assumed a Hubble constant $H_0 = 75$ km s^{-1} Mpc^{-1} throughout this paper.

2 SAMPLE

2.1 Rotation curves

Our sample consists of 31 nearby galaxies selected from the GHASP survey (which contains 203 galaxies) and having H I RCs and 3.4 µm photometric data. The GHASP survey produced high spectral (∼10 000) and spatial (∼2 arcsec) resolution Hα RCs. The Hα line was scanned using a Fabry–Perot interferometer at the 1.93 m telescope of the Observatoire de Haute Provence (Garrido et al. 2002; Epinat et al. 2008b). As we already applied a selection criteria on the quality of the Hα RCs in a previous study (Korsaga et al. 2018), we use the same Hα RCs which have both W_1-band photometric data and H I RCs available in the literature. The Hα RCs are computed from the 2D velocity field using the method described in Epinat et al. (2008a), making the synthesis between the method used in Papers I–IV; the one based on tilted-ring models (found for instance with the rotcur routine of GIPSY, Begeman 1987) and the one used by Barnes & Sellwood (2003). This method aims to reduce the degeneracy using physical constraints and χ^2-minimization methods on the velocity field (and not on the RC). The RC is computed in successive rings containing the same number of uncorrelated bins. Thus, the width in each ring is variable, and the velocity computed for each ring is then always the average of the same number of uncorrelated velocity measurements. The estimation of the errors of the Hα RC comes from the dispersion of velocity measurements divided by the square root of bins in each ring.

For the H I RCs, 15 galaxies were taken from van Eymeren et al. (2011) and the remaining 16 from Lelli et al. (2016), which can be accessed on the SPARC website.[1] The H I RCs are usually derived by fitting tilted-ring models to the observed velocity fields and the errors on the rotation velocities are based on the difference between the approaching and the receding sides of the galaxy (e.g. Begeman 1987; Swaters et al. 2009; Lelli et al. 2016).

In order to compute hybrid RCs, we need to combine Hα and H I data. The difference in inclination between H I and Hα discs may be an issue, the H I discs being usually more extended than the Hα ones and sometimes warped in the outskirts. Furthermore, using a mean inclination for the whole disc may be not correct outside the optical radius. Usually, even when tilted-ring models are used, the inclination is kept constant in the optical region both in Hα and H I due to the fact that warps in galactic discs rarely start within the inner disc. Outside, a correction of inclination to match H I and Hα RCs is not necessary because the plane of the disc at each radius is only traced by the H I component. Ideally, the inclination deduced from the internal H I RC should be used to make the best correction. However, our Hα sample is homogeneous whereas the H I data come from various sources (see Table 1). We therefore decided to use Hα inclinations (Epinat et al. 2008b) as a reference. For the same reason, we have also used the distances from Epinat et al. (2008b) rather than collecting distances from different works. We applied the following first-order corrections: (i) H I rotation velocities are multiplied by the ratio between the sine of H I and Hα inclinations, (ii) gas component velocities derived from H I surface brightness are multiplied by the root square of the ratio between Hα and H I distances, and (iii) galactic radii in H I curves are multiplied by the same ratio of distances. The different parameters of the H I RCs, collected in the literature as well as the one we use in this work, are shown in Table 1. The correction on the amplitude of the H I RC is below 10 per cent for 24/31 galaxies, and we do not observe any systematic trend towards lower or higher values. In addition, only 2/31 galaxies (UGC 8490 and UGC 8334) are clearly affected by H I warps, however the H I inclination provided for those two galaxies has been obtained from the inner disc. Furthermore, only UGC 8490 has a correction higher than 10 per cent. The warp issue therefore only marginally impacts our study. Finally, three galaxies only (UGC 2080, UGC 3574, and UGC 3734) have a low inclination (<30°). Due to deprojection effects, the Hα RCs of these galaxies exhibit furthermore high uncertainties and we notice either a poor sampling or a lack of data in the inner parts of their H I RCs.

[1] http://astroweb.cwru.edu/SPARC/

Table 1. Global properties of galaxies.

UGC (1)	$D_{\rm H\,I}$ (2)	$D_{\rm H\,\alpha}$ (3)	$i_{\rm H\,I}$ (4)	$i_{\rm H\alpha}$ (5)	t (6)	Flag (7)	H I beam (8)	Ref (9)
01913	9.3	9.3	54	48	SABd	d	30	VE11
02080*	13.7	13.7	28	25	SABcd	d/b	30	VE11
02800	20.6	20.6	62	52	Im	d	30	VE11
02855**	17.5	17.5	61	68	SABc	d/b	30	VE11
03574	21.8	21.8	31	19	SAcd	d/b	30	VE11
03734	15.9	15.9	22	43	SAc	d/b	30	VE11
04284	9.8	9.8	62	59	SAcd	d/b	30	VE11
04325**	9.6	10.9	41	63	SAm	d	30	SW09, SW02
04499	12.5	12.2	50	50	SABdm	d/b	30	SW09, SW02
05251	21.5	21.5	65	73	Sbc	d/b	30	VE11
05253	22.9	21.1	37	40	SAab	d	11.6	No07, No05
05414	9.4	10.0	55	71	IABm	d	30	SW09, SW02
06537	18.0	14.3	53	47	SAB(r)c	d/b	12	VS01, SV98
06778	18.0	15.5	49	49	SABc	d/b	12	VS01, SV98
07323*	8.0	8.1	47	51	SABdm	d	30	SW09, SW02
07766*	9.0	13.0	67	69	SABcd	d/b	17	Ba05
08334	9.9	9.8	63	66	SAbc	d	28	Bt06, Bl04, Th97
08490	4.7	4.7	50	40	SAm	d	30	SW09, SW02
09179	7.1	5.7	51	36	SABd	d/b	20	Bl99, Sa96, Co91
09649*	7.7	7.7	57	54	SBb	d	30	VE11
09858	38.2	38.2	70	75	SABbc	d/b	30	VE11
09969	39.7	36.0	60	61	SAB(r)b	d/b	14	Bl04, Br92
10075	17.0	14.7	61	62	SAcd	d	13	VM97
10359	16.0	16.0	44	44	SBcd pec	d/b	30	VE11
10470	21.2	21.2	37	34	SBbc	d/b	30	VE11
11012	6.3	5.3	74	72	SAcd	d	30	Be91, Be87
11597*	5.5	5.9	38	40	SABcd	d/b	12	Bo08
11670	12.7	12.8	67	65	SA(r)0 − a	d/b	30	VE11
11852*	80.0	80.0	46	47	SBa	d/b	30	VE11
11914	16.9	15.0	31	33	SA(r)ab	d/b	10.5	No07, No05
12754	8.9	8.9	49	53	SBcd	d/b	30	VE11

Note. (1) Name of the galaxy in the UGC catalogue. Columns (2) and (4) represent, respectively, the distance in Mpc and the inclination for H I data. Columns (3) and (5) show the distance in Mpc and inclination for H α data taken from Epinat et al. (2008b) used in this study. Column (6) shows the morphological type from the RC3 catalogue. Column (7) represents the baryonic components that have been used (d: for disc only; d/b: for disc and bulge). Column (8) shows the H I beam for the H I RCs in arcsec. Column (9) shows the H I data references (VE11: van Eymeren et al. 2011; SW09: Swaters et al. 2009; SW02: Swaters et al. 2002; No07: Noordermeer et al. 2007; No05: Noordermeer et al. 2005; VS01: Verheijen & Sancisi 2001; SV98: Sanders & Verheijen 1998; Ba05: Barbieri et al. 2005; Bt06: Battaglia et al. 2006; BI04: Blais-Ouellette et al. 2004; Th97: Thornley & Mundy 1997; BI99: Blais-Ouellette et al. 1999; Sa96: Sanders 1996; Co91: Cote, Carignan & Sancisi 1991; Br92: Broeils 1992; VM97: Verdes-Montenegro, Bosma & Athanassoula 1997; Be91: Begeman, Broeils & Sanders 1991; Bo08: Boomsma et al. 2008). Galaxy names marked with asterisks mean galaxies for which we do not need DM to describe their RCs: one asterisk when using only H α RC, two asterisks when it is the same case when using H α and hybrid rotation and H I curves.

2.2 Photometric data

The infrared surface photometry provides smaller dispersion for the M/L ratios compared to the optical photometry (Korsaga et al. 2019). Several models also predict that the values of the M/L ratios are approximately constant when using the NIR photometry (Bell & de Jong 2001; Lelli et al. 2016). Because our first step is to better constrain the M/L ratio, the W_1 band (3.4 μm) from the *WISE* (Jarrett et al. 2013) is suitable due to its weaker sensitivities to star formation activities and dust. The field of view is 47 × 47 arcmin^2 with an angular resolution of 6 arcsec. The decomposition of the surface brightness profiles into multiple components (bulge, disc, bar, spiral arm, ring, etc.) was already performed in Korsaga et al. (2018). From the whole sample of 31 galaxies, 11 did not need a decomposition (faint bulge) while the remaining 20 galaxies were decomposed. In order to reduce the number of parameters, we disentangle spherical components (bulges) from planar components (disc, bar, spiral arm, etc.) that we call disc in the mass models (Korsaga et al. 2018). The sample covers all morphological types (early-type to late spiral and irregular galaxies) from Sa to Im. We have 10 Sa-Sbc, 15 Sc to Sd, and 6 Sm-Im. The stellar mass contribution is obtained by scaling with the M/L ratio of both components. We first use the M/L ratio as a free parameter in the mass models corresponding to the minimal χ^2 value; secondly, we constrained the M/L to have a maximum stellar contribution, so higher than the M/L derived from the minimal χ^2 and lastly, we consider the M/L as a constant parameter calculated as a function of the colour index $(W_1 - W_2)$ using the following relation given by Cluver et al. (2014):

$$\log(M_{\rm stellar}/L_{W_1}) = -2.54(W_1 - W_2) - 0.17, \quad (1)$$

where L_{W_1} is the luminosity in the W_1 band and where W_1 and W_2 correspond to magnitudes in the W_1 and W_2 bands, respectively. In

that case, bulge and disc components are not treated separately (see Section 3.3).

2.3 H I density

To trace the mass of the galaxy at larger radii, the contribution of the neutral gas component is necessary, especially for late-type galaxies where H I can become an important (if not dominant) part of the luminous mass. As already mentioned in Section 2, from the whole sample of 31 galaxies, 15 galaxies were taken from van Eymeren et al. (2011) and the remaining 16 from Lelli et al. (2016). However, the H I density profiles for 15 galaxies were not available in van Eymeren et al. (2011). For those, we use the total H I maps of the galaxies at the 30 arcsec resolution from the WHISP (Westerbork observations of neutral Hydrogen in Irregular and SPiral galaxies) website. We derive the surface density profiles of the neutral hydrogen using the GIPSY[2] task ELLINT and the tilted-ring geometric parameters (de Blok et al. 2008). To take into account the presence of helium, the surface densities are corrected by a factor of 1.33. The RCs associated with those surface densities are derived by assuming an infinitely thin gas disc.

To check the consistency of the H I surface brightness profiles with those collected from the literature, we run the software BBAROLO (Di Teodoro & Fraternali 2015) on our sample. This software fits a 3D tilted-ring model directly on an observed emission line datacube. For each datacube, we compute the RC in determining the parameters for each ellipse of the tilted-ring model and we derive the H I surface brightness profiles. We convert the H I surface brightness profile into an H I surface density profile by normalizing the integrated surface brightness with the total H I mass $M_{\rm H\,I}$ of the galaxy that is derived from the total flux using

$$M_{\rm H\,I} = 2.36\ 10^5\ D^2 \int F(v){\rm d}v, \tag{2}$$

where $M_{\rm H\,I}$ is in solar units, D is the distance of the galaxy in Mpc, and $\int F(v){\rm d}v$ is the total flux in Jy km s^{-1}.

3 MASS MODELS

3.1 Densities, masses, and velocities

We used the extended hybrid RCs (Hα extended with the H I RCs) of 31 galaxies to study the mass distribution. Therefore, two main models are used to quantify the distribution of the DM within the galaxies: the observation motivated *ISO* sphere with a constant central density core profile (Begeman 1987) and the NFW cuspy central density profile derived from the ΛCDM N-body simulations (Navarro et al. 1996). The total rotation velocity $V_{\rm rot}$ is the quadratic sum of the individual contributions of stellar disc, bulge, gas disc, and DM halo. The expression is

$$V_{\rm rot}(r) = \sqrt{V^2_{\rm disc} + V^2_{\rm bulge} + V^2_{\rm gas} + V^2_{\rm halo}}, \tag{3}$$

where $V_{\rm disc}$ and $V_{\rm bulge}$ are, respectively, the stellar disc and bulge contributions inferred from light profiles decomposition modulated by their mass-to-light ratio, $V_{\rm gas}$ is the gas disc contribution inferred from the H I surface densities derived in Section 2.3, and $V_{\rm halo}$ is the contribution of the DM halo. For disc components, we are using a thin discs and the prescriptions of Pierens & Huré (2004). For the halo, we use either the *ISO* or NFW profiles described below. The core central density profile of the *ISO* model is a single power law given by

$$\rho_{\rm iso}(r) = \frac{\rho_0}{\left[1 + \left(\frac{r}{r_0}\right)^2\right]}, \tag{4}$$

where ρ_0 is the central density and r_0 the characteristic radius of the DM halo. The integration of relation (4) over a volume of radius r gives the total mass within this radius that will be used in Section 6.5:

$$M_{\rm iso}(r) = 4\pi\rho_0 r_0^2 \left[r - r_0 \arctan\left(\frac{r}{r_0}\right)\right]. \tag{5}$$

The corresponding circular velocity of a particule at radius r is

$$V^2_{\rm iso}(r) = 4\pi G\rho_0 r_0^2 \left[1 - \frac{r_0}{r}\arctan\left(\frac{r}{r_0}\right)\right], \tag{6}$$

which is an increasing function of r, asymptotically reaching

$$V_{\rm max} = V(r=\infty) = \sqrt{4\pi G\rho_0 r_0^2}.$$

The cuspy density profile of the NFW model is a two-power law given by

$$\rho_{\rm NFW}(r) = \frac{\rho_0}{\left(\frac{r}{r_0}\right)\left(1 + \frac{r}{r_0}\right)^2}, \tag{7}$$

where ρ_0 and r_0 are also, respectively, the central density and the characteristic radius of the DM halo. The integrated mass within the radius r is

$$M_{\rm NFW}(r) = 4\pi\rho_0 r_0^3 \left[\ln(1 + r/r_0) - \frac{r/r_0}{1 + r/r_0}\right].$$

The NFW profile is often characterized by the concentration parameter c of the halo defined as $c = R_{200}/r_0$, where R_{200} is the virial radius. This radius corresponds to the radius where the mean density is 200 times the cosmological critical density $\rho_{\rm c} = 3H_0^2/8\pi G \simeq 2.775\ 10^{11}\ h^2\ {\rm M}_\odot\ {\rm Mpc}^{-3}$ (where $h = H_0/100$ and H_0 the Hubble constant in km s^{-1} Mpc^{-1}). The velocity at the virial radius is $V_{200} = hR_{200}$ (McGaugh et al. 2007), where V_{200} is in km s^{-1} and R_{200} is in kpc. Using parameters c and V_{200}, the expression of the halo mass at a reduced radius $x = r/R_{200}$, used in Section 6.5, is

$$M_{\rm NFW}(x) = \frac{V^3_{200}}{Gh}\frac{\ln(1+cx) - cx/(1+cx)}{\ln(1+c) - c/(1+c)}. \tag{8}$$

The velocity at a reduced radius x for NFW is furthermore given by

$$V^2_{\rm NFW}(x) = V^2_{200}\frac{\ln(1+cx) - cx/(1+cx)}{x[\ln(1+c) - c/(1+c)]}. \tag{9}$$

3.2 Data weighting

Because the density of points of the Hα RCs is different from that of H I RCs, we do not have the same radial weighting for Hα and H I velocities. To construct the mass models with the hybrid RCs, we optimized an equal radial weighting for both Hα and H I data points when fitting the RCs. It was arbitrarily decided to attribute the same total weight (the weight of a point being the inverse of its uncertainty) to the Hα and to the H I data sets in order to have a similar contribution to the fit from inner and outer regions. Uncorrelated Hα velocities are generally more numerous and have usually larger uncertainties than H I measurements. It is therefore

[2]The Groningen Image Processing System.

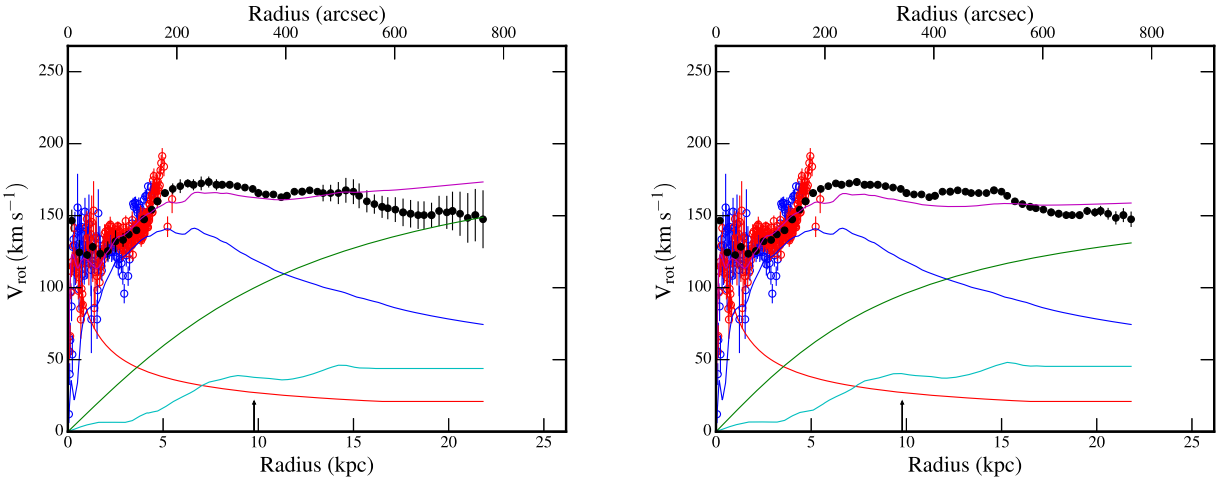

Figure 1. Example of mass model using *ISO* (BFM) with the hybrid RC of a galaxy UGC 11597. Left-hand panel corresponds to the model without optimizing the same weight of Hα and H I points. The right-hand panel shows the model after applying the same weight for the Hα and H I points. For each panel, the open blue and red circles corresponds, respectively, to the approaching and receding points of the Hα RC, the full black dots are the H I RC. The blue, red, cyan, and green lines correspond, respectively, to the disc, bulge, gas, and DM halo components. The magenta line is the model of the fit. The vertical arrow represents the isophotal radius R_{25} of the galaxy in kpc.

necessary to normalize the uncertainties. We made the choice not to modify the Hα uncertainties and to redistribute the new weights on the H I data only. We therefore compute new H I uncertainties as follows:

$$e_{n\mathrm{H\,I},i} = e_{\mathrm{H\,I},i} \left[\frac{\sum_{j=1}^{n} \left(1/e_{\mathrm{H\,I},j}\right)}{\sum_{k=1}^{m} \left(1/e_{\mathrm{H}\alpha,k}\right)} \right], \quad (10)$$

where $e_{n\mathrm{H\,I},i}$ is the new H I uncertainty for the ith point, $e_{\mathrm{H\,I},j}$ and $e_{\mathrm{H}\alpha,k}$ are the H I and Hα actual uncertainties, respectively, for individual points. This method accounts for the different error bars but also for the different sampling rate between Hα and H I RCs and allows the model to describe the hybrid RCs in the inner and outer regions using optimized uncertainties for the rotational velocities. Note that when we construct the mass model with the hybrid RCs without optimizing the weights, the model does not fit well the outer parts of the RCs where the H I points are, because of their smaller spatial sampling (see Fig. 1).

3.3 Mass-to-light ratios

The mass models are built using the same fitting procedures as used in Korsaga et al. (2018). We use two techniques for *ISO* and NFW models: (i) the best-fitting model (hereafter BFM) with a minimum χ^2 value, for which, all the parameters are free. This leads to three (or four if presence of a bulge) free parameters for both *ISO* (r_0, ρ_0, and $\mathrm{M/L_{disc}}$, and $\mathrm{M/L_{bulge}}$ if presence of a bulge) and NFW (c, V_{200}, and $\mathrm{M/L_{disc}}$, and $\mathrm{M/L_{bulge}}$ if presence of a bulge); (ii) the fixed M/L ratio for which the value of M/L is derived from the $(W_1 - W_2)$ colour described in Section 2.2. In this case, the M/L is considered as a fixed parameter, which leaves us with two free parameters for both *ISO* (r_0 and ρ_0) and NFW (c and V_{200}). For this technique, the same value of M/L for the disc and the bulge is used because the spectrophotometric models do not allow to disentangle them. We also look at the maximum disc model (hereafter MDM) for the *ISO* models. This technique allows to maximize the baryonic contribution by minimizing the DM haloes contribution. The M/L value for the MDM is constrained to be higher than the M/L value of the BFM and the χ^2 is allowed to increase up to 1.3 times the minimal χ^2 value. Minimal values were imposed to the parameters to avoid some unphysical values; $\mathrm{M/L} = 0.1\ \mathrm{M_\odot/L_\odot}$, $r_0 = 0.5$ kpc and $c = 1$. The value $0.1\ \mathrm{M_\odot/L_\odot}$ is imposed as a minimum value because we do not find a value of M/L below $0.1\ \mathrm{M_\odot/L_\odot}$ when using the colour index to calculate the M/L shown in equation (1).

4 ANALYSIS OF THE MASS MODELS FOR INDIVIDUAL GALAXIES

Different data sets are being used to build the mass models of the galaxies from the GHASP sample. In previous papers, the mass distribution was first determined using Hα RCs with the stellar mass component (disc and bulge, if presence of a bulge). We looked at the differences when using the mid-IR W_1 photometric band (Korsaga et al. 2018) versus the optical R_c-band (Korsaga et al. 2019) data. Since we found in those studies that it was better to use mid-IR photometry, *WISE* W_1 data will be used in the rest of this study.

In this paper, we also add the contribution of the neutral gas component, which was not considered in previous papers (Korsaga et al. 2018, 2019), to the total circular velocity. This is mainly important for the later types which are more gas rich. We first use Hα RCs. Secondly, we use the H I RCs. Finally we use hybrid (Hα/H I) extended RCs with the stellar and the neutral gas contributions. The different models and methods used for the three data sets are given for the whole sample in Appendix A. An example of mass models for the galaxy UGC 6537 is shown in Fig. 2.

In this section, we review the main properties and conclusions we can draw from a detailed examination of individual RC and mass models. We discuss the shape and the flat parts of the RCs; the consequence of limited spatial coverage and spatial resolution in H I RCs; the behaviour of intermediate and outer RCs; the constraints driven by the M/L estimates using stellar population models and we conclude by discussing the galaxies with a bar and with a bulge.

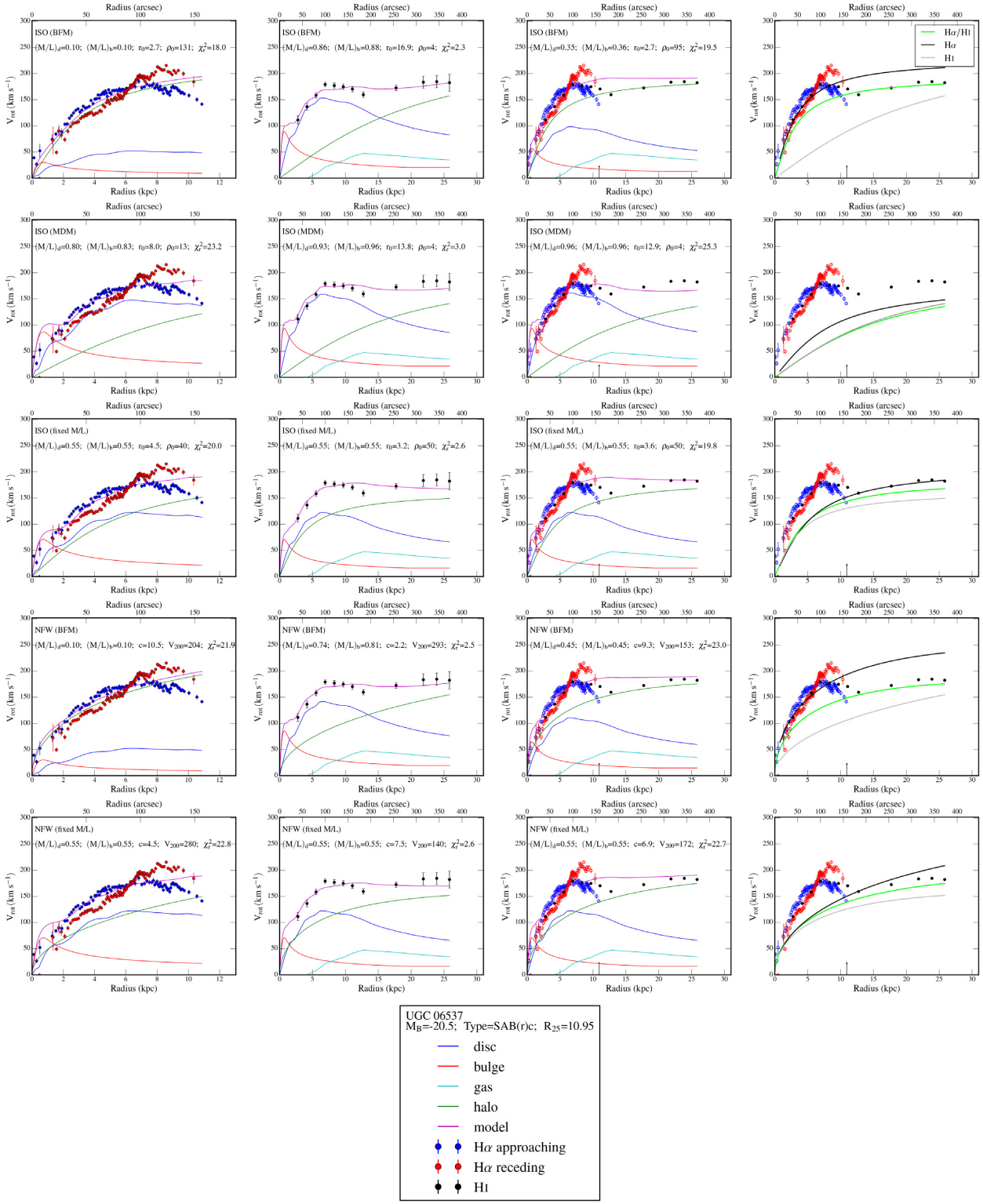

Figure 2. Example of mass models for the galaxy UGC 6537. Lines 1–3: *ISO* sphere density profiles. Lines 4–5: NFW density profiles. First line: BFM. Second line: MDM. Third line: Mass-to-Light ratio M/L fixed using W_1 - W_2 colour. Fourth line: BFM. Fifth line: Mass-to-Light ratio M/L fixed using $W_1 - W_2$ colour. The name of the galaxy, its *B*-band absolute magnitude, morphological type, and optical radius in kpc have been indicated in the inset located at line 6. Column 1: Models using H α RCs and no neutral gas distribution. Column 2: Models using H I RCs. Column 3: Models using the hybrid H α/H I RCs. Column 4: We show the halo derived from the different RCs. The vertical arrow represents the isophotal radius R_{25} of the galaxy in kpc. For each model, the fitted parameters and the reduced χ^2 have been indicated in each sub-panel.

4.1 Shapes of H α and H I rotation curves

As expected, H I RCs are more extended than H α ones for 30/31 galaxies. In some cases, the H I RC even starts when the H α one ends (e.g. UGC 10075, UGC 11670, UGC 11852, UGC 11914). In those cases, the combination of H α and H I RCs is really mandatory. H α RCs display larger wiggles, asymmetries when comparing both sides, and other irregularities, than H I RCs. In the inner regions, H α RCs are more affected than H I RCs by non-circular motions due to bars and by larger central rotation velocity peaks due to the bulge components (e.g. UGC 11670). Outside the central kpc where the bar and the bulge usually dominate, H α RCs display larger wiggles than H I RCs due to the presence of warm star-forming H II regions, expanding bubbles/supernova remnants and gas acceleration/deceleration when crossing spiral arms (e.g. UGC 1913, 6537).

4.2 Flat parts of the rotation curves

The flat part of the RCs is clearly reached in H α for 16/31 galaxies (UGC 1913, 2080, 2800, 4284, 4325, 4499, 5251, 5414, 6778, 7323, 8490, 9179, 9649, 10359, 11597, 11852). In some cases, the flat part in H α does not seem to be reached while in fact it is, when comparing to the H I RC (UGC 6778, 8490, 10359, 11597, 11852). This brings to 20/31 the number of galaxies for which the flat part is reached even if the H α data alone do not allow to estimate this fraction. In other cases, we can estimate that the flat part is reached even if the RC is still very slowly rising (e.g. UGC 3734).

14/31 H α RCs do not reach the optical radius (UGC 1913, 2800, 4325, 5251, 5253, 7766, 8334, 8490, 10075, 11012, 11597, 11670, 11852, 11914) meaning that the other 17/31 reach it. Nevertheless only 3/31 H α RCs do not reach 0.72 R_{25} (UGC 1913, 8334, 11597). Among the 17 H α RCs that reach the optical radius, only 4/17 do not reach the flat part. Surprisingly, the H I RC of UGC 11914, which is an early-type with its H I in a ring, does not reach the optical radius while the Im galaxy UGC 5414 barely reached it.

When the flat part is not reached within the optical disc, the halo parameters are generally not well modelled using the H α data alone (e.g. UGC 2800, 4284, 4325, 4499, 6537, 6778, 8490, 11012, 11597, 11852). Exceptions to this rule are noted when a minimum disc model (M/L = 0.1) is used to fit all the data sets (e.g. UGC 1913, 11670).

Even when the flat part is reached or almost reached in H α, the halo parameters strongly depend on the extension of this flat part; a small variation of the stellar M/L may considerably change the halo parameters in the case of the H α data alone while they do not impact so much the halo parameters in the case of the H I or hybrid RCs (e.g. UGC 2080, 3734, 4284, 4499, 6778, 9858, 9969, 12754).

When the flat part is never reached, neither in H α nor in H I, the halo parameters obtained using the H α RCs differ from those obtained with H I or hybrid RCs, which provides consistent results (e.g. UGC 5251, 8490, 10359, 11597, 11852).

In summary, the flat part of the RC as well as the optical radius are reached in H α for two-thirds of the sample even if it is sometimes barely reached. If the flat part is not reached within the optical disc, the halo parameters are poorly constrained using the H α data alone but if the flat part is almost reached or even reached in H α, the halo parameters strongly depend on the extension of this flat part. When the flat part is never reached, neither in H α nor in H I, the halo parameters are similar using H I or hybrid RCs but are different from those obtained using H α RCs.

4.3 Spatial coverage and spatial resolution in the galaxy inner regions

The M/L of the stellar component (disc and/or bulge) and the halo parameters are poorly estimated in H I when the H I RCs do not provide a sufficient spatial coverage or when the spatial resolution is too low to correctly sample the inner 0 to $\sim$3 kpc of the RC (e.g. UGC 9858, 10470, 11914, 12754). In some cases, the H α models give an RC that is less steep than the one fitted by the model when H I data are missing in the inner regions (e.g. UGC 9969, 10075) and in those cases, the M/L deduced from the H I data alone are obviously overestimated by the model.

The stellar M/L components could be identical using the three sets of data just by chance when the central density increases to compensate the core (e.g. UGC 1913, 2800, 2855, 4499, 9858, 10359, 10470, 11597, 11670). Even when the three data sets probe about the same spatial extension, i.e. when $R_{\rm H\,I} \leq 1.2$–$1.4\ R_{\rm H\,\alpha}$, the halo parameters may differ due to the difference of slope in the inner regions (e.g. UGC 2855, 7323, 9858, 11914, 12754).

When the baryonic components (disc alone or bulge plus disc) dominate the optical RC, the halo parameters are difficult to estimate from the H α data alone; it could be overestimated for the *ISO* model (e.g. UGC 2080, 2800, 4284, 6778, 7323, 11012) or at the opposite underestimated for the NFW model (e.g. UGC 2080). When the RC is slightly rising both in H α and H I, the NFW DM profiles provide a poorer fit to the data than the *ISO* ones.

In summary, the M/L of the stellar component and the halo parameters are weakly estimated in H I when the H I RC does not provide sufficient constraints in the inner regions. As a consequence, the halo parameters depend on the inner slope of the RC. The only way to estimate them correctly is to use high-resolution H α RC. If the baryonic components dominate the optical RC, the halo parameters tend to be over-/underestimated for the *ISO*/NFW models, respectively.

4.4 Intermediate and outer galaxy regions

As expected, H I RCs extend further out than H α RCs for 30/31 galaxies at the last measured velocity point. For a third of the sample H I RCs are 1–1.5 times more extended than the H α RCs; for another third of the sample the H I RCs are more than 2.5 times more extended than the H α RCs. The mean, median and standard deviation of the ratio between the H I and H α radii, is 2.4, 2.1, and 1.5, respectively. These values are similar for early-type galaxies (i.e. galaxies below the median morphological type $t = 6$), for which we get, respectively, 2.5, 1.9, and 1.8 and for late-type galaxies (i.e. galaxies above this median), for which we measured 2.3, 2.1, and 1.2, respectively. We reach the same conclusion when studying this ratio as a function of the stellar mass and luminosity. This indicates that, on average, the H I RC extension is correlated to the H α ones, regardless of the morphological type, the stellar mass or the luminosity of the galaxies.

Among the 31 galaxies, 12 RCs show a decrease (UGC 1913, 2080, 2855, 4284, 5253, 6778, 8334, 9179, 9969, 11597, 11852, 12754), 10 are flat (UGC 3574, 4325, 6537, 7766, 8490, 9858, 10075, 11012, 11670, 11914), and 9 are rising (UGC 2800, 3734, 4499, 5251, 5414, 7323, 9649, 10359, 10470). The case of UGC 11914 is particularly interesting: it shows a decreasing H α RC and increasing H I RC and when mixing both sets of data in the hybrid data set, the RC becomes finally flat. None of the H I decreasing RCs show a Keplerian decline. None of the H α RCs is decreasing except UGC 11914 mentioned just above and UGC 9858 that exhibits 3

velocity measurements much lower than the H I velocity points at the same radius; 7/31 are flat (UGC 2855, 3574, 5253, 8334, 9969, 10470, 11670). Among those seven flat H I RCs, four are finally decreasing in the outer regions in H I.

Outside the first kpc, usually smoothed out by beam smearing effects in H I (except in a few cases e.g. UGC 10470), H I and H α RC match fairly well up to the optical radius or up to the last H α data points in the case where the H α RC does not reach the optical radius (e.g. UGC 11597). For very extended and decreasing H I RCs, the halo parameters deduced from extended H α data alone match those deduced from H I and hybrid RCs, essentially because galaxies with decreasing RCs are massive galaxies showing a fast-rising inner RC, even in H I (e.g. 5253, 8334). For solid body RC or even for rising RCs, when the H I RC does not extent further out than the H α RC, the halo parameters match fairly well regardless of the model or of the data set (e.g. 5414, 7323).

In summary, the H I RCs presented here are on average a little more than twice as extended than the H α ones, nevertheless with a large standard deviation around this median value. In addition, this H I over H α radius ratio do not strongly depend neither on the morphological type, the stellar mass, nor on the luminosity. About a third of the galaxies show H I decreasing RCs, another third flat ones and the last third increasing ones. Nevertheless, none the H α RCs is decreasing (except maybe UGC 3574). At radii for which H I RCs are not affected by beam smearing effects, H I and H α RCs match reasonably well up to the last H α data points if those are within the optical radius. The three data sets lead to similar halo parameters in two cases: for large galaxies displaying decreasing H I RCs and for rising RCs when the three data sets provide RCs having about the same extension.

4.5 M/L computed from the colour index

When the M/L is fixed by the colour index, the stellar RC (disc and/or bulge) is higher than the H α RC at least within the first kpc for 10/31 galaxies (UGC 1913, 2800, 2855, 3734, 5253, 6537, 8334, 10470, 11597, 11670). When H I RCs are used, this happens for 13/31 galaxies (UGC 1913, 2800, 2855, 3734, 5251, 5253, 5414, 6537, 8334, 9858, 11597, 11670, 11852). It should be noted that the lack of constraints in H I results in the stellar RC does not overestimate the H I RC while it does in H α (UGC 10470). This means that for about 2/3 of our sample of 31 galaxies, M/L fixed by the colour indices provides a possible solution for mass modelling and this is not significantly different in H α or H I.

The M/L fixed by the colour index gives larger values than those computed using *ISO* MDM for 11/31 galaxies when using H α RCs (UGC 1913, 2800, 2855, 4325, 4499, 5251, 5253, 8334, 10470, 11597, 11670) and for 15/31 galaxies when using H I RCs (UGC 1913, 2800, 2855, 4325, 4499, 5251, 5414, 7323, 7766, 8334, 9858, 10359, 11597, 11670, 11914) or even 17/31 galaxies if we consider UGC 5253 and UGC 10470 for which H I is missing in the first 5 and 3 kpc, respectively, and thus unable to constrain the disc.

In order to quantify the disagreement between the RC and stellar component that can exceed the RC when the M/L ratio is fixed using the $W_1 - W_2$ colour indices, we compute $V_{\rm max}^{\rm d+b}$, the maximum of the stellar rotation velocity, disc (d) plus bulge (b) summed quadratically, and we compare it to the value of the RC at the same radius $V_{\rm max}^{\rm RC}$. The stellar (disc + bulge) component has a rotation velocity higher than the RC (i.e. $\Delta V = V_{\rm max}^{\rm d+b} - V_{\rm max}^{\rm RC} > 0$ km s^{-1}) for 6/31 galaxies. On the one hand, M/L grows as $W_1 - W_2$ decreases (see relation 1) and low values of $W_1 - W_2$ might overestimate the M/L; thus relation (1) might become inappropriate (Michelle Cluver, private communication). We check that the $\Delta V > 0$ km s^{-1} values for these six galaxies are not correlated to low colour indices $W_1 - W_2$. For our sample, $W_1 - W_2$ ranges from -0.08 to 0.21 with a median value of 0.05 and six galaxies have $W_1 - W_2 < 0$ (UGC 3574, 3734, 4284, 4325, 5414, 9649). Only one galaxy among those six has $\Delta V > 0$ (UGC 3734). On the other hand, the colour distribution of the six galaxies having $\Delta V > 0$ km s^{-1} is the same than the one the 25 others having $\Delta V < 0$ km s^{-1}. Finally, we find no correlation between ΔV and any other parameters except maybe with the galactic absorption Ag. Indeed, among the five galaxies having the largest Ag, four of them have the four lowest ΔV of the sample ($\Delta V < -50$ km s^{-1} for UGC 2855, 3734, 11597, 11670). This might suggest that M/L are too large for those galaxies, i.e. $W_1 - W_2$ too low, due to a difficult galactic absorption correction at low galactic latitude.

In summary, the M/L values estimated from the colour index overestimate the disc component in one-third and one-half of the cases using H α and H I RCs, respectively.

4.6 Bulgy galaxies

Twenty galaxies among the 31 have a bulge component (see Section 2.2). Constrained by the physics of stellar evolution, we force the M/L of the bulge to be larger or at minimum equal to the M/L of the disc. This has some impacts on the mass distribution since the bulge component dominates the very inner central regions and furthermore minimizes the M/L of the disc, the halo central density and increases the halo core radius. Regarding the difference of inner slope in H α and H I RCs and regarding the spatial coverage at both wavelengths this have different consequences. If the H I spatial coverage is not good in the central regions, the M/L of the bulge could be larger with respect to the constraints imposed by the high spatial coverage of H α RC (e.g. UGC 4284, 6537, 9179, 9969, 10470, 11852, 11914, 12754) or alternatively smaller (e.g. UGC 3574, 6778, 9858, 10359, 11670). This can also be seen for galaxies with an important bulge component ($L_{\rm bulge}/L_{\rm disc} > 0.2$; UGC 3574, 3734, 6778, 9858, 10470, 11852) or not ($L_{\rm bulge}/L_{\rm disc} < 0.2$; e.g. UCG 9969, 10359). In addition, due to beam smearing smoothing, H α RCs are usually steeper than the H I RCs in the inner regions, thus the bulges tend to have lower M/L with H I data than with H α or hybrid data sets (e.g. UGC 2080, 3574, 5251, 6778, 7766, 9858).

Regarding the halo of bulgy galaxies, the halo shape at large radius is almost the same regardless of the data sets but this could be just by chance. Indeed, due to the lack of constraint in the central H I RC, the high M/L for the bulge observed in the case of steep H α RC becomes smaller using lower resolution H I RC but this effect is compensated by a larger central halo density without significantly changing the core radius (e.g. UGC 3574, 7766).

In summary, the presence of a bulge usually leads to lower both the stellar M/L and the halo central mass density, and to increase the halo core radius. Nevertheless, it could lead to very different trends if the inner RC is affected by beam smearing or low spatial coverage because the bulge component can thus be, respectively, lower or higher than what it should be.

4.7 Barred galaxies

Twenty-two galaxies among the 31 have a bar which is consistent with the expected ratio in the MIR. Due to non-circular motions, when the bar is aligned with the major axis, the slope of the RC is artificially lowered by radial motions along the bar while, on the

Table 2. Median, 16th, and 84th percentiles values of the M/L for *ISO* models.

	M/L ($M_\odot/L_\odot$) (1)	Median (2)	16th (3)	84th (4)
	BFM	0.13	0.1	0.55
H α	MDM	0.51	0.22	1.02
	Fixed M/L	0.50	0.28	0.77
	BFM	0.26	0.1	0.96
H I	MDM	0.49	0.15	1.36
	Fixed M/L	0.50	0.28	0.77
	BFM	0.35	0.1	1.37
H α/H I	MDM	0.55	0.19	1.37
	Fixed M/L	0.50	0.28	0.77

contrary, this slope increases when the bar is aligned with the minor axis (Dicaire et al. 2008; Randriamampandry et al. 2015). If the bar ranges around the median of these two axes, the bar does not affect the slope of the RC that traces in this case only circular motions. Sixteen galaxies among 22 have their bar located at 20° or less from the major axis and 2 have their bar located at 25° or less from the minor axis; the 4 others range in between.

We verify this effect by comparing the inner slopes of the RC and of the stellar RC computed from the surface density profile distribution. Among the 16 having a bar within 20° from the major axis, the slope of the stellar RC overestimates the H α RC for 10 galaxies (UGC 1913, 2800, 2855, 4284, 4499, 5251, 6537, 6778, 7323, 9969, 10470). For six cases they overestimate one side of the RC only. This is even worse for H I RCs: the stellar RCs overestimate the H I RC for 13 cases over 16. None of the 15 remaining galaxies shows a stellar RC overestimating the H α RC. This could be true as well for the H I RC, nevertheless the inner constraints are often not strong enough to discard some cases. Beam smearing observed on H I RCs has the same effect than a bar aligned with the major axis or diminish the effect of a bar aligned with the minor axis while a lack of coverage in the inner RC does not allow to observe the shape induced by the bar.

In summary, the presence of a bar changes the inner shape of RCs that are better constrained with H α or hybrid RCs than with H I RCs.

5 RESULTS

In the previous section, we reviewed the main properties of individual cases. In this section we study the global properties. The aim of using different data sets to construct the mass distribution is to study how the DM halo parameters may vary when including the neutral gas component or using a hybrid RC or only H α or only H I kinematics. Median values and the 16th and 84th percentiles[3] of M/L (Table 2) and halo parameters (Table 3) are provided for various models and data sets.

5.1 Mass models − H α + stars

The mass distribution is determined by combining the H α RCs with the W_1-band photometric data for the stellar component (Korsaga et al. 2018). The distribution of the baryonic matter is characterized by the M/L ratios (Table 2). For the *ISO* model, we find median values of 0.13, 0.51, and 0.50 $M_\odot/L_\odot$, respectively, for BFM, MDM, and fixed M/L. These values are consistent with Lelli et al. (2016), who found M/L minimum and maximum values of $\sim$ 0.2 and $\sim$0.7 $M_\odot/L_\odot$, respectively. The median value of the fixed M/L (0.5 $M_\odot/L_\odot$) is similar to the fixed M/L assumed by Lelli et al. (2016) and Richards et al. (2018), who used 3.6 µm photometric data. The M/L value obtained using the MDM model is $\sim$4 times higher than the value of the BFM.

For the *ISO* model, we study how the DM parameters (r_0, ρ_0) are distributed. The general relation between ρ_0 in 10^{-3} $M_\odot$ pc^{-3} and r_0 in kpc is

$$\log\ \rho_0 = (a \pm \delta a)\ \log\ r_0 + (b \pm \delta b), \quad (11)$$

where the parameters a, δa, b, and δb are shown in Table 4.

Before doing the study, we exclude galaxies for which DM is not needed to build the mass models, the RCs are well modelled with only the contribution of the baryonic matter when using the *ISO* MDM (these galaxies are marked with an asterisk in Table 1). We find an anticorrelation between the two parameters where smaller r_0 tend to have higher ρ_0, which is in agreement with previous studies made by Kormendy & Freeman (2004), Randriamampandry & Carignan (2014). However, when looking at the relation between the DM parameters and the luminosity of the galaxies, we find no clear correlation between r_0 and the luminosity, which is not in agreement with Kormendy & Freeman (2004) and Randriamampandry & Carignan (2014). As we already explained in Korsaga et al. (2019), the difference between our results and the previous authors is due to the fact that their studies were based mostly on late-type galaxies (mostly composed of bulge-poor galaxies), while we cover all morphological types.

For NFW models, we can look at the relation between the concentration parameter c and the velocity at the virial radius (V_{200}). Before doing the fit, we exclude galaxies for which $c \leq 1$ and $V_{200} \geq 500$ km s^{-1} because these values are non-physical in the CDM context (de Blok et al. 2008). We find that low-mass haloes are more concentrated. We find a median value of $c = 9.0 \pm 11.5$ which is close to the value of $c = 10$ found by Bullock et al. (2001) for BFM and $c = 6.3 \pm 8.2$ for fixed M/L, meaning that the halo appears more concentrated for BFM than for fixed M/L. The general relation between c and V_{200} is

$$\log\ c = (a \pm \delta a)\ \log\ V_{200} + (b \pm \delta b), \quad (12)$$

where the parameters a, δa, b, and δb are shown in Table 4.

5.2 Mass models − H α + stars and gas

The mass models are constructed in this case using H α RCs, W_1-band photometric data and the neutral gas component from radio H I observations. The reason for including the gas component is to check if the presence of this component could change the distribution of the luminous and DM in galaxies. For the *ISO* models, we find median values of M/L equal to 0.14, 0.54, and 0.50 $M_\odot/L_\odot$, respectively, for BFM, MDM, and fixed M/L. We see that despite a slightly higher value for the BFM and MDM (0.14 versus 0.13 and 0.54 versus 0.51), the M/L values for fixed M/L are the same with or without considering the gas component. This may not be completely surprising since the M/L is a parameter for the stellar disc, which is in the inner parts while H I is more abundant in the outer parts.

Similarly, the relation between ρ_0 and r_0 and between the DM parameters and the luminosity of the galaxies are very similar. This is why, in the rest of the paper, we will not discuss those

[3]For a normal distribution, observations within one standard deviation σ to either side of the mean m accounts for about 68.3 per cent of the distribution; $-\sigma$ represents the $\sim$16th percentile and $+\sigma$, the $\sim$84th percentile.

Table 3. Median, 16th, and 84th percentiles values of the DM halo parameters for *ISO* and NFW models.

		Median (1)	16th (2)	84th (3)
Hα: r_0 (kpc) (*ISO*)	BFM	2.44	1.77	4.16
	MDM	4.33	2.03	7.63
	Fixed M/L	3.74	1.56	17.16
Hα/H I: r_0 (kpc) (*ISO*)	BFM	2.71	1.39	5.55
	MDM	3.81	1.75	7.41
	Fixed M/L	2.73	1.40	7.59
H I: r_0 (kpc) (*ISO*)	BFM	2.70	1.46	5.69
	MDM	4.06	1.89	6.59
	Fixed M/L	3.34	1.70	8.74
Hα: ρ_0 ($\times 10^{-3}$ $M_\odot$ pc^{-3}) (*ISO*)	BFM	110.00	26.00	171.31
	MDM	31.00	13.23	114.24
	Fixed M/L	40.90	14.49	270.14
Hα/H I: ρ_0 ($\times 10^{-3}$ $M_\odot$ pc^{-3}) (*ISO*)	BFM	54.54	14.55	169.31
	MDM	21.79	5.56	83.44
	Fixed M/L	34.61	10.79	299.35
H I: ρ_0 ($\times 10^{-3}$ $M_\odot$ pc^{-3}) (*ISO*)	BFM	53.09	13.23	145.98
	MDM	30.79	9.85	92.97
	Fixed M/L	30.77	6.82	137.84
Hα: c (NFW)	BFM	8.97	2.77	25.84
	Fixed M/L	6.32	2.04	18.39
Hα/H I: c (NFW)	BFM	12.23	4.61	19.95
	Fixed M/L	10.45	5.46	19.14
H I: c (NFW)	BFM	9.86	2.61	25.09
	Fixed M/L	9.57	3.68	21.68
Hα: V_{200} (km s^{-1}) (NFW)	BFM	187.5	114.19	460.99
	Fixed M/L	211.59	76.84	479.25
Hα/H I: V_{200} (km s^{-1}) (NFW)	BFM	120.65	85.45	168.03
	Fixed M/L	128.63	96.59	161.62
H I: V_{200} (km s^{-1}) (NFW)	BFM	118.18	82.44	343.21
	Fixed M/L	116.48	74.54	188.52

models anymore. As for the NFW models, we find slightly more concentrated haloes with the median values of the concentration c equal to 9.4 ± 9.1 and 7.8 ± 10.9, respectively, for BFM and fixed M/L compared to what found using Hα and stars.

5.3 Mass models − hybrid Hα/H I + stars and gas

It is well known that H I RCs are well suited to study DM in the outer parts of galaxies. However, mass models parameters are very sensitive not only in the outer regions but also to the exact velocity

Table 4. Relation between the DM halo parameters for *ISO* and NFW models.

		a	δa	b	δb
Hα: ρ_0 versus r_0 (*ISO*)	BFM	−1.47	0.22	−0.45	0.11
	MDM	−1.45	0.22	−0.56	0.15
	Fixed M/L	−1.10	0.14	−0.59	0.11
Hα/H I: ρ_0 versus r_0 (*ISO*)	BFM	−1.45	0.16	−0.61	0.08
	MDM	−1.32	0.22	−0.88	0.15
	Fixed M/L	−1.78	0.16	−0.48	0.09
H I: ρ_0 versus r_0 (*ISO*)	BFM	−1.53	0.17	−0.56	0.09
	MDM	−1.54	0.18	−0.62	0.12
	Fixed M/L	−1.74	0.12	−0.47	0.09
Hα: c versus V_{200} (NFW)	BFM	−1.24	0.16	+3.73	0.38
	Fixed M/L	−0.77	0.22	+2.53	0.51
Hα/H I: c versus V_{200} (NFW)	BFM	−1.17	0.22	+3.48	0.47
	Fixed M/L	−1.07	0.38	+3.24	0.80
H I: c versus V_{200} (NFW)	BFM	−1.22	0.19	+3.58	0.42
	Fixed M/L	−0.93	0.25	+2.89	0.52

gradient in the inner parts of the RCs (Blais-Ouellette et al. 2001), where the H I data can be affected by beam smearing. Therefore, the best combination is to use the high spatial resolution H α RC which probes the inner regions and extends it with the H I RC in the outer parts.

To construct the mass models, we use those hybrid RCs, W_1-band photometric data, and the neutral gas component from radio H I observations. Using the hybrid RCs will allow us to see how the DM is distributed in the inner and outer regions of galaxies and also to compare the results with those obtained using only H α (Section 5.1) and only H I (Section 5.4) kinematics. We find median values of the baryonic M/L ratio equal to 0.35, 0.55, and 0.5 $M_\odot/L_\odot$ for BFM, MDM, and fixed M/L, respectively. Naturally, the fixed M/L value will always remain the same. While the values of M/L using the MDM are very similar ($\sim$1.1 times larger) those for the BFM are around twice as large as when using only the H α kinematics.

For the NFW models, the median value of the concentration parameter c is equal to 12.2 ± 7.7 and 10.5 ± 6.8 for BFM and fixed M/L, respectively. While between 30 per cent and 50 per cent higher than when using only the H α kinematics, these values are still in the range $10 \leq c \leq 20$ defined by Martinsson et al. (2013). The halo is more concentrated for BFM than for fixed M/L.

5.4 Mass models – H I + stars and gas

The mass models are constructed in this case using the 21cm H I RCs, the W_1-band photometry and the neutral gas component. Even, when it is already known that the H I RCs may suffer from beam smearing in their central parts, we decide to use these data as is in order to compare these results with what we find using only H α kinematics (Section 5.1) or the hybrid (H α/H I) RCs (Section 5.3). For the baryonic matter, we find median values of M/L corresponding to 0.26, 0.49, and 0.5 $M_\odot/L_\odot$ for BFM, MDM, and fixed M/L, respectively. Curiously, those values are closer to what was obtained using H α only than using the hybrid RCs. For the NFW model, we find as usual that galaxies with a low V_{200} tend to have a higher concentration. The median values of the concentration c is 9.9 ± 11.2 for BFM and 9.6 ± 9.0 for fixed M/L. Those values are intermediate between what was found for H α only and for the hybrid RCs.

A detailed comparison of the results for the different data sets is presented in Section 6.

6 DISCUSSION

In the first two papers of this series (Korsaga et al. 2018, 2019), we studied the different parameters of the mass models as a function of the photometric band used. The main aim of this paper is to compare the results of mass models, both for the luminous disc and for the DM halo components, using RCs derived from the four different data sets: 1a and b – using H α kinematics only including or excluding the contribution of the neutral gas component; 2 – using H I kinematics only; and 3 – using hybrid RCs combining the high spatial resolution optical data in the inner parts to the more extended radio data in the outer parts. We saw in the previous section that mass models using H α RCs including and excluding the H I gas component provide comparable disc M/L. Furthermore, in this discussion, we will not consider anymore the H α RCs including the H I component because, from a practical point of view, when the H I densities are available, the H I RC is available as well while, when H α RCs alone are used, this generally means that no H I data are available.

In this paper, with the 3 data sets mentioned above (1a, 2, and 3), we use 2 different halo shapes (*ISO* and NFW), 3 different methods (BFM, MDM, fixed-M/L), 4 free parameters per model for BFM and MDM (ρ_0 the central halo mass density, r_0 the halo core radius and the disc and bulge M/L ratios) for the 20 galaxies with a bulge, 3 free parameters per model for the 11 disc-only galaxies, and finally 2 or 3 free parameters for disc-only and bulge galaxies, respectively, for the fixed (by colour) M/L models. So, the number of free parameters to explore per galaxy ranges from 48 for disc-only galaxies to 66 for galaxies with a bulge. This is because of this huge number of free parameters that we force the M/L of the disc and of the bulge to be the same for the fixed M/L model.

Naturally, it is not possible to present here a systematic search of the whole parameter space. Instead, we tabulate some key median values and illustrate the most important relations in different plots. In this section, we study the relationships between the DM parameters of *ISO* and NFW models (Table 4 and Figs 3–6) and we discuss the values of those parameters (Table 3).

6.1 *ISO* models

For the *ISO* models, let us first concentrate on the first three rows of Table 4 and on Fig. 3. We see that the agreement is very good for the three data sets for the BFM, especially between the H α only and the H I only, as compared to the hybrid RCs. On the other hand, the best agreement is between H α and H I RCs for the MDM and hybrid RCs and H I for the fixed M/L models. Clearly, the relation between the parameters of the *ISO* model varies from one data set to the other depending on the fitting technique used. So, the relation between the parameters of the *ISO* functional form (ρ_0 and r_0) vary by $\sim$20 per cent and equation (11) becomes

$$\log \rho_0 = (-1.43 \pm 0.22) \log r_0 - (0.60 \pm 0.15). \quad (13)$$

Figs 4 and 5 explore the relations between the *ISO* DM parameters and the absolute galaxy luminosity M_B. There is no clear trend of those parameters as a function of the luminosity. There may however exist a trend with morphological types but a larger sample would be necessary to confirm this. This was already suggested in Korsaga et al. (2018, 2019).

Table 3 allows us to examine the physical values of the DM parameters. For *ISO* (r_0 and ρ_0), it can be seen that the three data sets give consistent estimates of the parameters with the BFM having the more concentrated haloes (2.4 ± 1.2 kpc and $110 \pm 73 \times 10^{-3}$ $M_\odot$ pc^{-3}), followed by the fixed M/L (3.7 ± 7.8 kpc and $41 \pm 128 \times 10^{-3}$ $M_\odot$ pc^{-3}), and finally, by the MDM (4.3 ± 2.8 kpc and $31 \pm 51 \times 10^{-3}$ $M_\odot$ pc^{-3}).[4] Naturally, the result for the MDM is expected by definition since maximizing the M/L necessarily minimizes the halo by pushing it out. Clearly, the differences between the fitting procedures are larger than between the different data sets. Galaxies that do not need a DM halo are not the same depending on the model and on the data set used. Since they are excluded from the analysis, this impacts the sample used to compute medians. Those galaxies have both low r_0 and ρ_0 values. We checked that including those galaxies to compute medians does not change the above trends.

[4]Values are given for H α RCs.

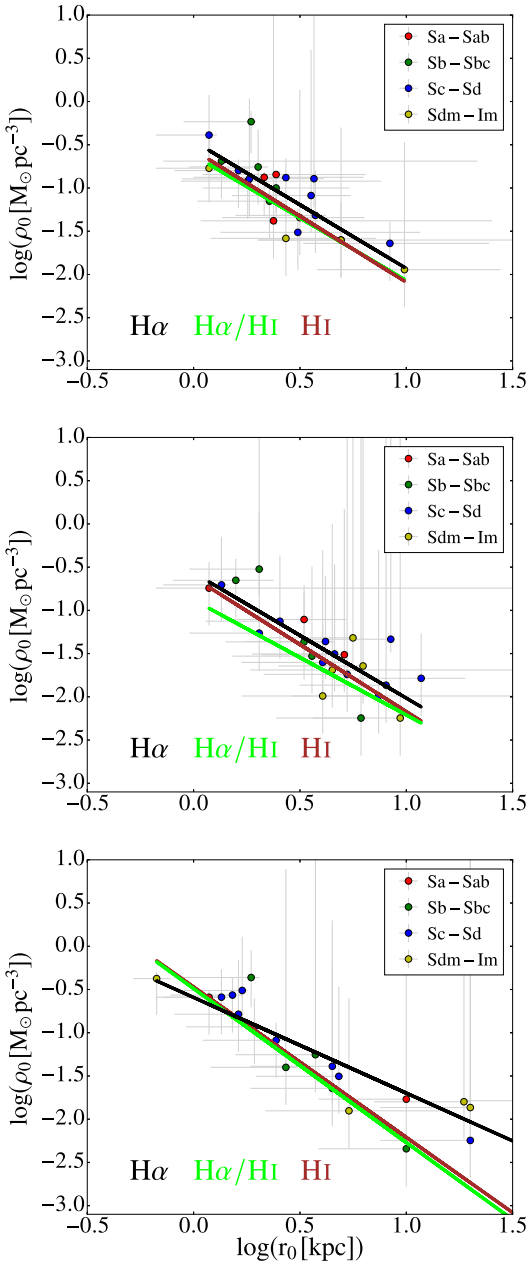

Figure 3. Central halo density as a function of halo core radius for *ISO* models. From top to bottom: BFM, MDM, and fixed M/L. The points are obtained using Hα RCs. The black line represents the fits of the points. The lime and red lines represent the fit found using the hybrid and H I RCs, respectively.

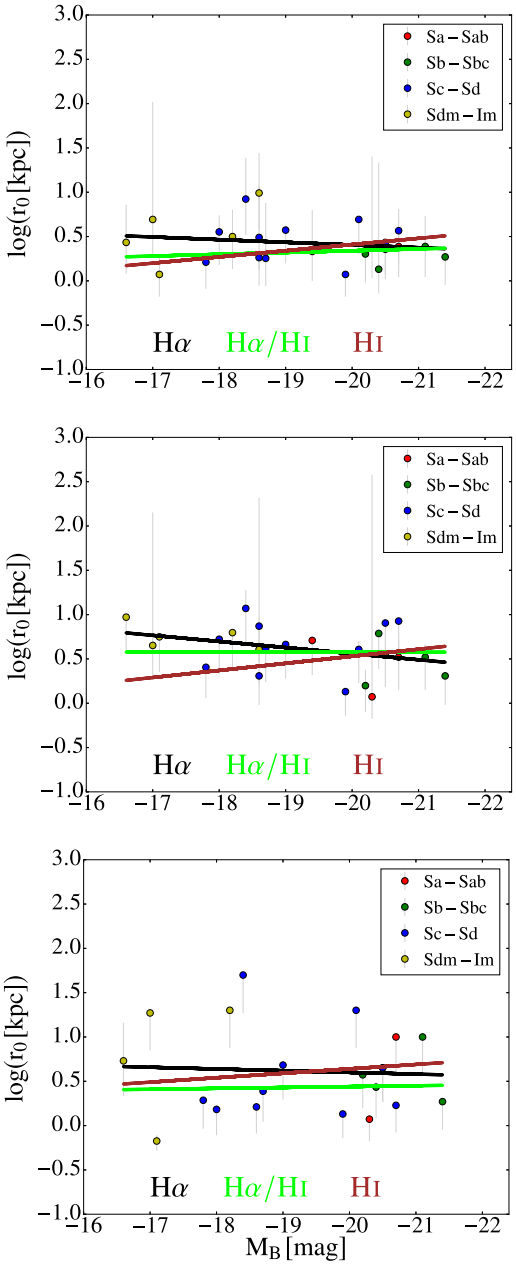

Figure 4. Halo core radius as a function of *B*-band absolute magnitude for *ISO* models. From top to bottom: BFM, MDM, and fixed M/L. Colours and symbols are similar as in Fig. 3.

6.2 NFW models

It is interesting to note in the last three rows of Table 4 and in Fig. 6, that the relation between the parameters of the NFW functional form (c and V_{200}) is less affected by either different data sets (Hα, H I, or hybrid) or fitting techniques (BFM or fixed M/L), which is quite different from the situation with *ISO* models. The parameters of the relation vary by less than 10 per cent and equation (12) becomes

$$\log\ c = (-1.07 \pm 0.19)\ \log\ V_{200} + (3.24 \pm 0.46). \qquad (14)$$

This suggests that Hα kinematics in the inner parts is sufficient to characterize a NFW halo. As for the value of the concentration parameter c, we get from all the data sets and fitting techniques $c \sim 10 \pm 2$, which is exactly the value found by Bullock et al. (2001), who did ΛCDM *N*-body simulations and had a statistical sample of $\sim$5000 haloes in the range 10^{11}–$10^{14}\,h^{-1}$ M$_\odot$. We observe in Section 5 that the haloes appear more concentrated for BFM than for fixed M/L, whatever the data set. In addition, the halo concentration parameter is the lowest for the Hα data set, it increases when including gas mass distribution, and still grows using the H I data set to reach the highest value for the hybrid RCs. Galaxies with critical values of c or V_{200}, which are excluded from the analysis, differ depending on the model and on the data set. Considering those galaxies in the analysis to keep a constant sample does not change the previous trends.

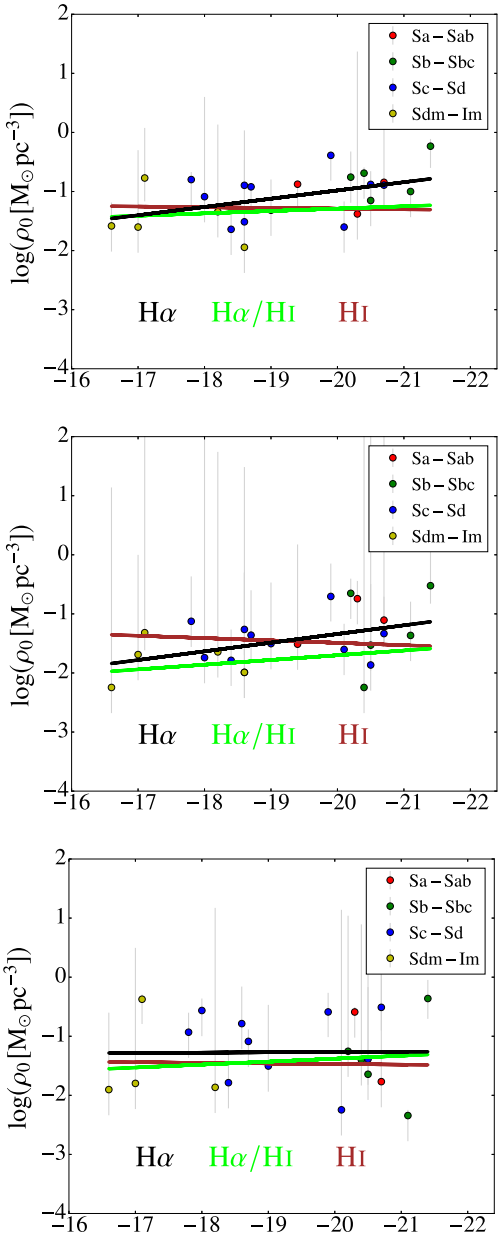

Figure 5. Central halo density as a function of *B*-band absolute magnitude for *ISO* models. From top to bottom: BFM, MDM, and fixed M/L. Colours and symbols are similar as in Fig. 3.

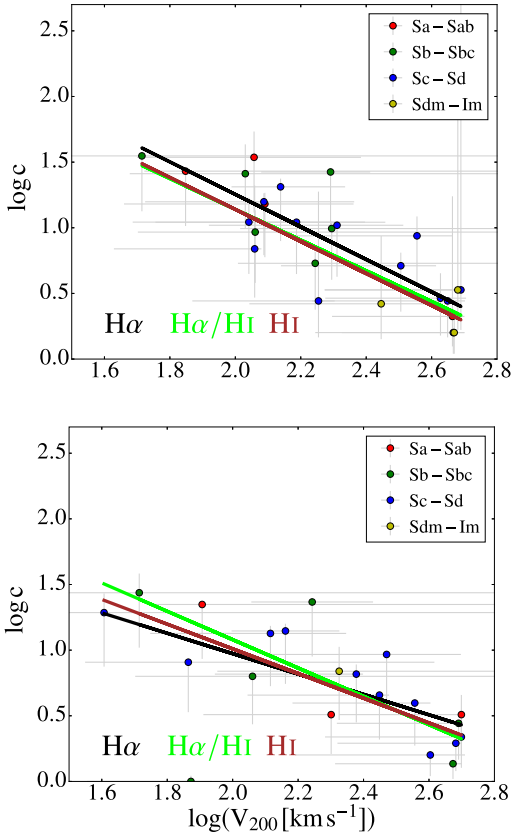

Figure 6. Concentration as a function of V_{200} for the NFW models: top for BFM and bottom for fixed M/L. Colours and symbols are similar as in Fig. 3.

Figs 7 and 8 show the variation of the NFW parameters (c and V_{200}) as a function of the luminosity (M_B). We can see that c is nearly constant. However, while V_{200} seems also to be constant when using only Hα kinematics, H I and hybrid RCs suggest that it increases with luminosity.

6.3 Shape of dark haloes within the optical disc

All the models are given in Appendix A to which must be added the example given in Fig. 2. It is interesting to look closely at the last column on the right in which we plot the Hα and H I kinematical data with the different fits for the halo components of the three data sets using the Hα, H I, and hybrid RCs. For 2/3 of the sample, the halo components are very similar while for the other 1/3, the Hα halo component is much less constrained than when using the H I or hybrid data. For the *ISO* (BFM) model, the contributions of the halo component derived from the Hα RCs generally exceed those derived from the H I data at large radii. In fact, the figures show that the *ISO* (BFM) halo velocities derived from Hα are higher than when derived from the H I data for about 58 per cent of the sample (UGC 2080, 2800, 3734, 4284, 4325, 4499, 6537, 6778, 8490, 9649, 9969, 10075, 10359, 10470, 11012, 11597, 11852, 12754). For the *ISO* (MDM) model, the Hα-derived halo contribution is more important than the H I-derived halo contribution for about 25 per cent of the sample (UGC 4284, 4325, 4499, 6778, 8490, 10359, 10470, 11012). For the *ISO* model with fixed M/L, $\sim$ 30 per cent of the sample (UGC 4284, 4325, 4499, 5253, 10359, 10470, 11012, 11852, 12754) present a halo contribution higher when derived from Hα data than from H I.

As for the NFW (BFM) model, the Hα-derived halo velocities are higher than the H I-derived contribution for about 40 per cent of the sample (UGC 2080, 4284, 4325, 6537, 6778, 7766, 8490, 9179, 10359, 10470, 11012, 11852, 12754). For the NFW model with fixed M/L, only $\sim$ 30 per cent of the sample (UGC 4284, 6537, 6778, 8490, 10359, 10470, 11012, 11852, 12754) present a higher Hα-derived halo contribution. From these numbers, we conclude that the DM halo models derived using the Hα RCs are overestimated and less constrained at large radii compared to those derived from H I data. The fraction of galaxies for which the Hα RCs are overestimated is $\sim$ 58 per cent for *ISO* (BFM), while only $\sim$ 40 per cent for NFW (BFM); this implies that the *ISO* model does not constrain the halo parameters as well as the NFW model. However, when using the fixed M/L technique,

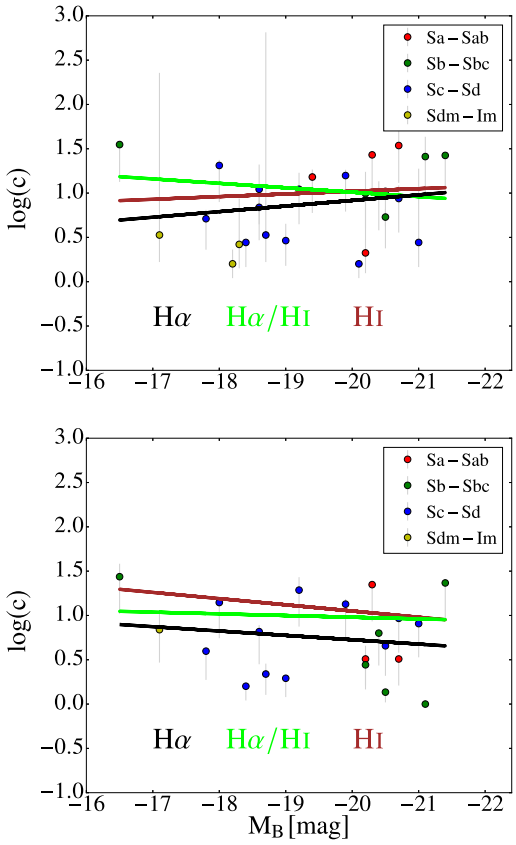

Figure 7. Concentration as a function of *B*-band absolute magnitude for the NFW models: top for BFM and bottom for fixed M/L. Colours and symbols are similar as in Fig. 3.

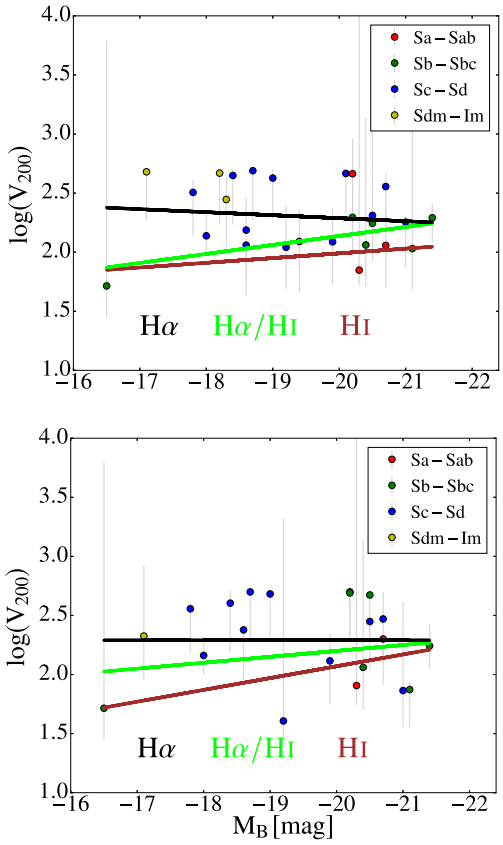

Figure 8. V_{200} as a function of *B*-band absolute magnitude for the NFW models: top for BFM and bottom for fixed M/L. Colours and symbols are similar as in Fig. 3.

$\sim$ 30 per cent of the sample galaxies present halo models that are not well constrained at large radii for both the *ISO* and NFW models. It should therefore be preferred to use the fixed M/L or the MDM technique to derive the halo models when using only Hα RCs.

6.4 Core or cusp?

One reason for using Hα RCs to constrain mass models is to study in details the inner DM density profiles. Indeed, Hα RCs are usually less affected by beam smearing than H I ones and therefore usually better trace the rising part of the RCs. One of the results obtained using Hα RCs in Korsaga et al. (2018) is that mass models with core haloes are favoured for their sample, i.e. *ISO* BFM provides lower reduced χ^2 values than NFW BFM on average. Thanks to the present data set, we can study the impact of the RC on this result. We made the comparison for each RC between *ISO* and NFW BFM reduced χ^2 values for all the 31 galaxies in our sample. We find that *ISO* (NFW) provides better fit to the data for 22 (9), 21 (10), and 17 (13) galaxies for Hα, hybrid, and H I RCs, respectively (the case of hybrid RCs is illustrated by Fig. 9). For one galaxy, the H I RC does not provide enough constraints to discriminate between *ISO* and NFW. Whatever the data set, we find that *ISO* is preferred to NFW (e.g. UGC 5251, UGC 8490, UGC 9179, see in Appendix A, Figs A10, A17, and A18, respectively). Nevertheless, the agreement between Hα and hybrid RCs is very good, whereas the result is less strong using H I RCs alone. This shows that the use of Hα RCs has to be favoured over H I ones, and that hybrid RCs provides fair constraints for this specific aim.

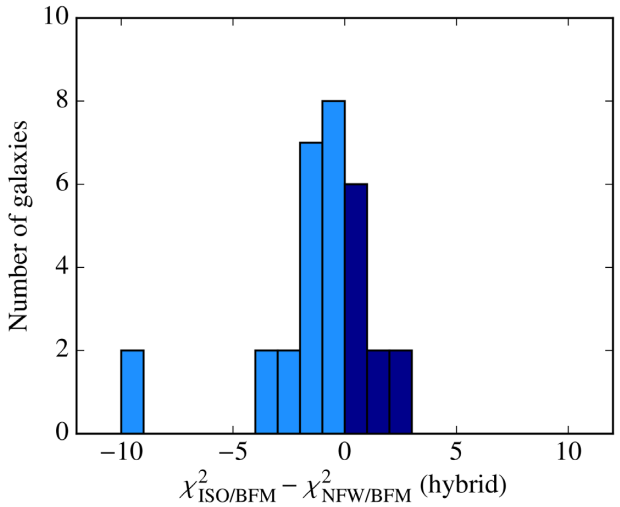

Figure 9. Distribution of the reduced χ^2 difference between *ISO* and NFW models. The whole sample of 31 hybrid RCs has been used. BFM χ^2 for *ISO* and NFW models are, respectively, in light and dark blue blue.

6.5 Halo masses at the optical radius

In Section 6.3, we discussed the halo shapes directly derived from the RCs. In this section, we discuss the halo masses based on the integrated mass of the halo within the optical radius based on relations (5) and (8). The goal is here to evaluate the dark halo mass budget error at the optical radius when we use only Hα or H I RCs instead of hybrid RCs.

The mass distribution grows roughly as rV^2 so, at large radius r where the RC is flat or slowly growing, the rotation velocity V is almost constant and the mass is roughly proportional to r. At small radius where the velocity gradient is large, the mass is still proportional to the radius r but is very sensitive to the rotation velocity variation ($\propto V^2$). Hα data usually constrain the inner RC while H I data the outskirts.

Mass models are not constrained by the data when the solutions are degenerate, i.e. when different models provide χ^2 that are not significantly different. For instance, when there are no inner points in the solid body region of the RC (e.g. UGC 10075), the disc component could reach the maximum rotation velocity with a large M/L or, alternatively being equal to zero and be replaced by a large halo without changing the χ^2 of the fit. When the H I RC is decreasing at larger radii than the Hα one, a specious effect could occur, the disc M/L becomes much larger in H I than in Hα. For instance in the case of UGC 12754, almost no halo is requested to fit the H I data while the Hα RC is completely dominated by the DM halo.

The analysis of inner regions of the individual RCs shows that H I RCs do not constrain the inner region of 9/31 galaxies and weakly constraint 15/31 other ones while only 2/31 Hα RCs do not provide strong constraints. The spatial resolution of Hα RCs is usually higher than the H I ones. Nevertheless, the beam smearing correction applied on H I RCs (Swaters et al. 2009) is usually not strong enough but sometimes the RCs are overcorrected (e.g. UGC 8490, UGC 11597, UGC 12754, UGC 12754). This means that in the latter cases the H I inner shape is artificially more cuspide than the Hα ones, thus the actual difference of inner slopes between Hα and H I RCs is even larger than what numbers show.

The same analysis has been done on the outskirts of the RCs: 18/31 Hα RCs do not strongly constrain and 10/31 weakly constrain while all the H I RCs constrain the mass distribution at the optical radius. Optical data are often but not always sufficient to reach the optical radius, as we discussed in the previous section, and even when it is the case, optical RCs might sometimes show a disagreement between both sides of the galaxy (bifurcation – e.g. Fuentes-Carrera et al. 2019, lack of data on one side, few measurements, large error bars, etc.) that do not constrain the fit enough. In addition, when the RCs extend much beyond the optical radius, as it is usually the case with H I data (in low-density environment), the mass distribution at the optical radius is constrained by the behaviour of the RC far beyond the optical radius.

By definition, MDM maximize the disc/bulge component(s) and of course fixed M/L do not allow this ratio to vary while BFM dispatch more uniformly the mass between the baryons and the DM. Nevertheless, the range of possible M/L ratios is wider for BFM and sometimes tends towards maximum or minimum disc models. This depends on the shape of the RCs both in the inner and outer parts.

In this paper we used 5 models (*ISO* BFM, *ISO* MDM, *ISO* Fixed M/L, and NFW fixed M/L) to analyse the mass distribution for the whole sample of 31 galaxies. In order to describe the differences obtained using the three data sets (hybrid, Hα, and H I RCs) for the typical halo masses measured at 1, 0.5, and 0.25 R_{25} for those five models, we decided to use, as a reference, the halo masses deduced from hybrid RCs because we expect that these curves combine all the constraints both at small and large radii. We present the results in Table 5 for each of the 15 cases (5 models $\times$ 3 radii). For each model, the first row of Table 5 contains the masses obtained with this data set and the two other lines show the values obtained with the two other data sets with respect to this reference. We always indicate the median and the 16th and 84th percentiles.

We find that:

(i) For *ISO* (both MDM and fixed M/L) and NFW fixed M/L, the halo mass at the optical radius could be equal to zero for $\simeq 10 \pm 5$ per cent of the sample, as indicated in the last column of Table 5. BFM always provide a solution with a DM halo, this is due to the degree of freedom of the fit that is larger than in the case of MDM or fixed M/L.

(ii) For both *ISO* and NFW BFM, the mass at the optical radius is better recovered using H I than Hα RCs. Hα RCs tend to overestimate the mass. However, the mass offset decreases for the Hα RCs when the mass is estimated at smaller radii (R_{25}/2 and /4), whereas it increases for the BFM *ISO* H I RCs. This indicates that the mass at the optical radius is dominated by the RC at large radius while in the inner regions, the inner shape of the RC becomes more and more important as the halo mass is measured near the centre. Fig. 10 illustrates the case of the BFM *ISO* at the optical radius and shows that the mass offset with respect to hybrid RCs is noticeable (median offset of $\sim$10 per cent, black arrow) for the Hα RCs but not for the H I ones (grey arrow). The masses determined for NFW BFM using H I or Hα RCs are however the same than with the hybrid RCs down to 0.25 R_{25}; this is due to the cuspide profile that force the fit down to the central regions.

(iii) For *ISO* MDM, halo masses determined at the optical radius using the H I or Hα RCs are overestimated but in that case, H I RCs lead to a larger overestimation than Hα RCs. This shift increases when the halo masses are measured at smaller radius. This is due to the fact that many H I RCs do not allow one to constrain correctly the M/L of the stellar distribution, contrarily to Hα and hybrid RCs.

(iv) Using a fixed M/L (*ISO* or NFW) slightly changes the situation since the baryonic contribution is identical for all data sets. We observe a slight trend of the halo mass being overestimated, at the optical radius, using the Hα RCs, but at small radius we do not observe anymore shifts between Hα and H I RCs.

(v) And finally we stress that masses computed from the hybrid RCs are within the 16th and 84th percentiles for all the cases, which means that statistically, the masses determined using either Hα or H I RCs are realistic. We also note that the discrepancies around the median (measured as the difference between 16th and 84th percentiles) increases from fixed M/L, BFM, and MDM.

7 SUMMARY AND CONCLUSIONS

We have studied the mass distribution of a sample of 31 galaxies covering morphological types from Sa to Irr. We first constructed the mass models using the optical high-resolution Hα RCs using W_1-band surface brightness profiles. Secondly, the mass models were constructed using H I kinematics instead of Hα RCs, with W_1-band surface brightness profiles and moreover we include the contribution of the neutral gas component obtained from radio H I observations. Thirdly, we combined the Hα with H I RCs as well

Table 5. DM halo masses (median, 16th and 84th percentiles) within a fraction of the optical radius for the various models. For each model, the first row presents the logarithm of the mass (in $M_\odot$) obtained with the hybrid data set used as a reference. The second and third rows provide the comparison of the masses (logarithm of the ratio) obtained with the hybrid and H α or H I RCs. The last column indicates the number of galaxies for which the model is compatible with a null DM halo mass.

Model	Data sets	R_{25}			$R_{25}/2$			$R_{25}/4$			
		Median	16th	84th	Median	16th	84th	Median	16th	84th	$N_{M=0}$
	$\log(M_{\rm hybrid})$	10.15	9.62	10.77	9.46	9.00	10.35	8.77	8.19	9.73	0
ISO BFM	$\log(M_{\rm H\alpha}/M_{\rm hybrid})$	0.09	−0.00	0.19	0.06	−0.06	0.14	0.02	−0.09	0.15	0
	$\log(M_{\rm HI}/M_{\rm hybrid})$	0.01	−0.10	0.11	0.04	−0.12	0.17	0.05	−0.12	0.24	0
	$\log(M_{\rm hybrid})$	9.96	9.16	10.64	9.38	8.51	10.15	8.58	7.65	9.55	1
ISO MDM	$\log(M_{\rm H\alpha}/M_{\rm hybrid})$	0.04	−0.22	0.23	0.02	−0.18	0.15	0.00	−0.28	0.21	4
	$\log(M_{\rm HI}/M_{\rm hybrid})$	0.07	−0.03	0.34	0.09	−0.07	0.45	0.11	−0.13	0.46	2
	$\log(M_{\rm hybrid})$	10.04	9.25	10.72	9.46	8.51	10.20	8.77	7.68	9.68	4
ISO fixed M/L	$\log(M_{\rm H\alpha}/M_{\rm hybrid})$	0.05	−0.01	0.10	0.00	−0.03	0.08	−0.00	−0.10	0.0	5
	$\log(M_{\rm HI}/M_{\rm hybrid})$	0.00	−0.04	0.06	−0.01	−0.07	0.04	−0.01	−0.13	0.11	3
	$\log(M_{\rm hybrid})$	10.41	9.71	10.75	9.96	9.16	10.25	9.43	8.59	9.73	0
NFW BFM	$\log(M_{\rm H\alpha}/M_{\rm hybrid})$	0.05	−0.02	0.14	0.02	−0.04	0.11	0.01	−0.10	0.16	0
	$\log(M_{\rm HI}/M_{\rm hybrid})$	0.01	−0.11	0.12	0.00	−0.10	0.18	0.02	−0.09	0.22	0
	$\log(M_{\rm hybrid})$	10.02	9.30	10.70	9.48	8.70	10.20	8.90	8.10	9.66	3
NFW fixed M/L	$\log(M_{\rm H\alpha}/M_{\rm hybrid})$	0.04	−0.14	0.10	0.01	−0.04	0.04	0.00	−0.08	0.07	4
	$\log(M_{\rm HI}/M_{\rm hybrid})$	0.00	−0.03	0.11	0.02	−0.03	0.13	0.03	−0.04	0.18	3

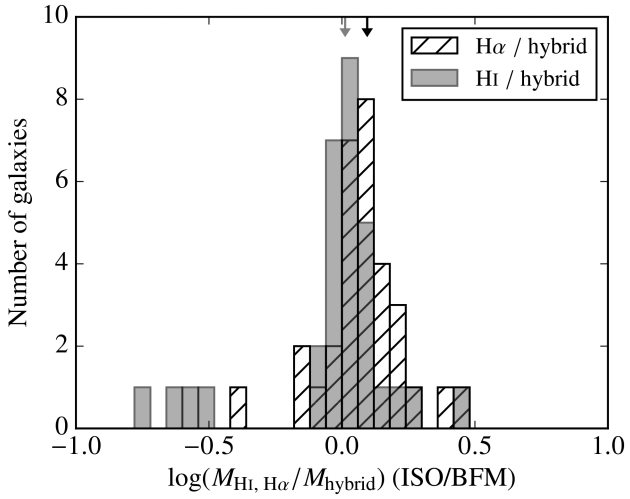

Figure 10. Distribution of the logarithm of relative halo mass difference for the BFM using the three families of RCs (H α, H I, and hybrid) at the optical radius for the whole sample of 31 galaxies. Vertical arrows represent the median values of the two distributions which are, in filled grey, the difference between H I and the hybrid RCs, and in hatched black, the difference between H α and hybrid RCs.

taking into account the neutral gas component. We call this data set the hybrid H α/H I RCs, and also use the W_1-band surface brightness profiles to build the mass models. To study the mass distribution, we used two models, the *ISO* sphere and the NFW with different techniques: a BFM, an MDM, and a fixed M/L calculated using the $(W_1 - W_2)$ mid-IR colour. The objective of this work is to study how the baryonic and DM halo's parameters distributions are recovered when including the H I gas component or using hybrid RCs instead of only H α or H I RCs.

a. Shape and extension of the RCs

Mostly depending on the mass, luminosity, and morphology of the galaxies, the shape of RCs ranges from a compact solid body behaviour to a quickly reached extended flat plateau. Comparing the data sets we find:

(i) High-resolution H α data are needed to constrain the inner part of the RCs, in particular when a bar or a bulge is present. In those cases, mass models are better constrained with H α or hybrid RCs than with H I RCs alone.

(ii) The presence of bars may change the inner shape of RCs, which requires higher resolution in the central parts. Therefore the use of H α or hybrid RCs should be preferred to constrain the inner part of the RC and mass models of barred galaxies should require specific care since this effect might not be reflected accordingly in mass models.

(iii) The flat part of the RC and the optical radius are reached in H α for two-thirds of the sample but when the flat part is not reached with the H α data only, additional H I data are mandatory to derive the halo's parameters.

(iv) The sample is divided into three subsamples with an almost equivalent size, having respectively rising, flat, and decreasing H I RCs, but none of the H α RC is decreasing. H α and H I RCs match fairly well outside their rising part, up to the optical radius, when reached in H α.

b. Baryonic components

Using W_1-band surface brightness profiles for the different data sets we find :

(i) A median value for M/L of 0.50 $M_\odot/L_\odot$ in the W_1 band when M/L is fixed, that of course does not depend on the data sets.

(ii) The amplitude of the stellar component RC obtained using fixed M/L values estimated from *WISE* colour indices is larger than the amplitude of H α and H I observed RCs in one-third and half of the cases, respectively. This incompatibility between dynamic and spectrophotometric baryonic mass distribution is an issue that should be addressed.

(iii) For H α RCs without the gas component, the median values of M/L are equal to 0.13 and 0.51 $M_\odot/L_\odot$ for *ISO* with BFM and MDM, respectively.

(iv) In the case of H α RCs including the gas component, the median values of M/L for BFM and MDM are equal to 0.14 and 0.54 $M_\odot/L_\odot$, respectively, which is close to what was found when the gas component was not included.

(v) Mass models built using H I RCs and the neutral gas component give M/L median values equal to 0.26 and 0.49 $M_\odot/L_\odot$ for BFM and MDM, respectively.

(vi) When using hybrid RCs and neutral gas components, the median values of M/L for BFM and MDM are, respectively, 0.35 and 0.55 $M_\odot/L_\odot$ which are higher to those found in the previous cases.

In summary H α RCs without considering the H I gas component give results close enough to those obtained with the gas component and could be safely used to estimate the M/L ratio when the H I gas component is not available and the M/L values are larger when using hybrid RCs than only H α or H I RCs.

c. DM components

The mass distribution within DM haloes strongly depends on the physical models used but also on the data sets that set the constrains on the models. We find:

(i) In the cases of MDM or fixed M/L models, a DM halo is not requested for only $\simeq 10 \pm 5$ per cent, regardless the data set (H α, H I, or hybrid) while BFM always find a solution including a DM halo.

(ii) Hybrid and H I RCs lead to higher M/L values for both *ISO* and NFW BFM but lower central densities ρ_0 for *ISO* haloes and higher concentration c for NFW haloes than when using purely H α kinematics.

(iii) The relation between the parameters of the NFW functional form (c and V_{200}) is less affected by either different data set (H α, H I, or hybrid) or fitting technique (BFM or fixed M/L) than the one between the parameters of the *ISO* (ρ_0 and r_0) models. This means that H α kinematics in the inner parts is sufficient to characterize a NFW halo.

(iv) The correlations between the DM halo parameters and the luminosity of the galaxy remain the same whatever the RC used: optical RCs including and excluding the contribution of the neutral gas component, optical RC extended with H I RC or H I RC alone.

(v) Regardless the data set, *ISO* density profile is to be preferred to NFW ones. *ISO* (NFW) provides better fit to the data for 22 (9), 21 (10), and 17 (13) galaxies for H α, hybrid, and H I RCs, respectively (the fit is not constrained with H I data alone for one galaxy). The agreement between the fit done with H α and hybrid RCs is very good, whereas the result is less strong using H I RCs alone. This shows that the use of H α or hybrid RCs has to be favoured over H I ones to optimize the fits.

(vi) H I and hybrid data sets give consistent halo masses at R_{25}, except for MDM for which the halo mass at R_{25} is slightly overestimated using H I data alone due to incorrect M/L estimation. For all the models, the halo mass at R_{25} is slightly overestimated when using H α RCs only. However, when the halo mass is measured at smaller radii (0.25 or 0.50 R_{25}), the agreement between the mass obtained using H α and hybrids RCs improves, whatever the model, whereas H I RCs tend to overestimate the mass for *ISO* models. Nevertheless, halo masses determined using either H α, H I, or hybrid RCs give statistically the same values within the 16th and 84th percentiles and discrepancies between the data sets are lower using fixed M/L models.

(vii) The relations between the parameters of the models depend more on the fitting technique (BFM, MDM, or fixed M/L) than on the data set (H α RCs, hybrid RCs, or H I RCs).

This work is not intended to describe a representative sample of galaxies but rather a sample of galaxies of different morphological types, sizes, and brightnesses. These results should be confirmed by studying a larger sample, representative of a complete Universe volume.

ACKNOWLEDGEMENTS

We warmly thank the referee for useful comments which helped us to improve the analysis. We also thank Prof. Tom Jarrett for the help with the *WISE* photometry and Prof. Michelle Cluver for discussions on the *WISE* photometry. Most of the research of MK was done while she was having a PhD Scholarship from the Science faculty of the University of Cape Town. CC's work is based upon research supported by the South African Research Chairs Initiative (SARChI) of the Department of Science and Technology (DST), the Square Kilometre Array South Africa (SKA SA), and the National Research Foundation (NRF). We acknowledge financial support from 'Programme National de Cosmologie et Galaxies' (PNCG) funded by CNRS/INSU-IN2P3-INP (Centre national de la recherche scientifique/Institut national des sciences de l'Univers - Institut national de physique nucleaire et de physique des particules – Institut de physique), CEA (Commissariat à l'Energie atomique et aux Energies alternatives), and CNES (Centre national d'etudes spatiales) in France.

REFERENCES

Amram P., Le Coarer E., Marcelin M., Balkowski C., Sullivan W. T., III, Cayatte V., 1992, A&AS, 94, 175
Barbieri C. V., Fraternali F., Oosterloo T., Bertin G., Boomsma R., Sancisi R., 2005, A&A, 439, 947
Barnes E. I., Sellwood J. A., 2003, AJ, 125, 1164
Battaglia G., Fraternali F., Oosterloo T., Sancisi R., 2006, A&A, 447, 49
Begeman K. G., 1987, PhD thesis, Kapteyn Institute
Begeman K. G., Broeils A. H., Sanders R. H., 1991, MNRAS, 249, 523
Bell E. F., de Jong R. S., 2001, ApJ, 550, 212
Blais-Ouellette S., Carignan C., Amram P., Côté S., 1999, AJ, 118, 2123
Blais-Ouellette S., Amram P., Carignan C., 2001, AJ, 121, 1952
Blais-Ouellette S., Amram P., Carignan C., Swaters R., 2004, A&A, 420, 147
Boomsma R., Oosterloo T. A., Fraternali F., van der Hulst J. M., Sancisi R., 2008, A&A, 490, 555
Bosma A., 1978, PhD thesis, Univ.Groningen
Broeils A. H., 1992, PhD thesis, Univ. Groningen
Bullock J. S., Kolatt T. S., Sigad Y., Somerville R. S., Kravtsov A. V., Klypin A. A., Primack J. R., Dekel A., 2001, MNRAS, 321, 559
Carignan C., Freeman K. C., 1985, ApJ, 294, 494
Cluver M. E. et al., 2014, ApJ, 782, 90
Cote S., Carignan C., Sancisi R., 1991, AJ, 102, 904
de Blok W. J. G., Walter F., Brinks E., Trachternach C., Oh S.-H., Kennicutt R. C., Jr, 2008, AJ, 136, 2648
Dicaire I. et al., 2008, MNRAS, 385, 553
Di Teodoro E. M., Fraternali F., 2015, MNRAS, 451, 3021
Epinat B. et al., 2008a, MNRAS, 388, 500
Epinat B., Amram P., Marcelin M., 2008b, MNRAS, 390, 466
Freeman K. C., 1970, ApJ, 160, 811
Fuentes-Carrera I. et al., 2019, A&A, 621, A25
Garrido O., Marcelin M., Amram P., Boulesteix J., 2002, A&A, 387, 821
Jarrett T. H. et al., 2013, AJ, 145, 6
Kormendy J., Freeman K. C., 2004, in Ryder S., Pisano D., Walker M., Freeman K., eds, IAU Symp. Vol. 220, Dark Matter in Galaxies. Astronomical Society of the Pacific, San Francisco, p. 377

Korsaga M., Carignan C., Amram P., Epinat B., Jarrett T. H., 2018, MNRAS, 478, 50
Korsaga M., Amram P., Carignan C., Epinat B., 2019, MNRAS, 482, 154
Lelli F., McGaugh S. S., Schombert J. M., 2016, AJ, 152, 157
McGaugh S. S., de Blok W. J. G., Schombert J. M., Kuzio de Naray R., Kim J. H., 2007, ApJ, 659, 149
Martinsson T. P. K., Verheijen M. A. W., Westfall K. B., Bershady M. A., Andersen D. R., Swaters R. A., 2013, A&A, 557, A131
Navarro J. F., Frenk C. S., White S. D. M., 1996, ApJ, 462, 563
Navarro J. F., Frenk C. S., White S. D. M., 1997, ApJ, 490, 493
Noordermeer E., van der Hulst J. M., Sancisi R., Swaters R. A., van Albada T. S., 2005, A&A, 442, 137
Noordermeer E., van der Hulst J. M., Sancisi R., Swaters R. S., van Albada T. S., 2007, MNRAS, 376, 1513
Pierens A., Huré J.-M., 2004, ApJ, 605, 179
Randriamampandry T. H., Carignan C., 2014, MNRAS, 439, 2132
Randriamampandry T. H., Combes F., Carignan C., Deg N., 2015, MNRAS, 454, 3743
Richards E. E. et al., 2018, MNRAS, 476, 5127
Sanders R. H., 1996, ApJ, 473, 117
Sanders R. H., Verheijen M. A. W., 1998, ApJ, 503, 97
Spano M., Marcelin M., Amram P., Carignan C., Epinat B., Hernandez O., 2008, MNRAS, 383, 297
Swaters R. A., van Albada T. S., van der Hulst J. M., Sancisi R., 2002, A&A, 390, 829
Swaters R. A., Sancisi R., van Albada T. S., van der Hulst J. M., 2009, A&A, 493, 871
Thornley M. D., Mundy L. G., 1997, ApJ, 484, 202
van Eymeren J., Jütte E., Jog C. J., Stein Y., Dettmar R.-J., 2011, A&A, 530, A29
Verdes-Montenegro L., Bosma A., Athanassoula E., 1997, A&A, 321, 754
Verheijen M. A. W., Sancisi R., 2001, A&A, 370, 765

Appendix A: MASS MODELS OF GALAXIES

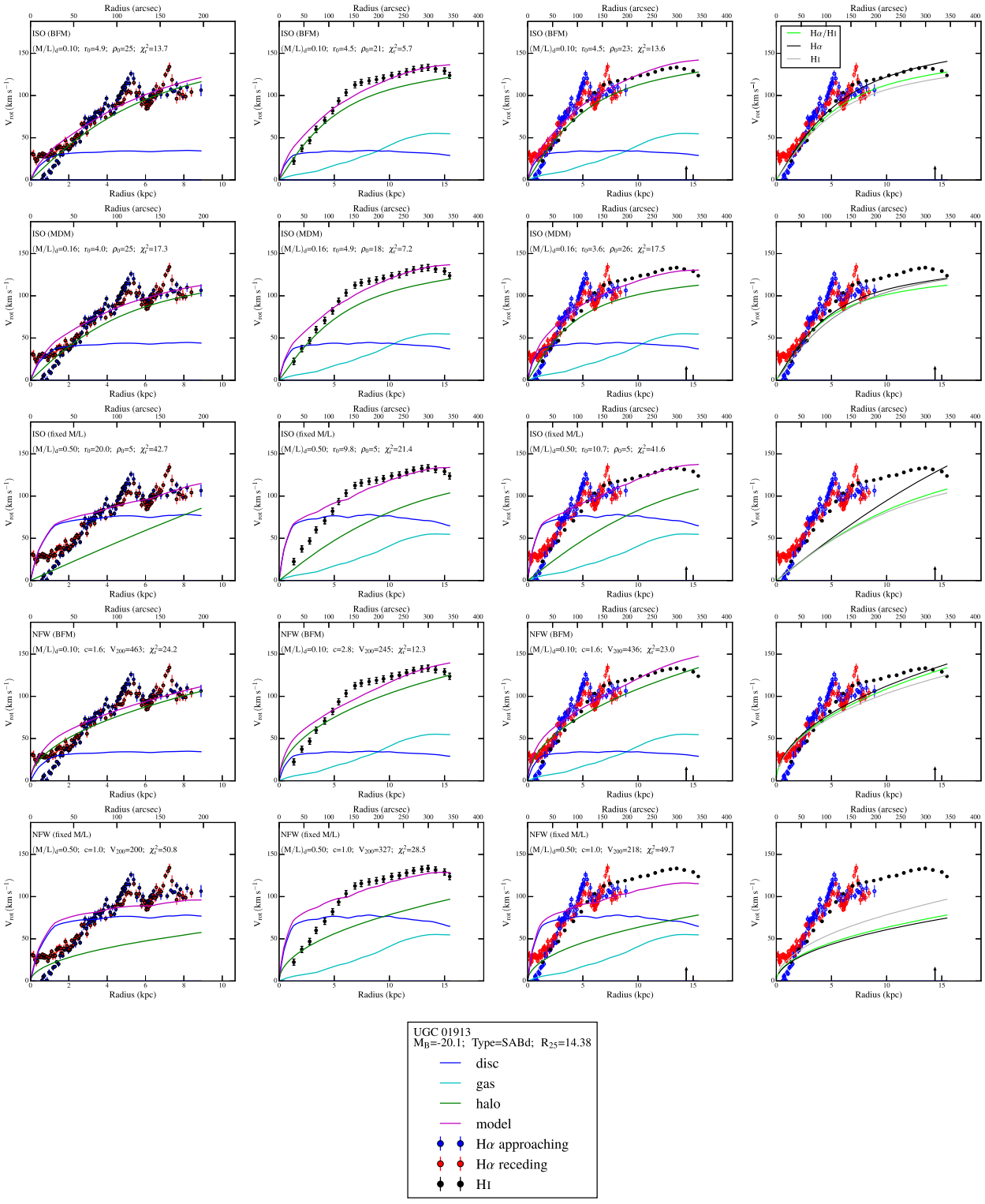

Figure A1. Mass models of the whole sample of galaxies except for UGC 6537 that is displayed in Fig. 2. The legends of Figs. A1–A30 are the same as that of Fig. 2.

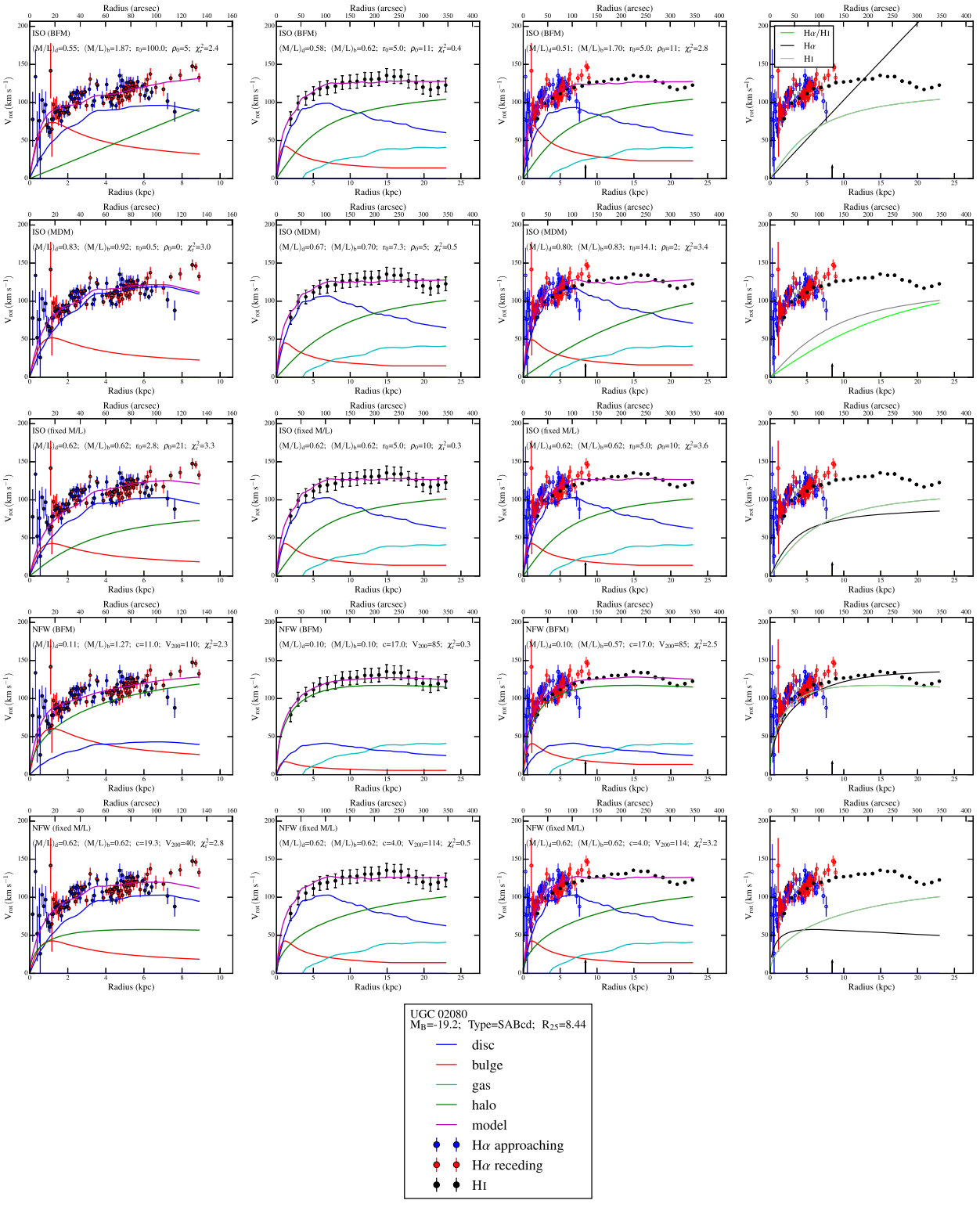

Figure A2.

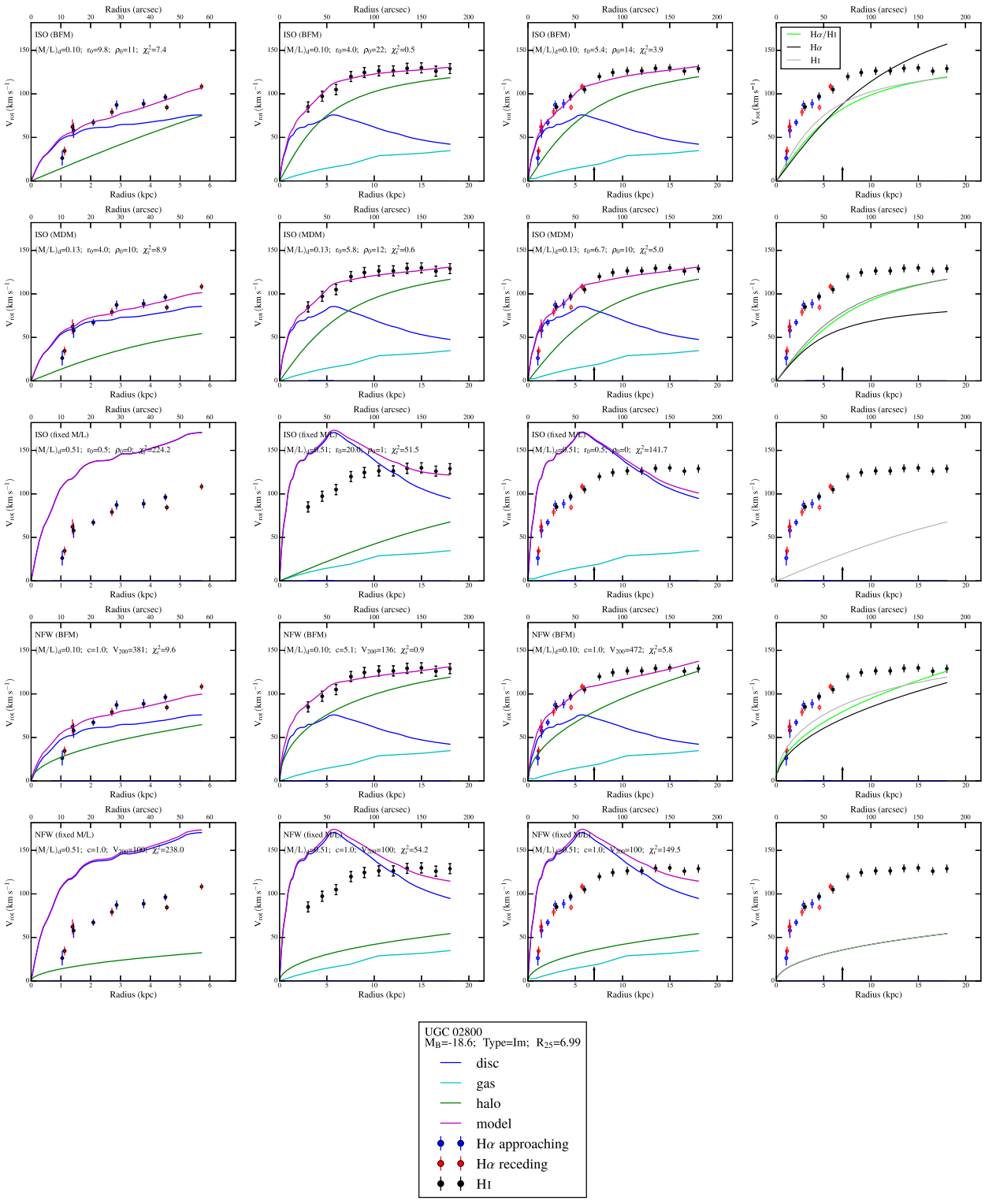

Figure A3.

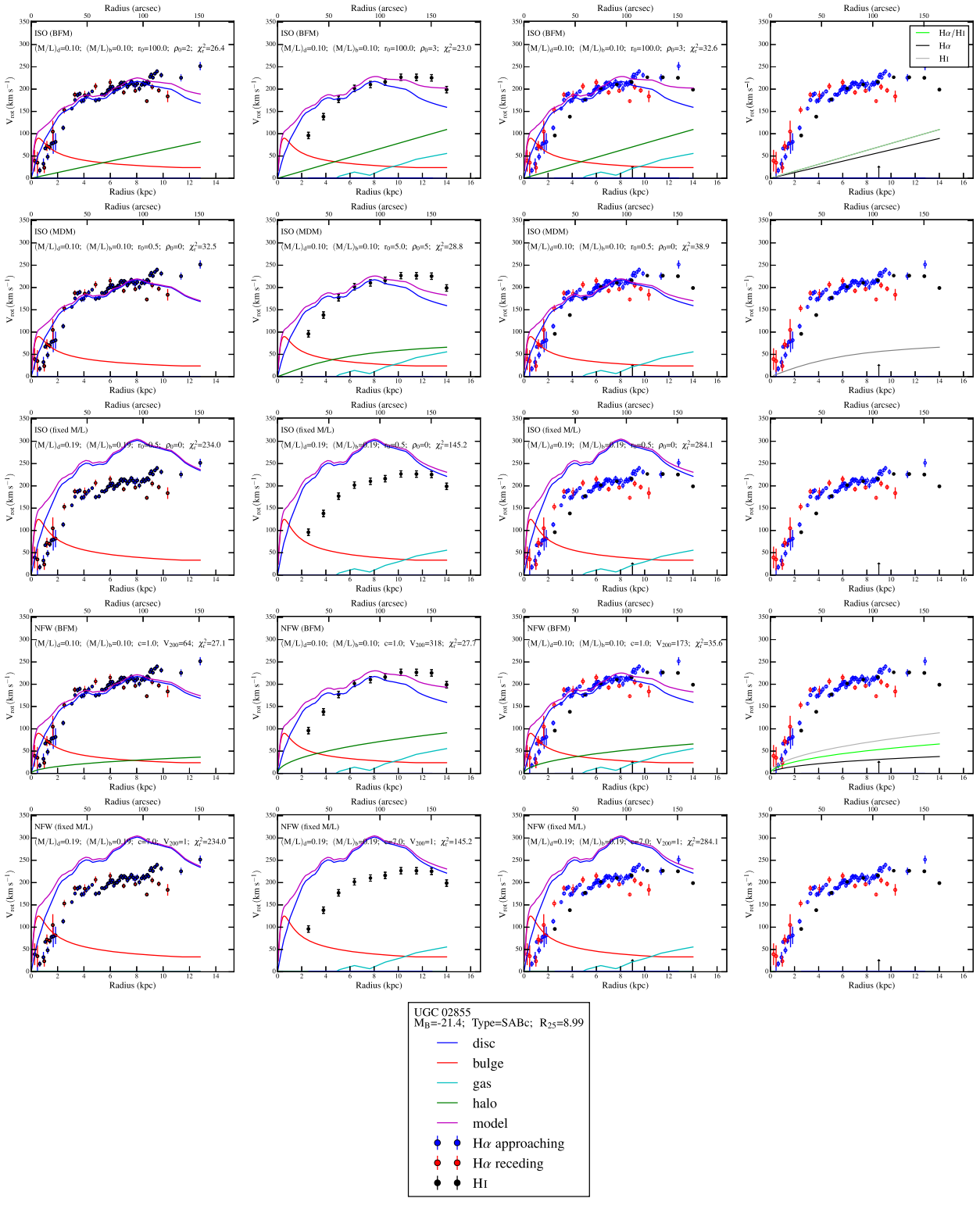

Figure A4.

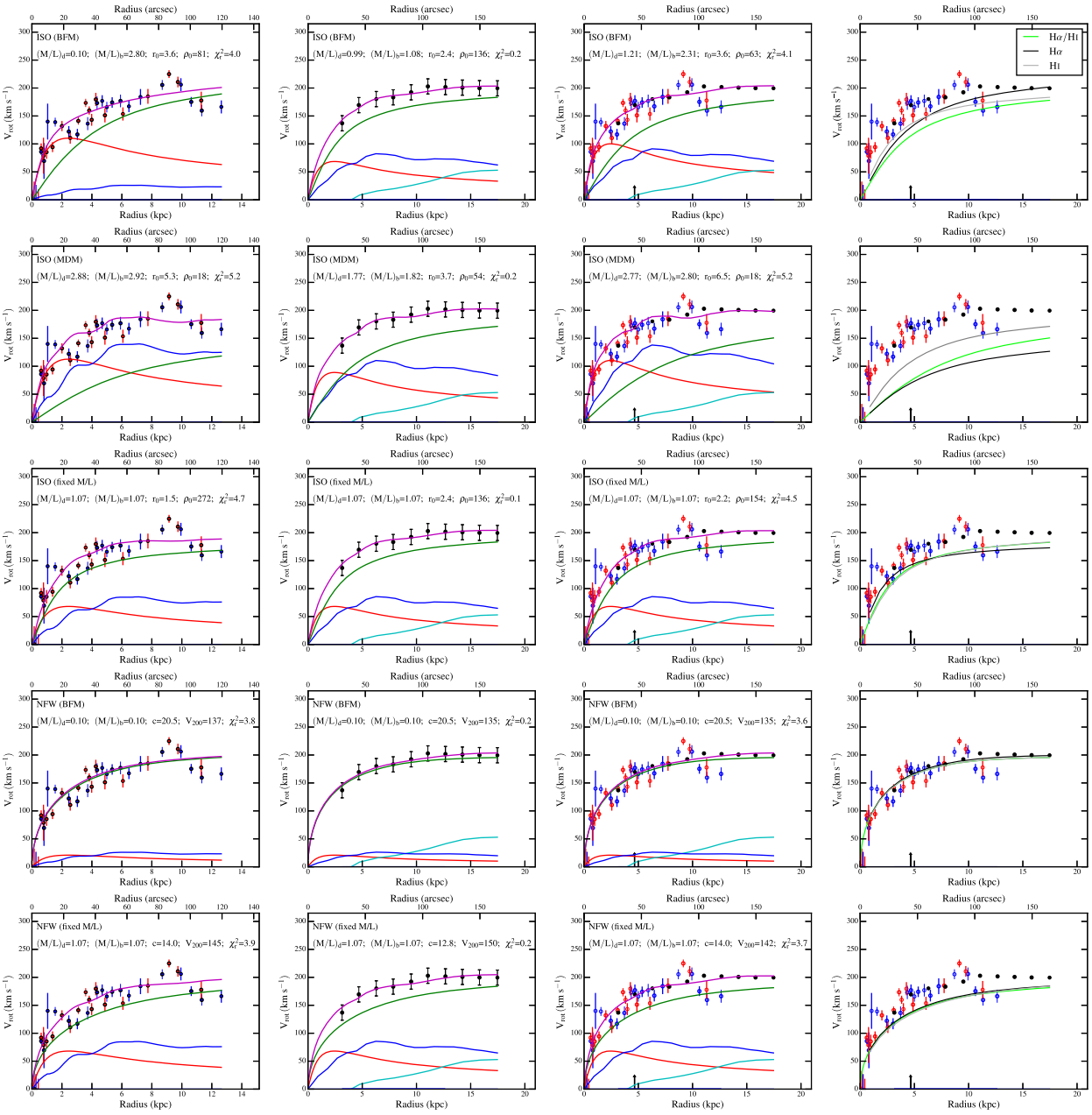

Figure A5.

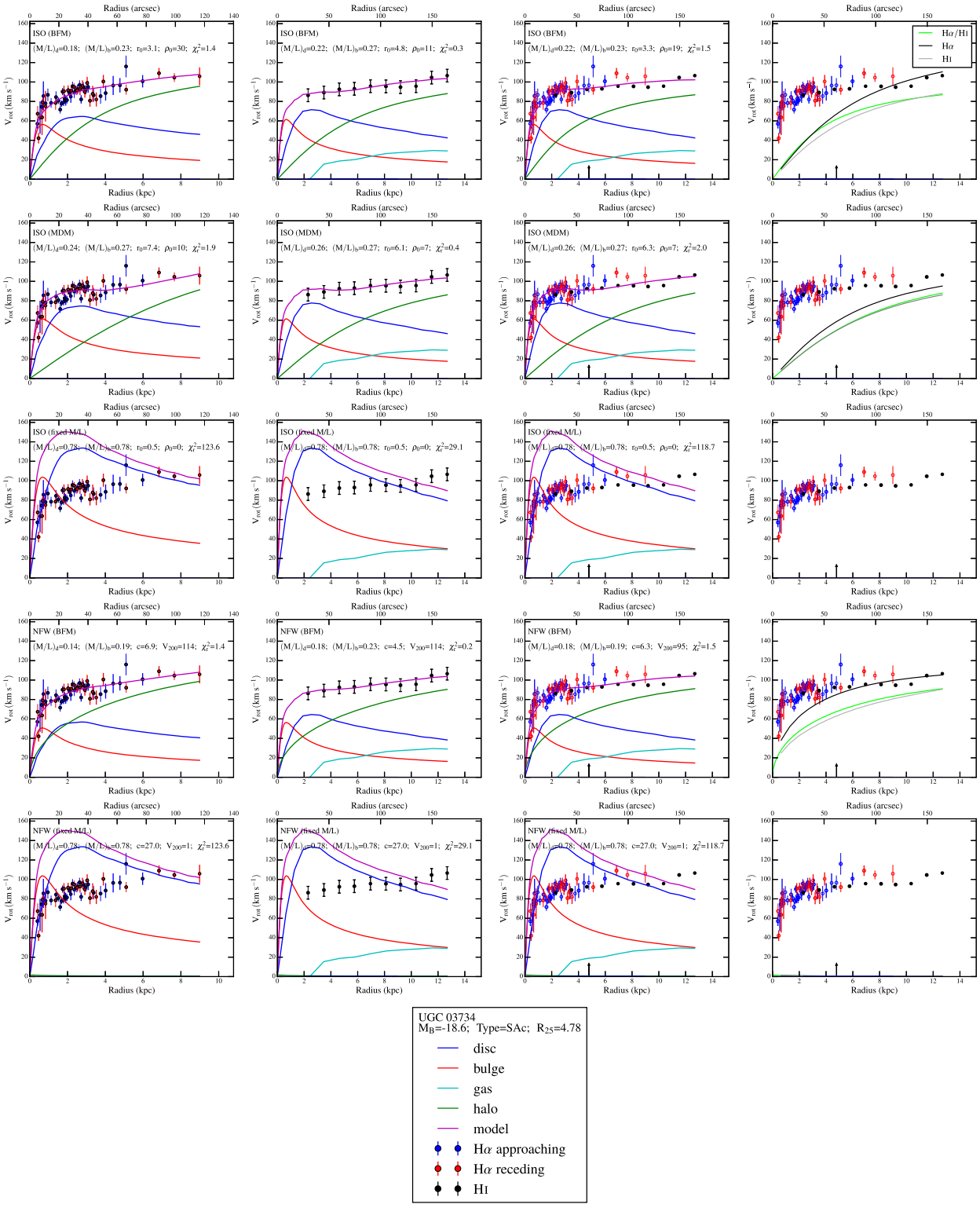

Figure A6.

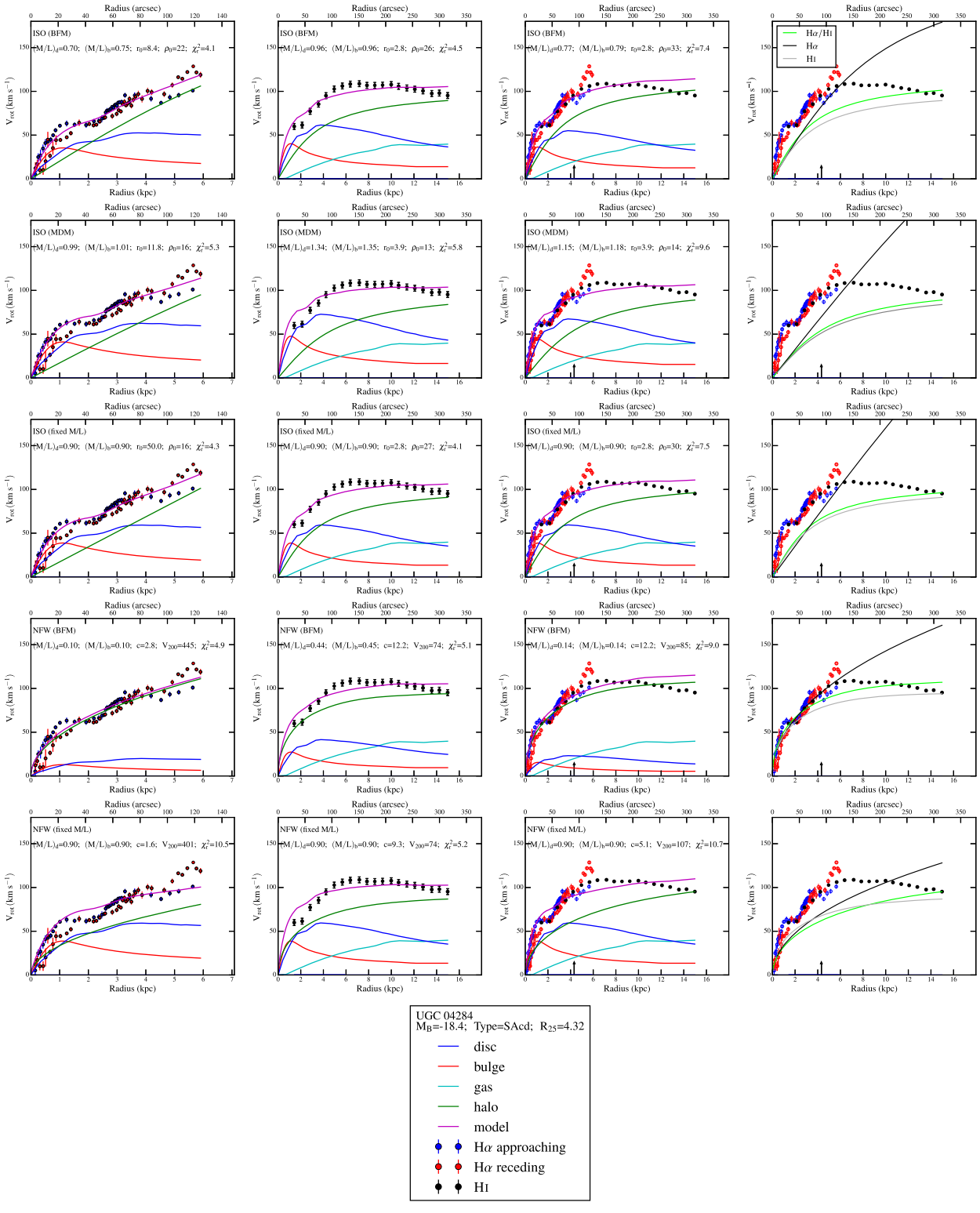

Figure A7.

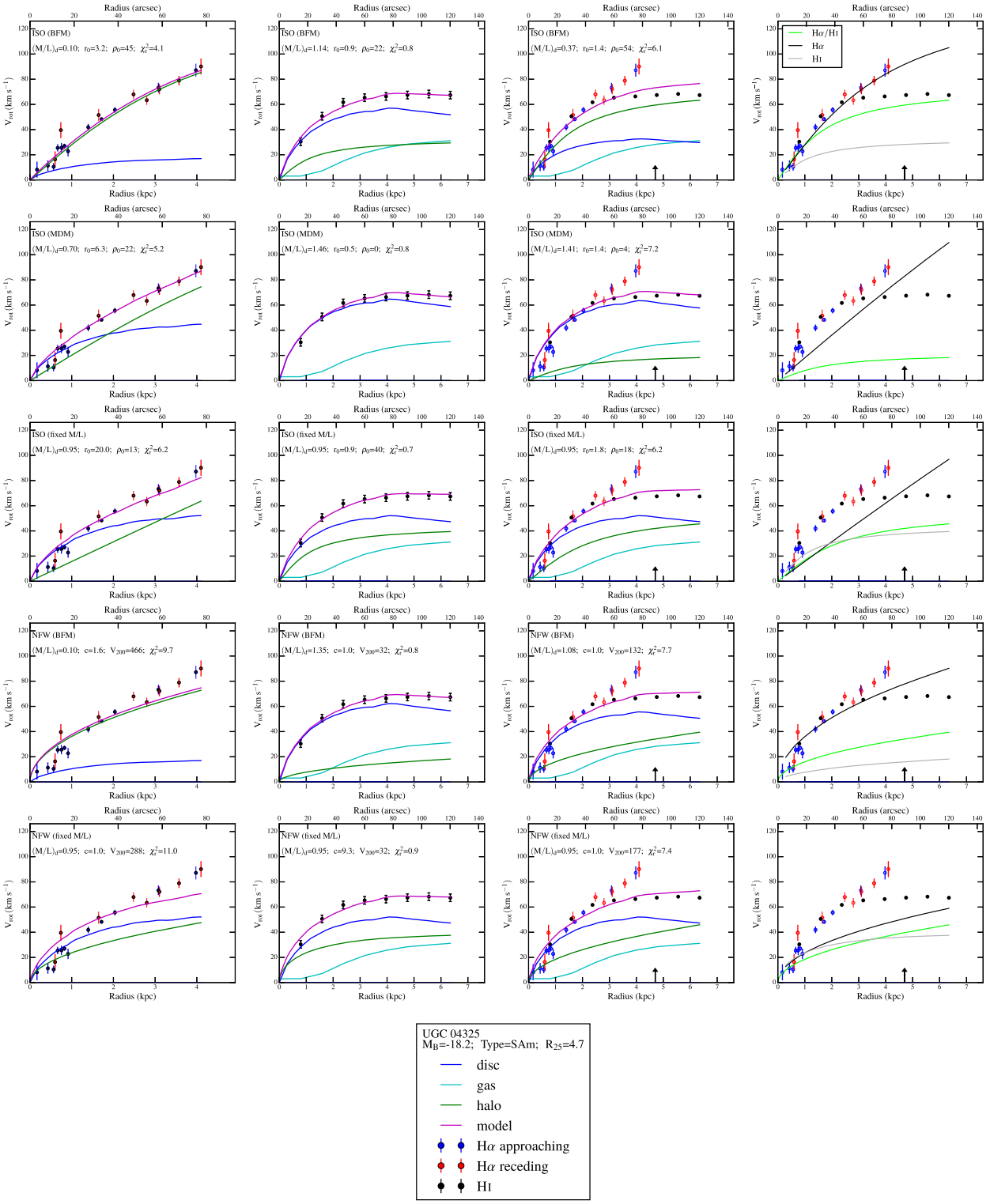

Figure A8.

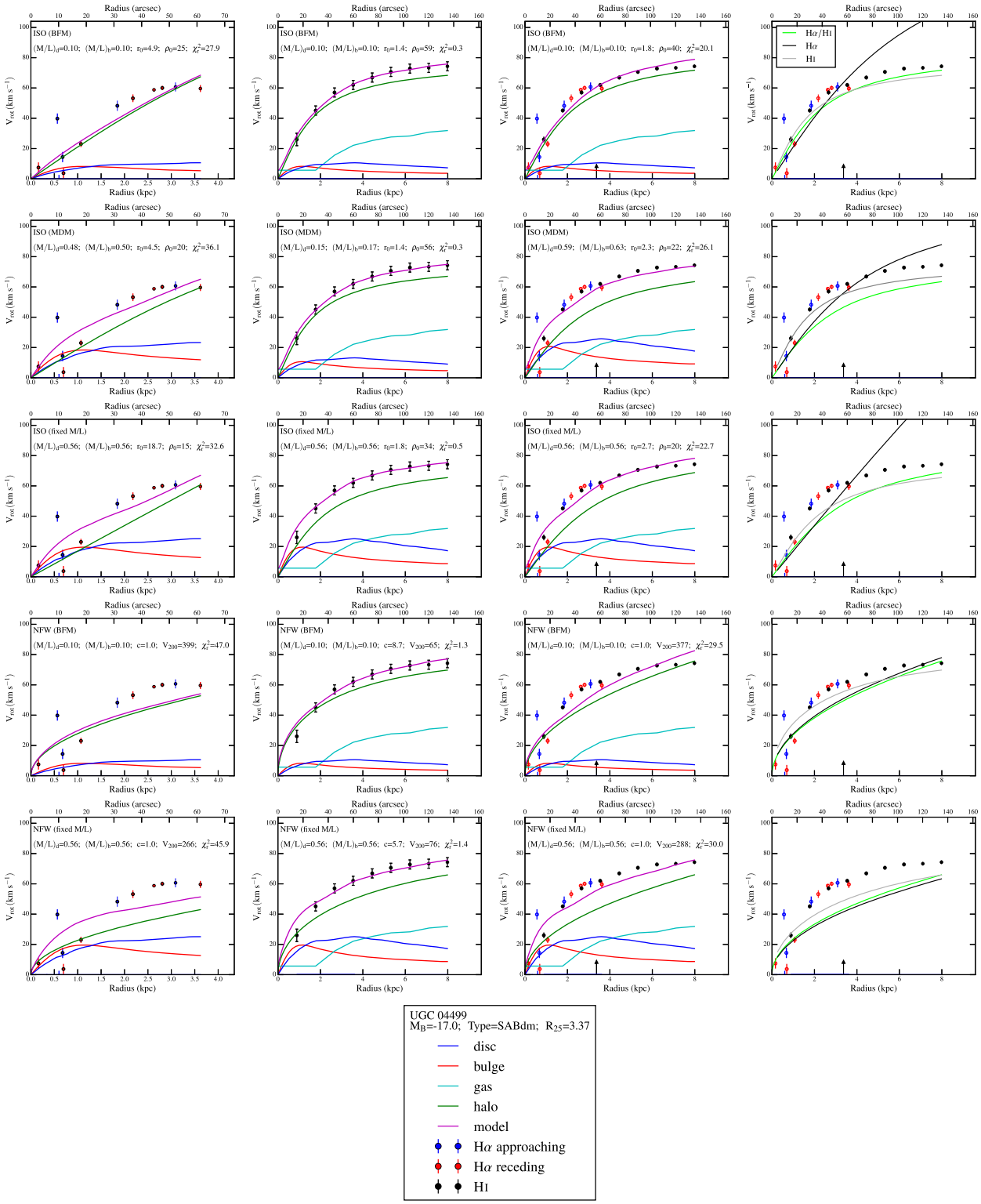

Figure A9.

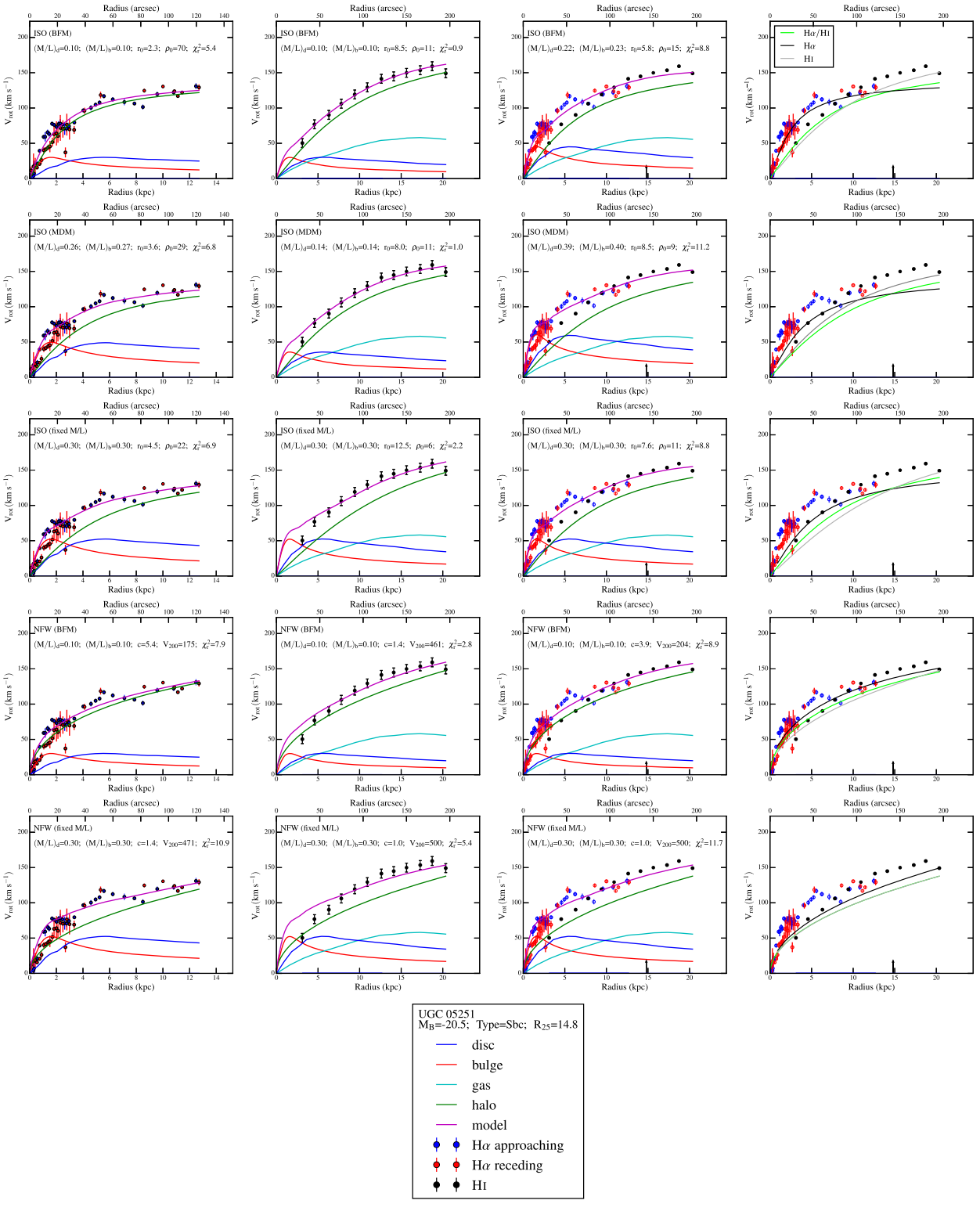

Figure A10.

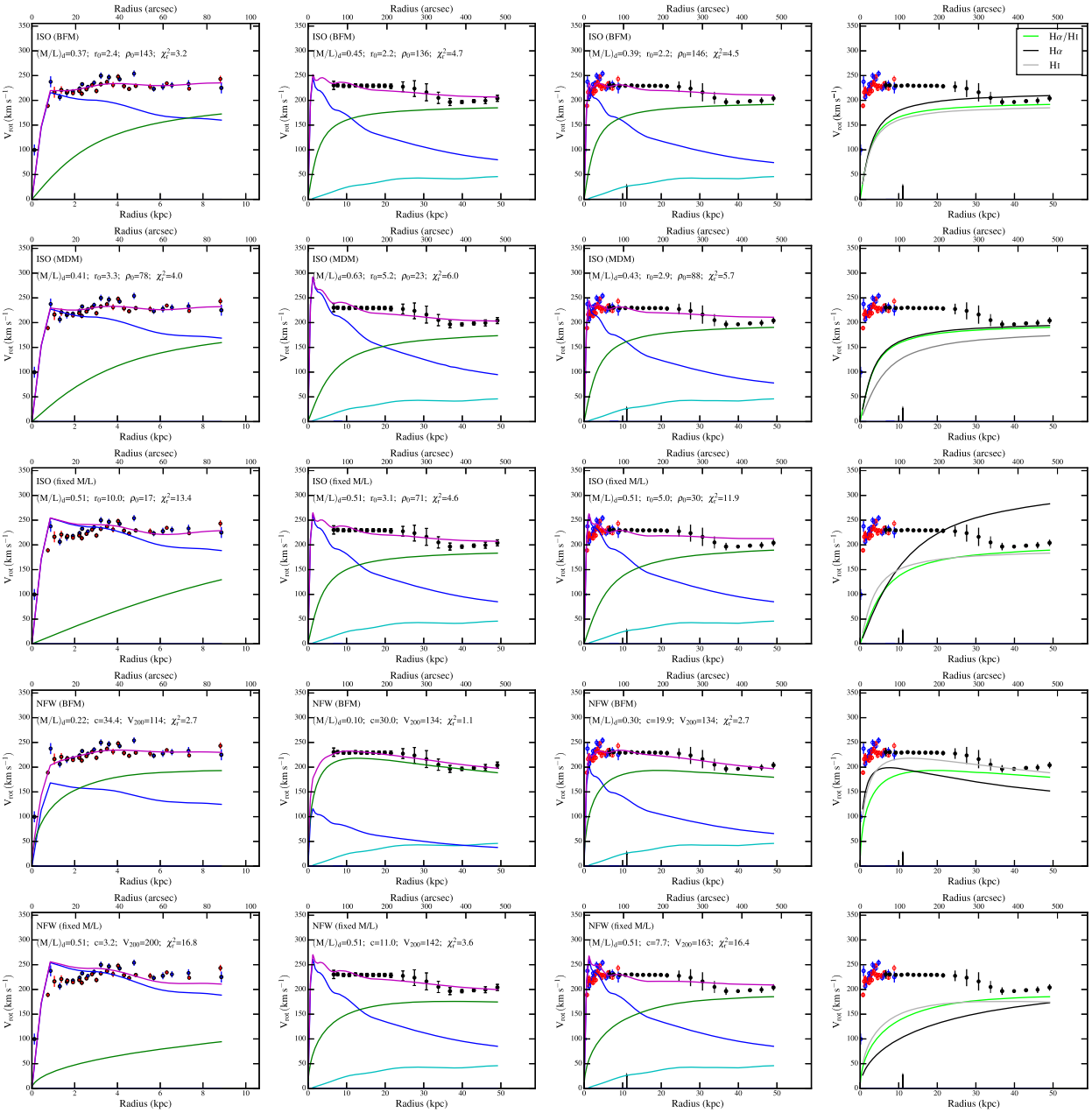

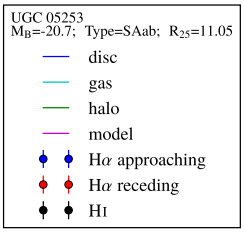

Figure A11.

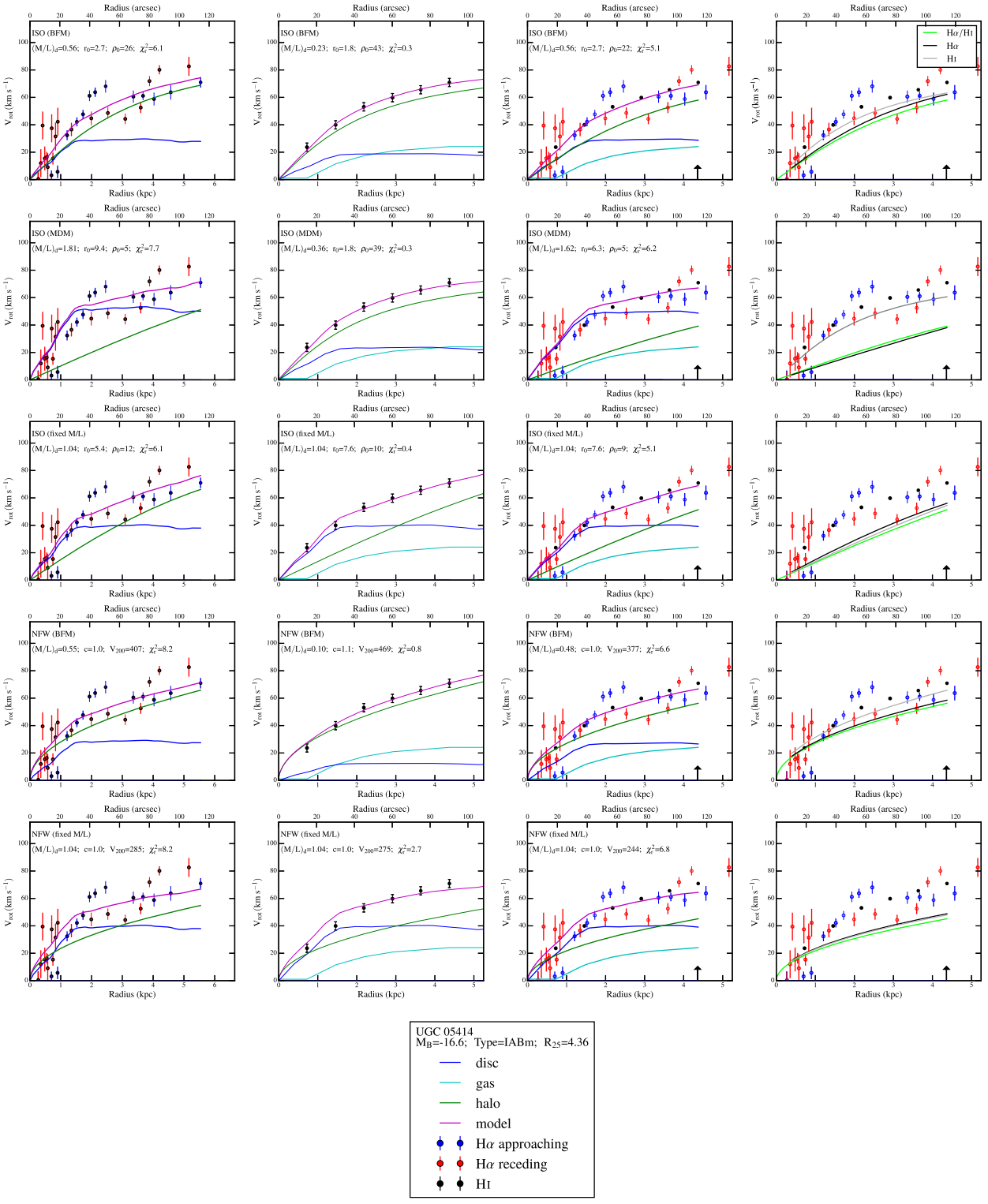

Figure A12.

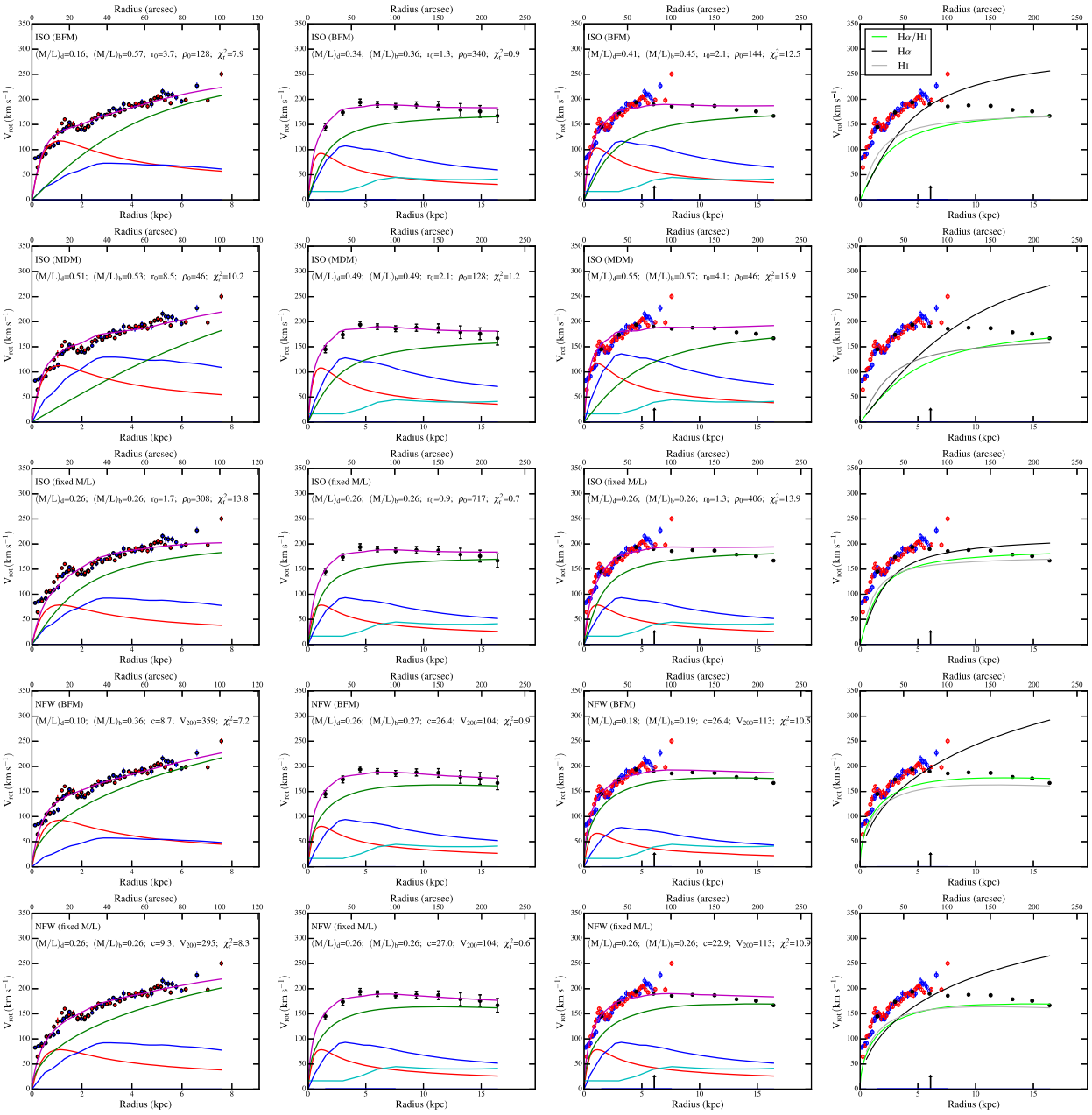

Figure A13.

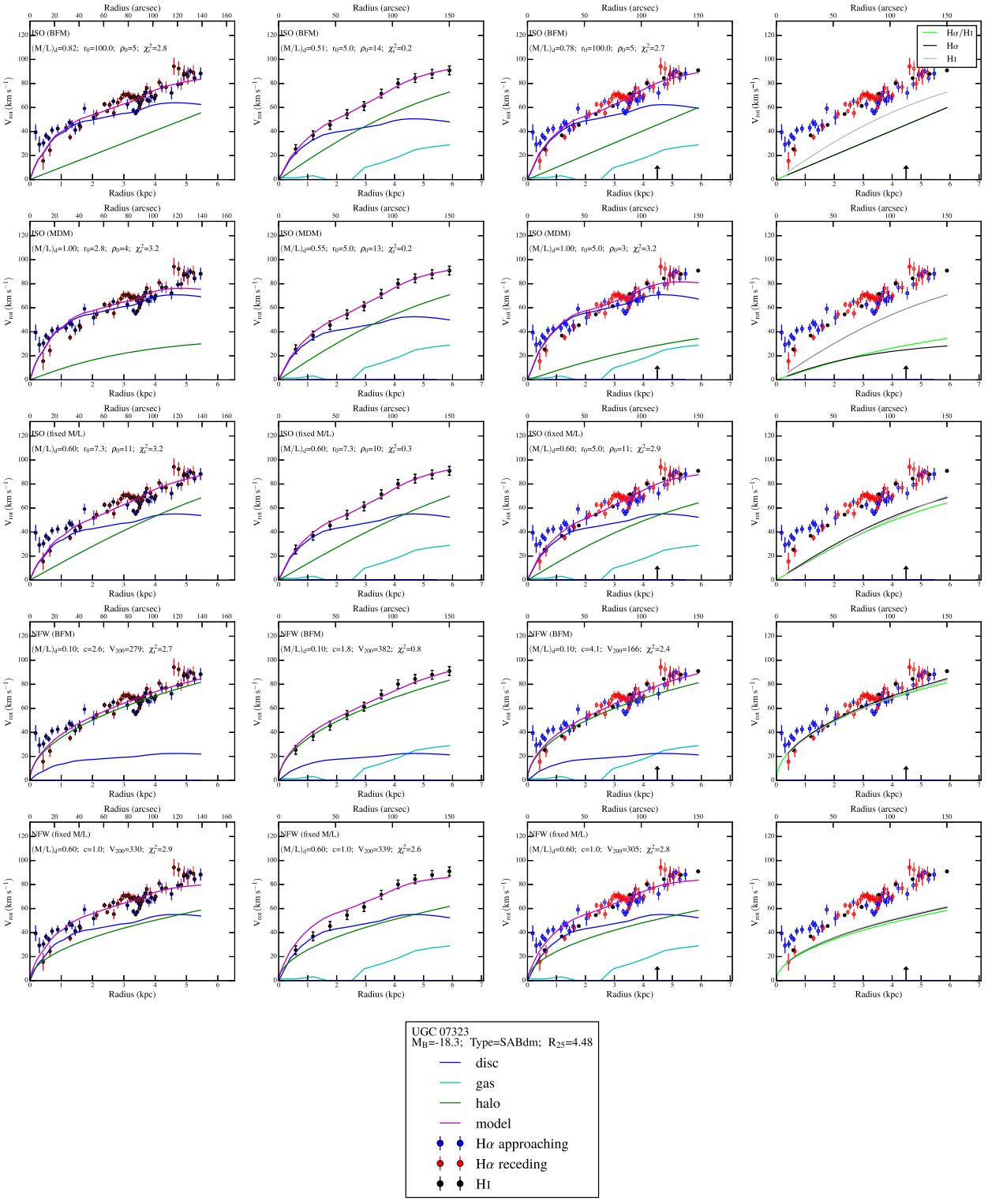

Figure A14.

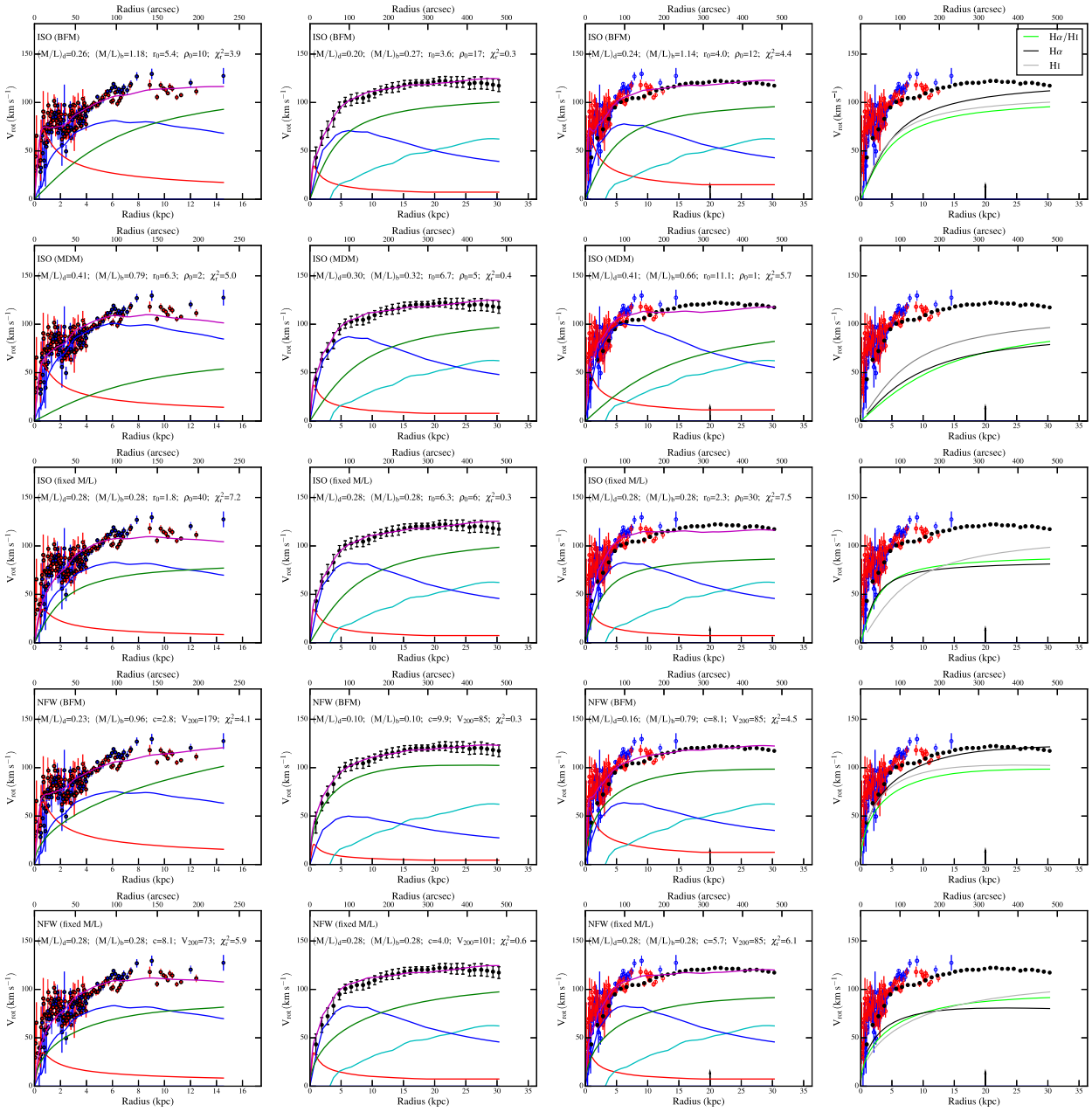

Figure A15.

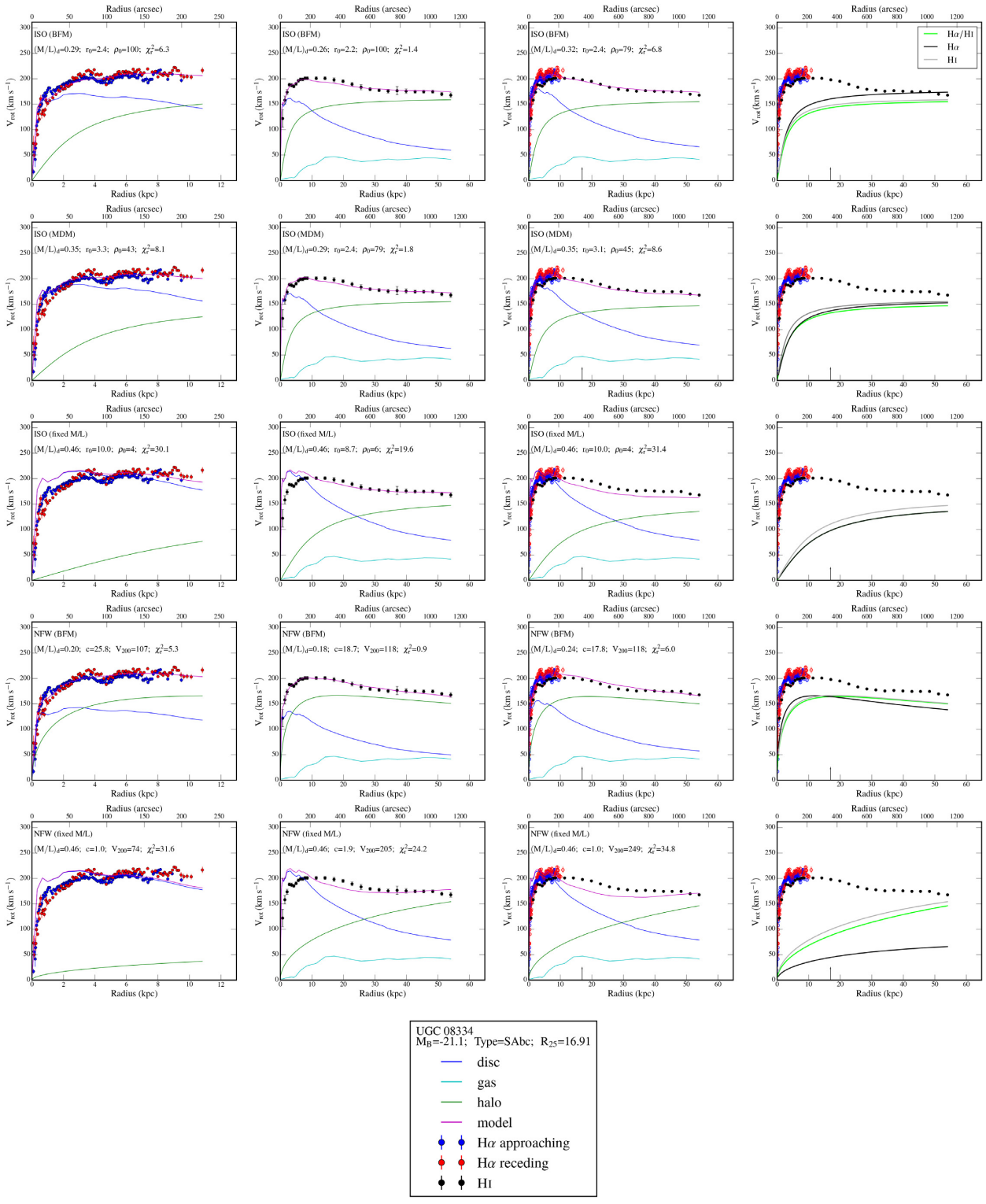

Figure A16.

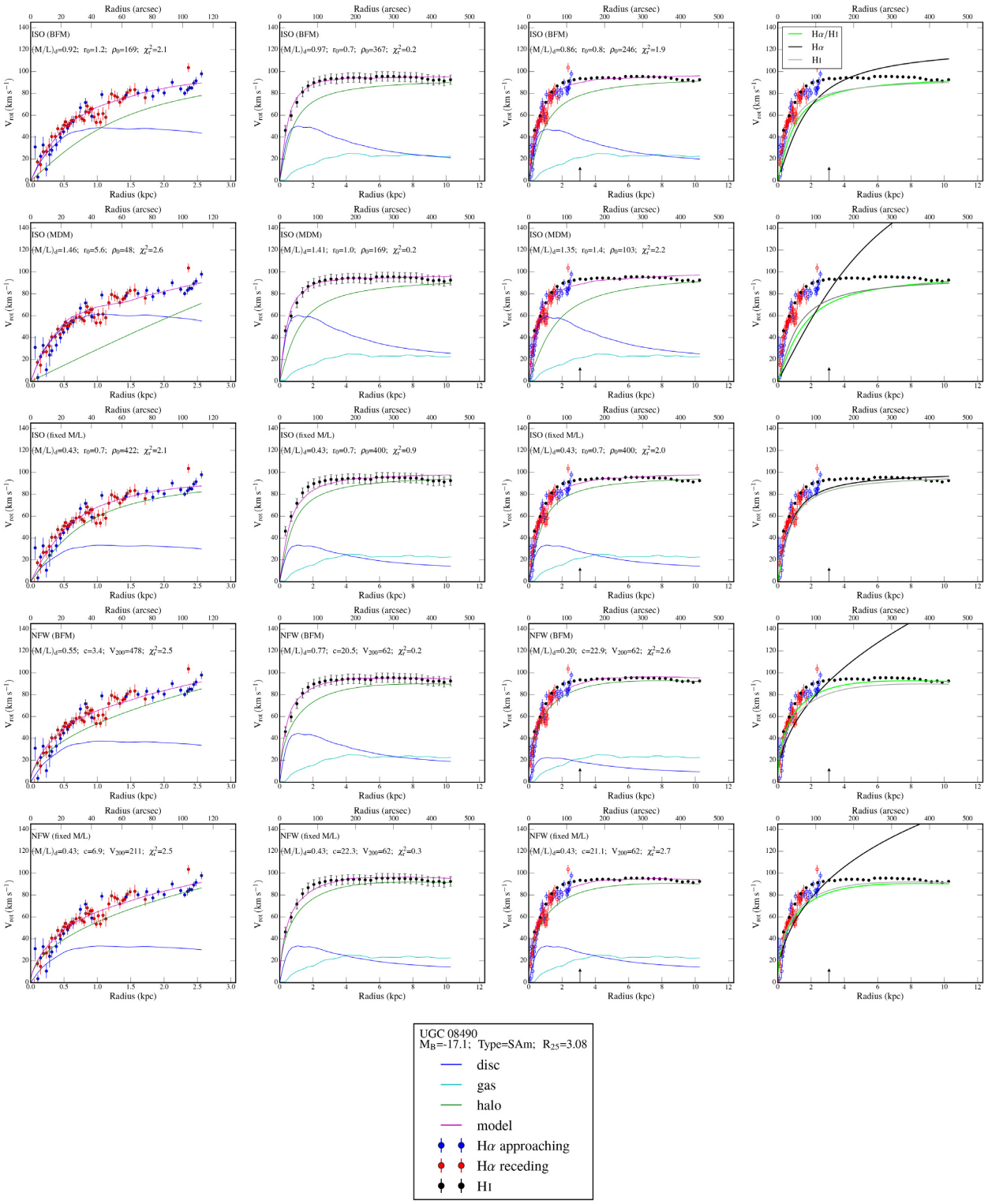

Figure A17.

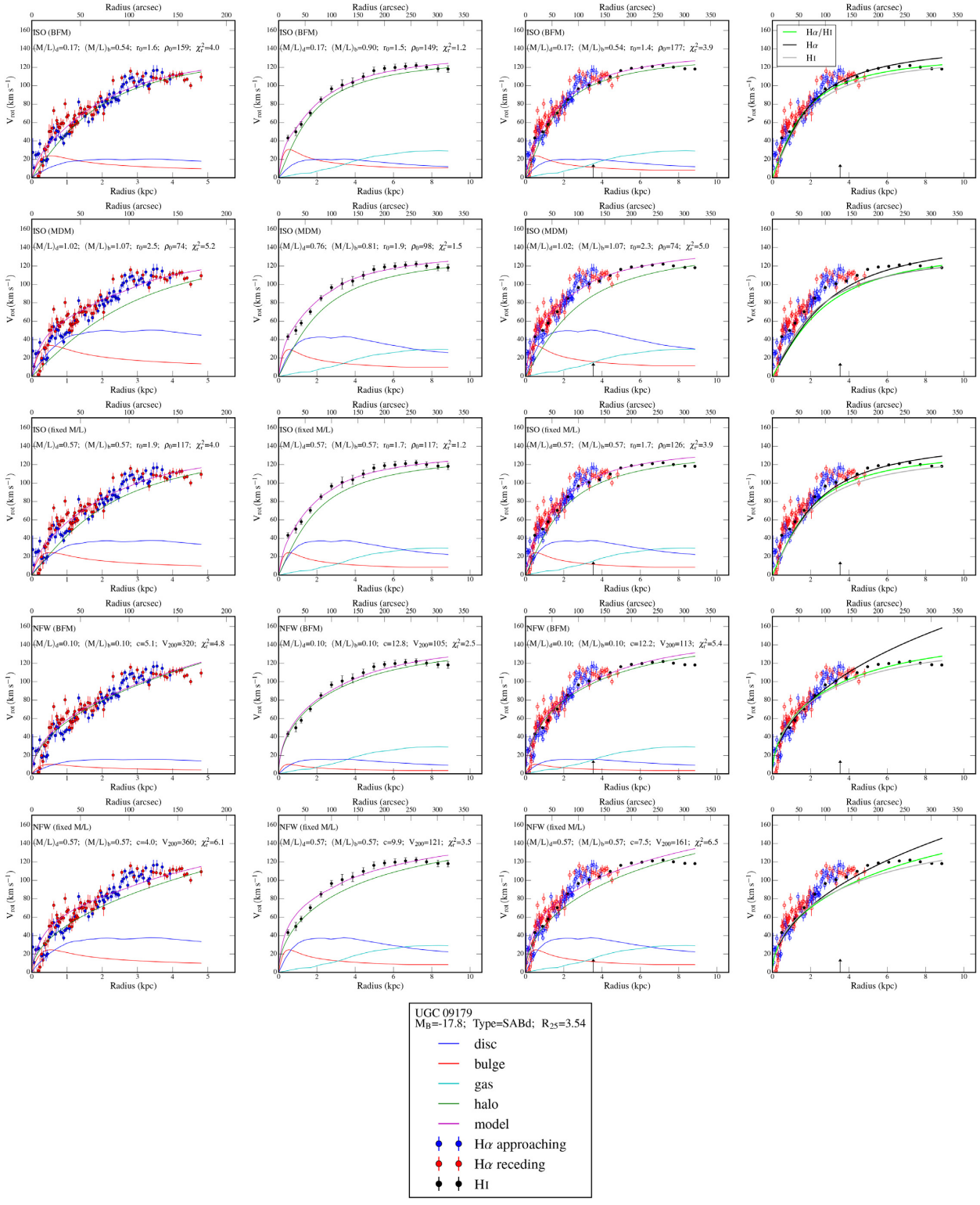

Figure A18.

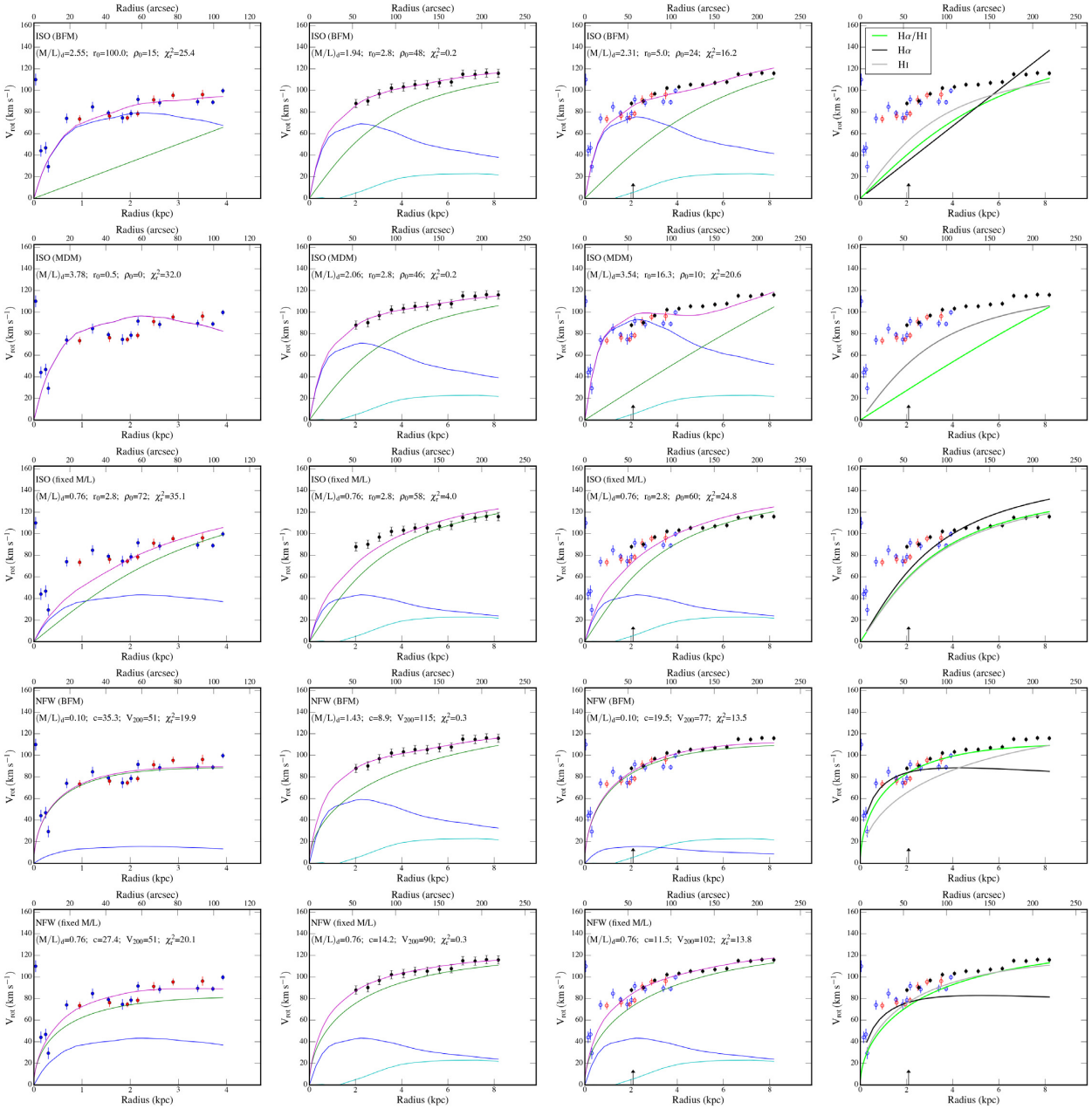

Figure A19.

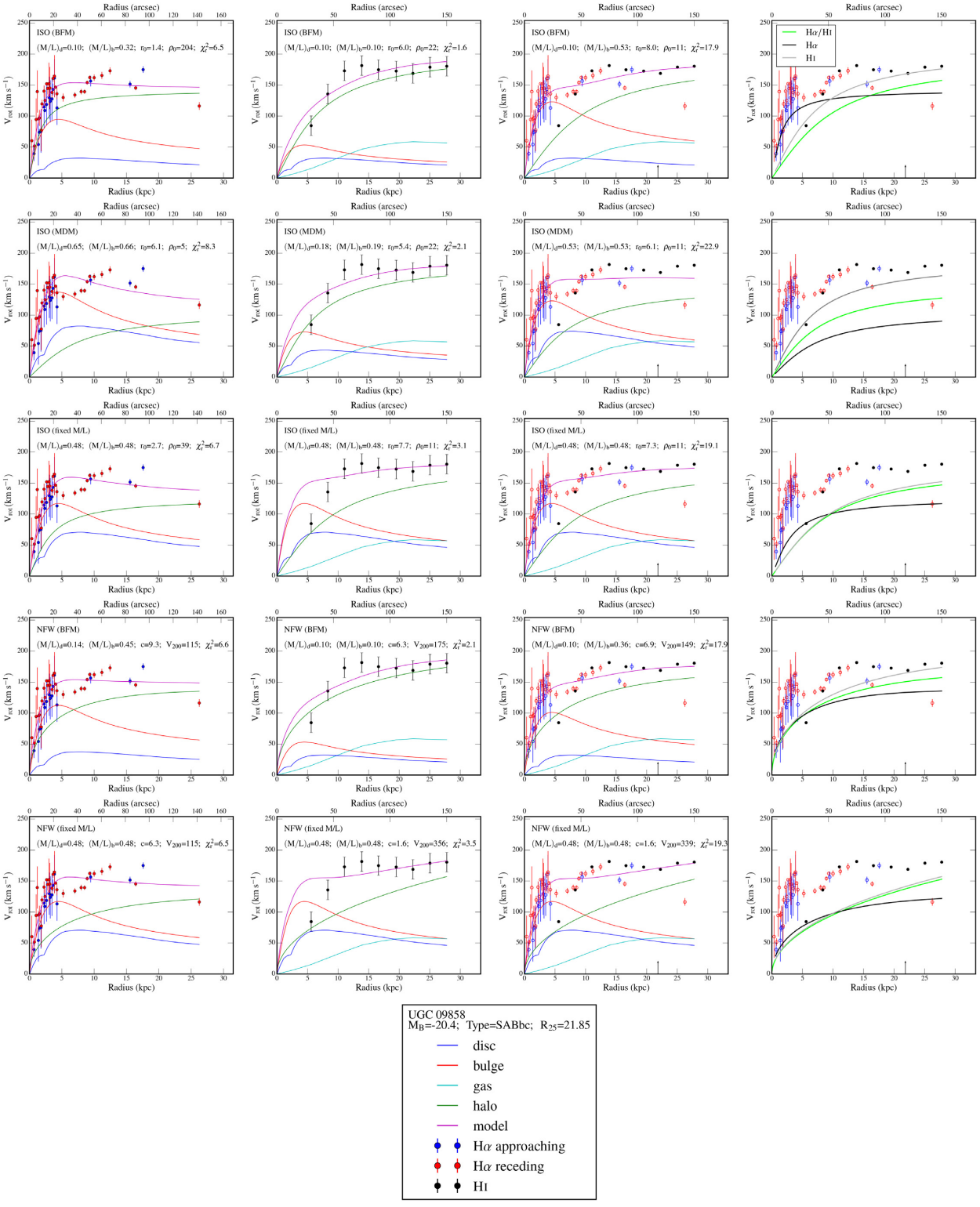

Figure A20.

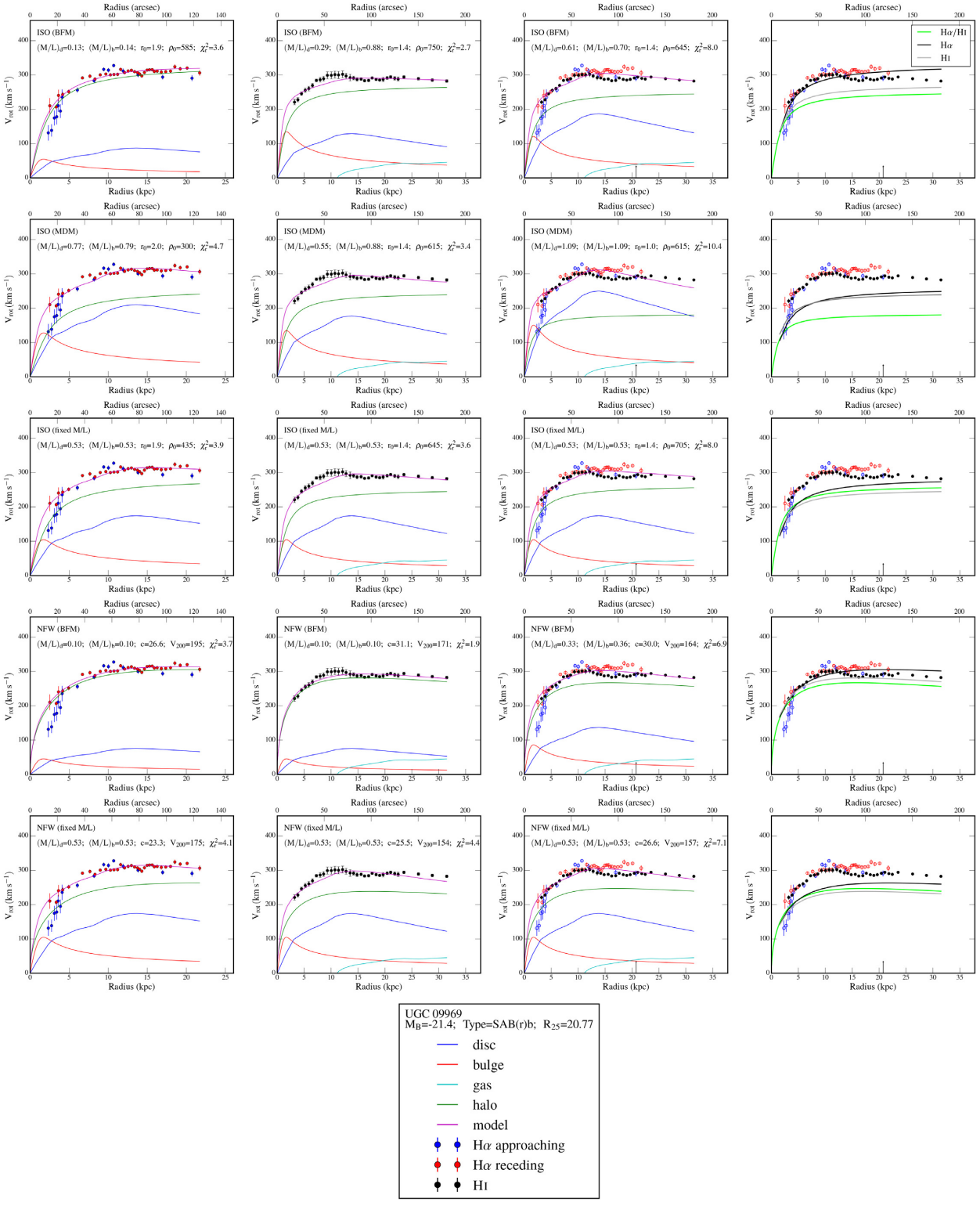

Figure A21.

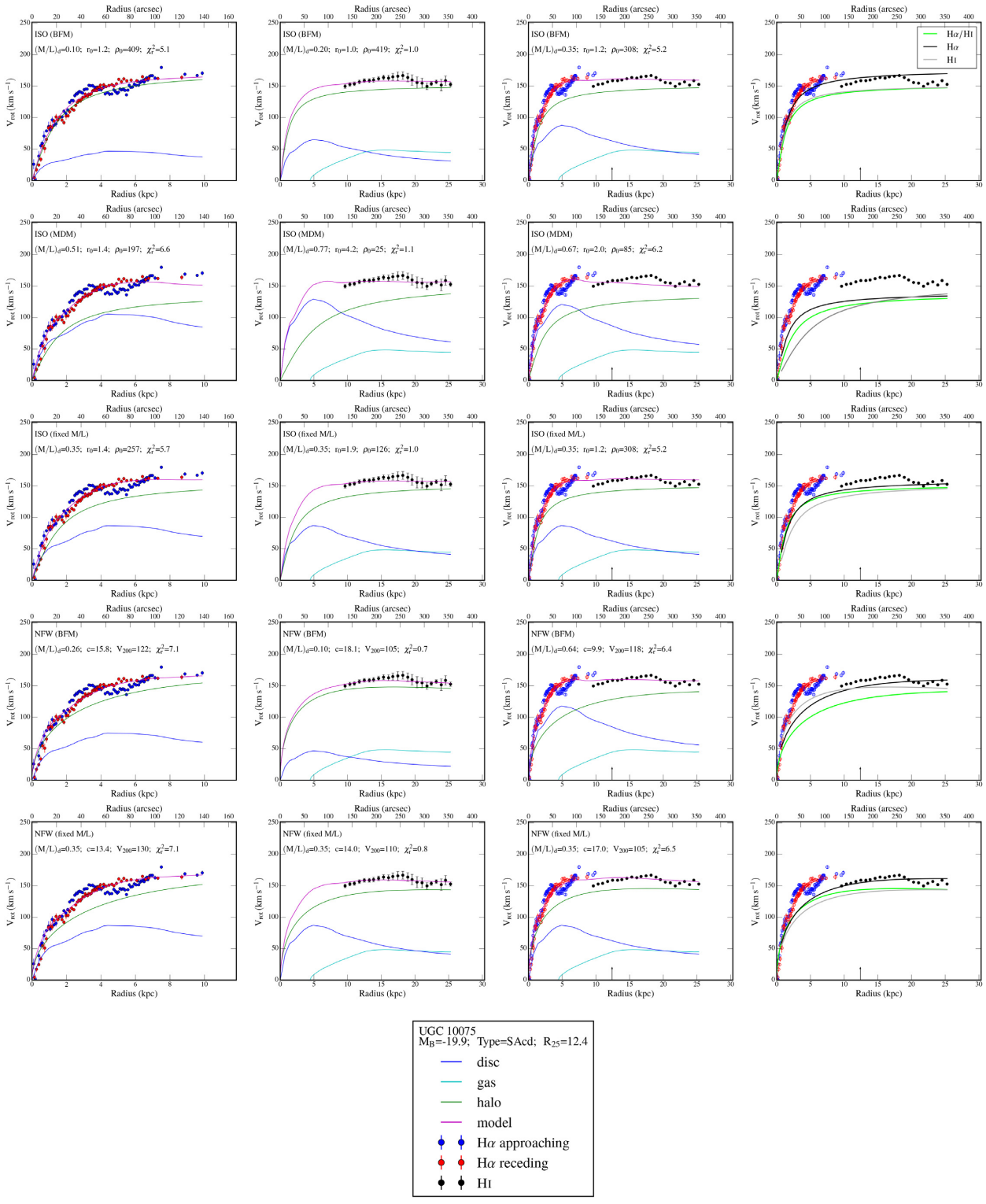

Figure A22.

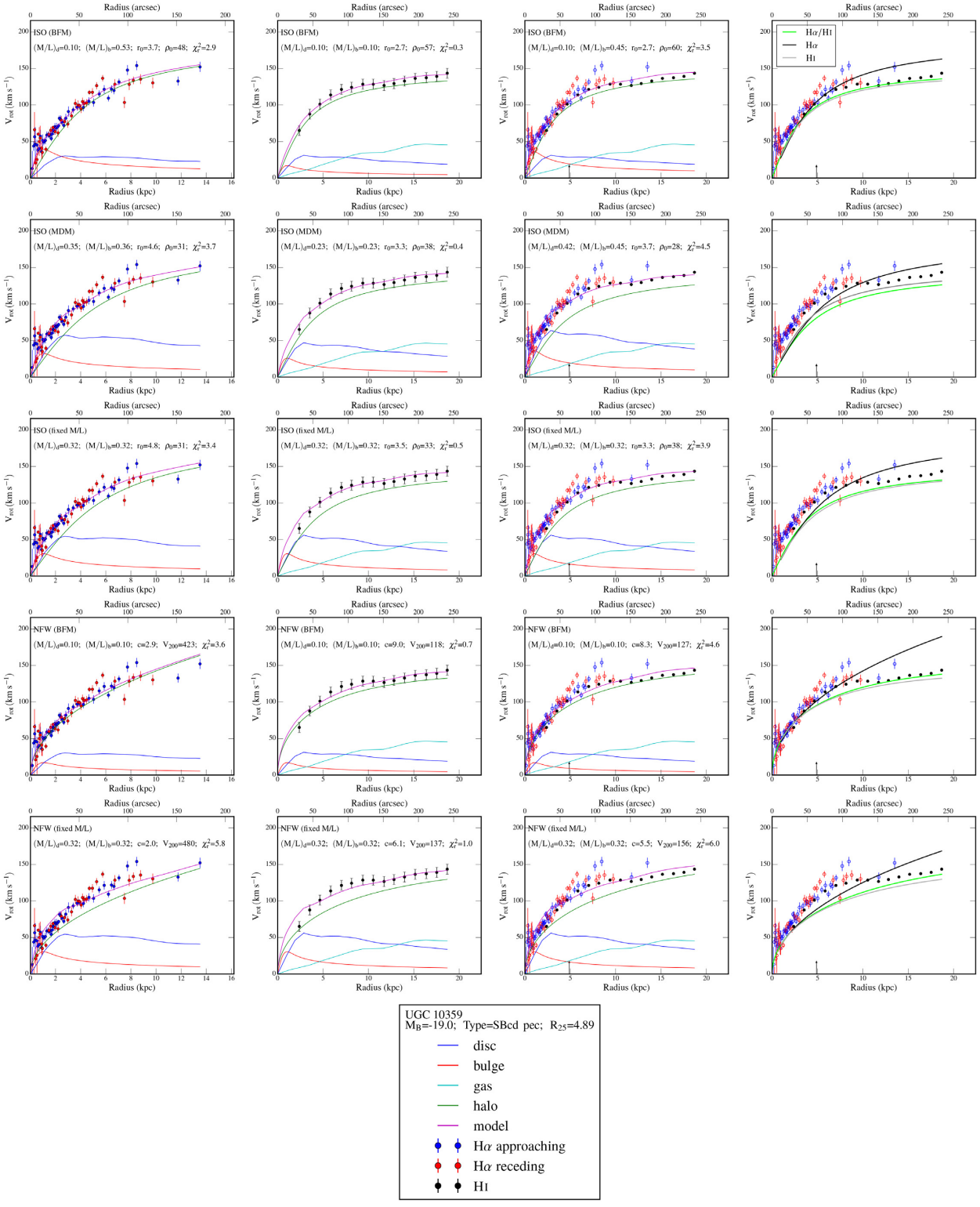

Figure A23.

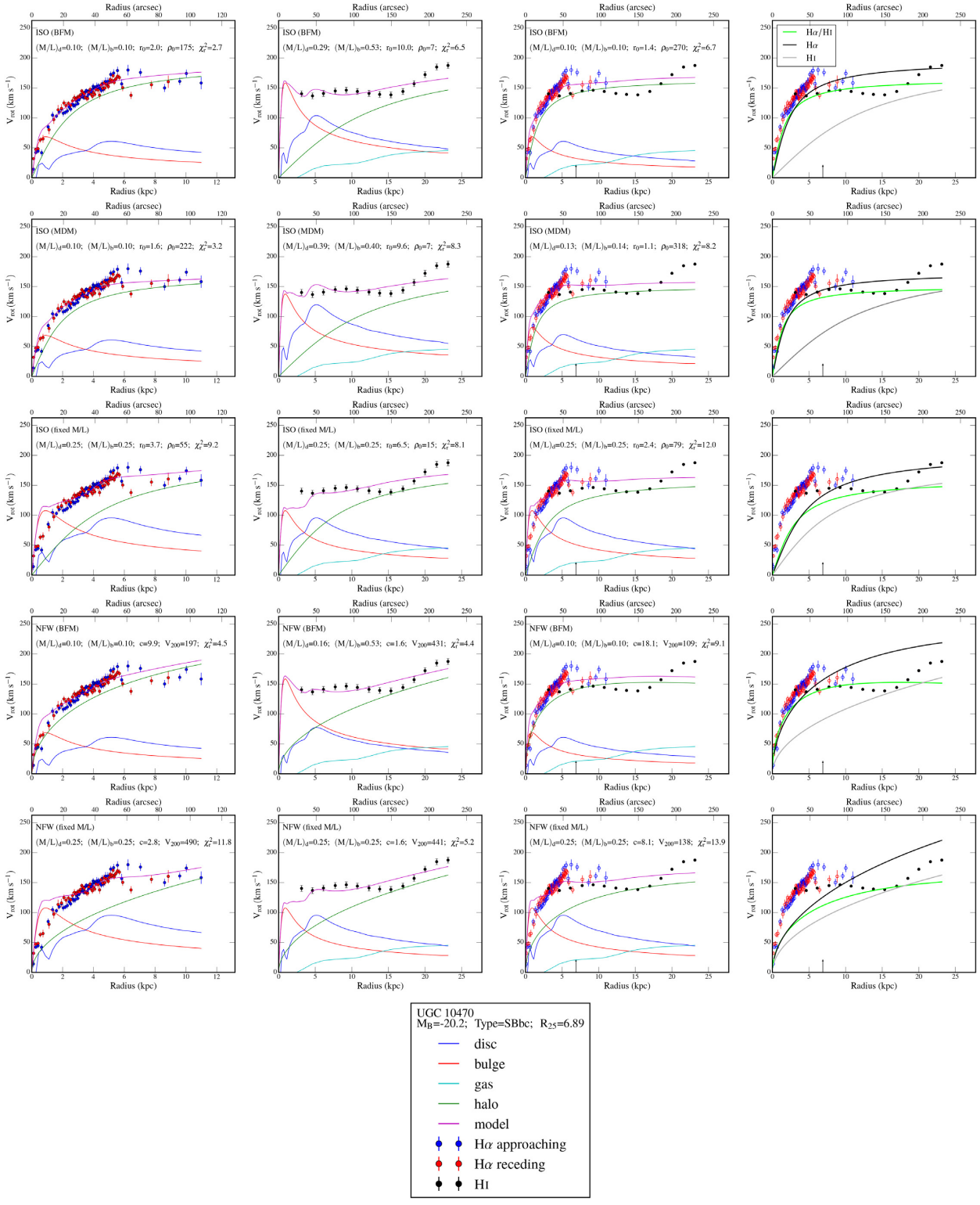

Figure A24.

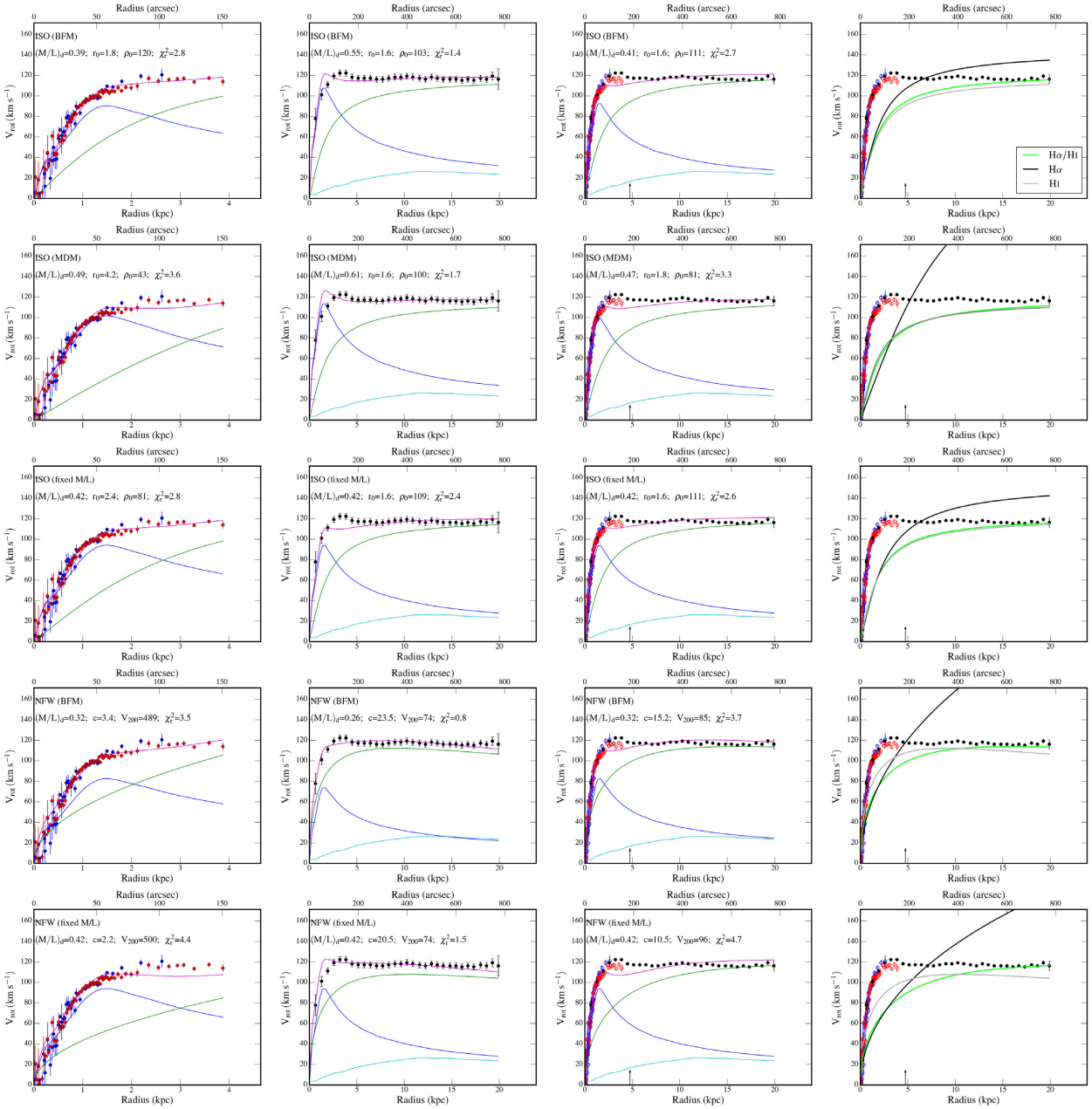

Figure A25.

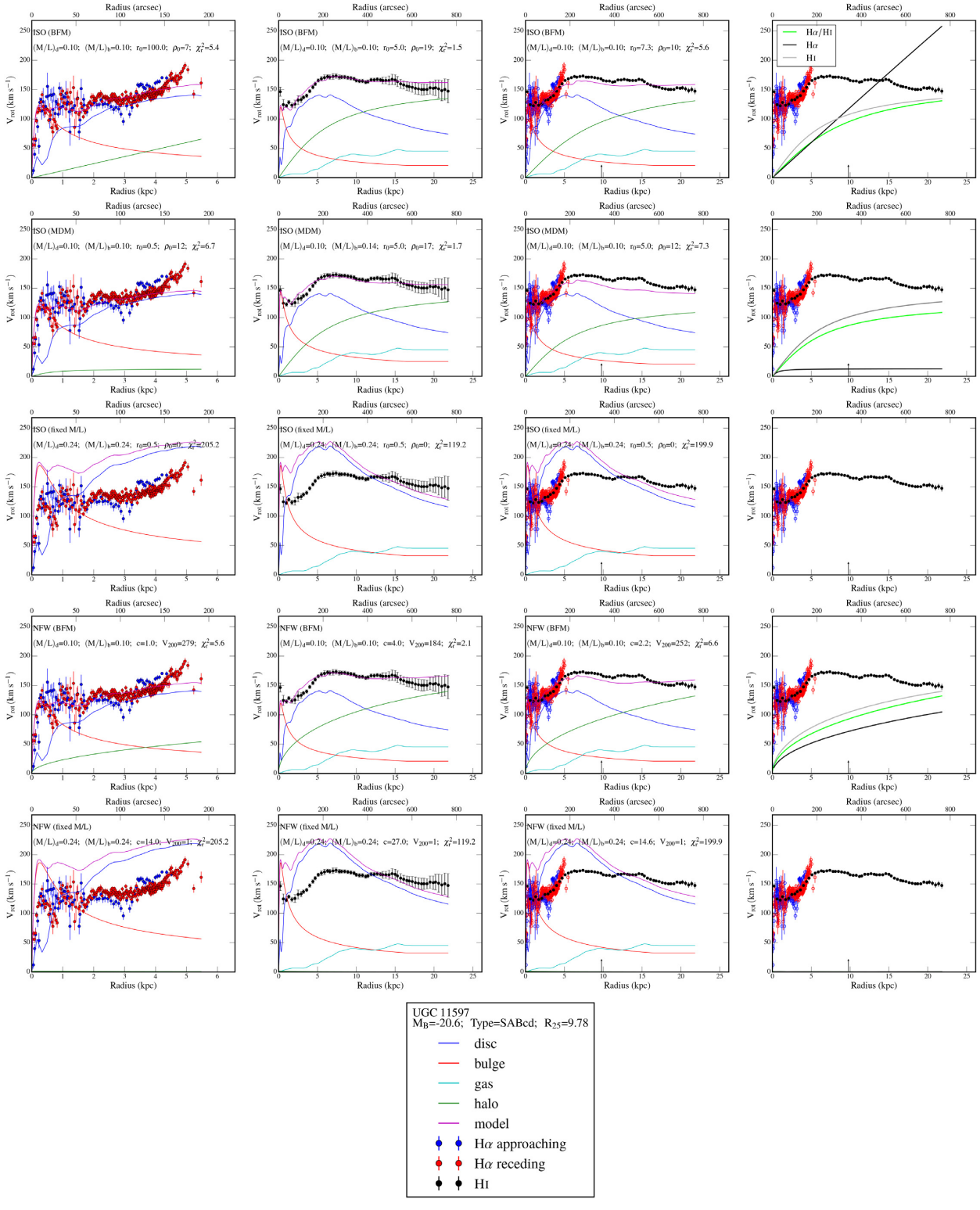

Figure A26.

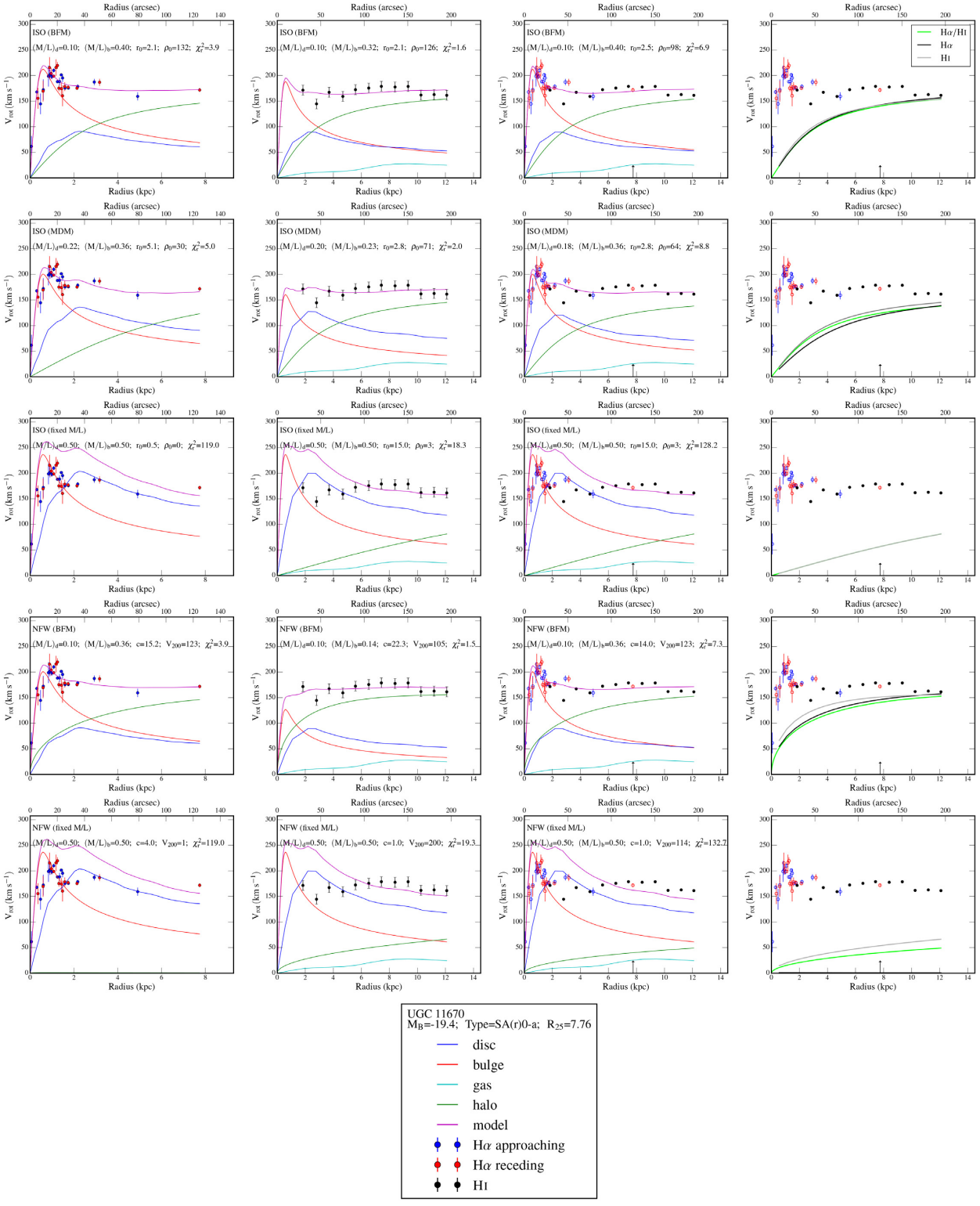

Figure A27.

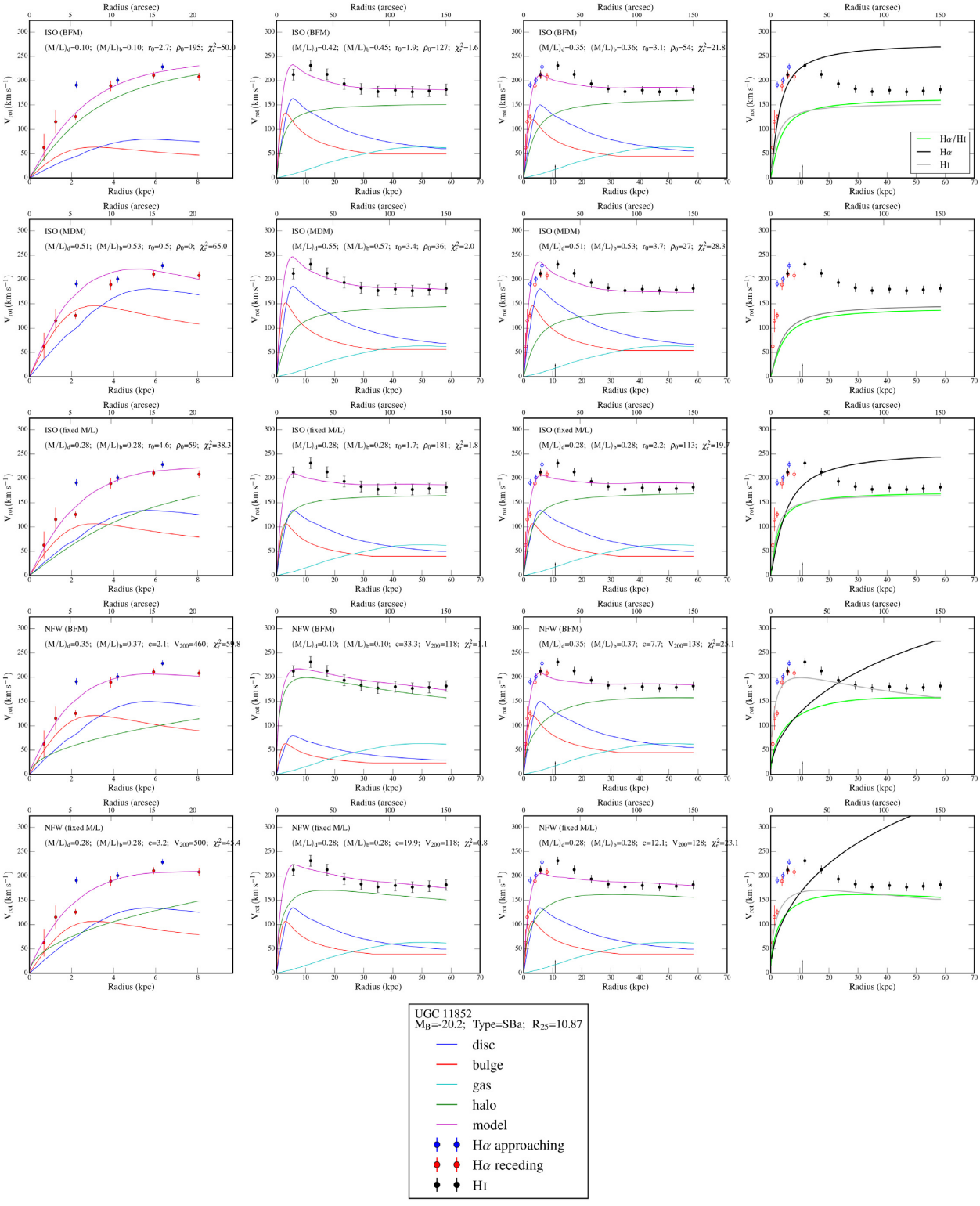

Figure A28.

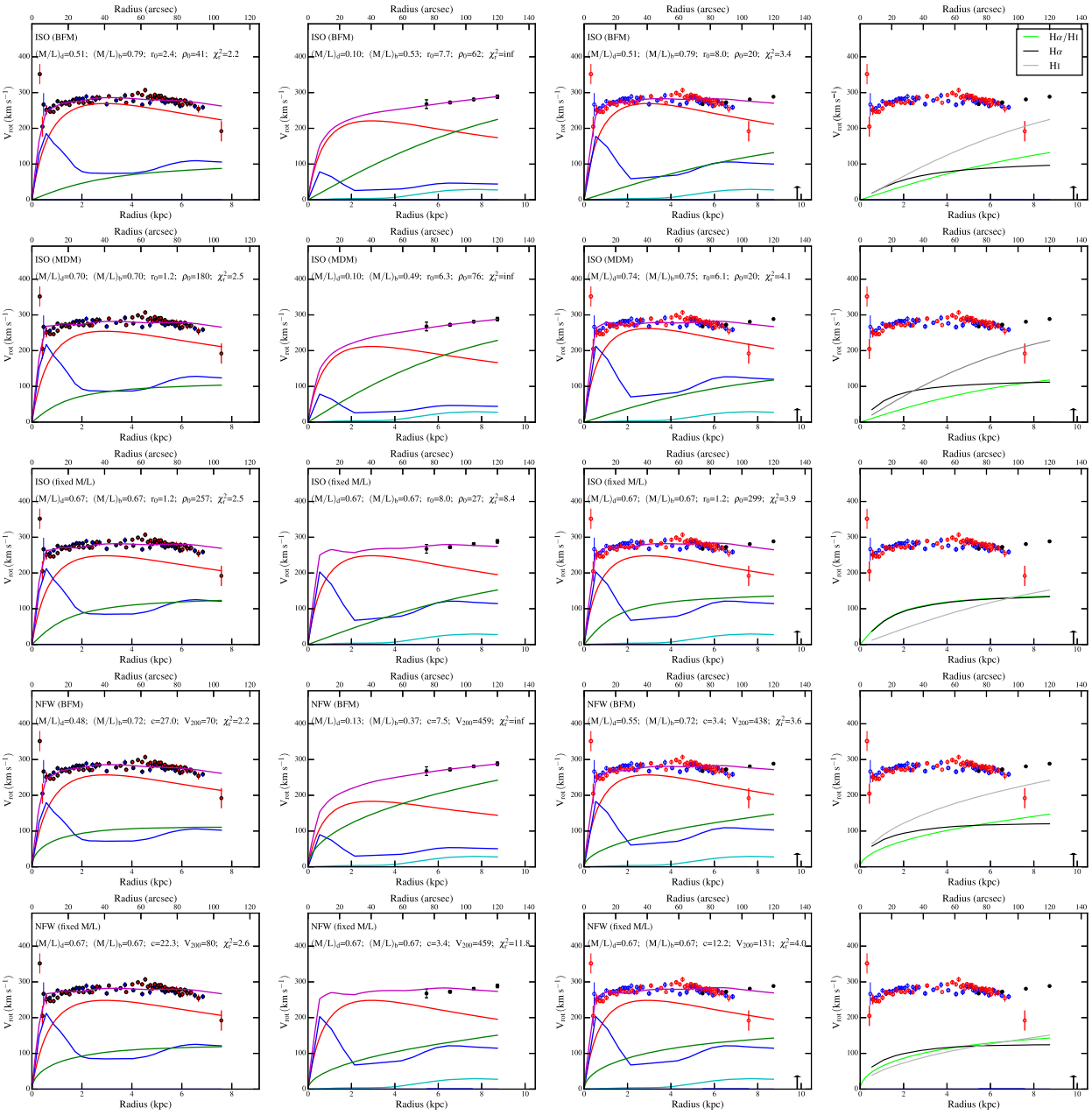

Figure A29.

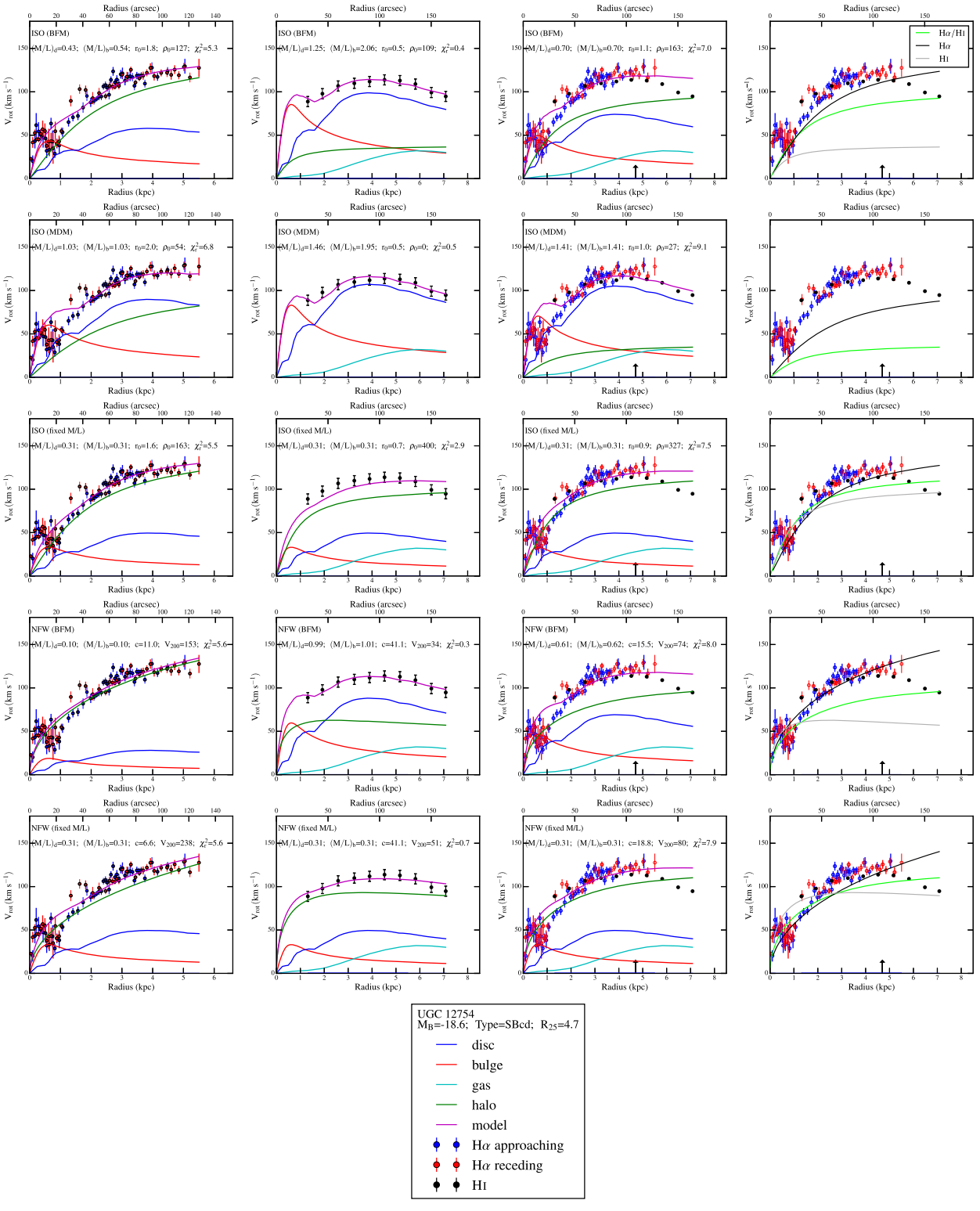

Figure A30.

This paper has been typeset from a TEX/LATEX file prepared by the author.